CHARLES UNIVERSITY IN PRAGUE

Faculty of Science

Molecular biology, genetics and virology

Mgr. Jan BLECHA

Molecular bases of sensitivity to electron transport chain inhibition-induced cell death

Molekulární podstata citlivosti k buněčné smrti indukované inhibicí elektron-transportního řetězce

Dissertation Thesis

Supervised by Mgr. Jakub Rohlena, Ph.D.
Laboratory of Molecular Therapy
Institute of Biotechnology AS CR, v.v.i.

Praha, 2019

Statement of originality:

This thesis was composed at the Institute of Biotechnology, Czech Academy of Sciences, in the Laboratory of Molecular Therapy. Experimental data included herein were published in two original research articles.

I declare that I have accomplished this final thesis independently under supervision of Mgr. Jakub Rohlena Ph.D. and that I have included all cited literature and used sources of information. Neither the work as the whole nor any its substantial part has been previously submitted to achieve a different or similar academic degree. I further declare that I have truthfully stated my contribution to the works published with the collective authorship in the chapter 3 Results.

In Prague.....

Signed: . . . . . .

Mgr. Jan BLECHA

CONTRIBUTION OF AUTHOR JAN BLECHA TO PRESENTED RESULTS

Data in the thesis were generated by Jan Blecha, unless stated otherwise. Papers related to this thesis are attached in the end of thesis.

Paper I. - Blecha J, Novais SM, Rohlenova K, Novotna E, Lettlova S, Schmitt S, Zischka H, Neuzil J, Rohlena J.; *Antioxidant defense in quiescent cells determines selectivity of electron transport chain inhibition-induced cell death*. Free Radic Biol Med. 2017 Nov.
Impact factor at the time of publishing = 6.32

The vast majority of the experimental work was performed by the first author (JB). He also participated in writing and revising of the manuscript and prepared all figures. SN helped with preparation of expression plasmid, generation and selection of manipulated cell lines. JR supervised and coordinated the project and contributed to writing and revision the manuscript. JR together with KR performed preliminary data as well as two-photon microscopy experiments and *in vivo* mice experiments. The mouse-derived materials were then analysed by JB. SL, EN, SS and HZ generated preliminary data and performed important confirmatory experiments that are not included in this work. SS and HZ developed and optimized an improved method for mitochondrial isolation from cultured cells, which has been used throughout the paper. JN provided important insights with respect to the overall direction of the work and participated in writing and revision of the paper.

Paper II. - Rohlenova K, Sachaphibulkij K, Stursa J, Bezework-Geleta A, **Blecha J**, Endaya B, Werner L, Cerny J, Zobalova R, Goodwin J, Spacek T, Pesdar EA, Yan B, Nguyen MN, Vondrusova M, Sobol M, Jezek P, Hozak P, Truksa J, Rohlena J, Dong LF, Neuzil J.; *Selective disruption of respiratory supercomplexes as a new strategy to suppress Her2^{high} breast cancer*. Antioxid Redox Sign. 2017 Jan.
Impact factor at the time of publishing = 6.53

JB contributed to this work by performing activity assays for respiratory complexes, measuring activity of the glycolytic pathway and by assisting with the evaluation of tumour growth. He also contributed to respiratory measurements.

Paper III. Is in preparation/unpublished but outlined in: Novais SM, **Blecha J**, Rohlenova K, Neuzil J, Rohlena J,; *P-115 - Functional electron transport chain is necessary for stress resistance in quiescent cells.* Free Radic Biol Med. 2018 May

The unpublished preliminary and pilot experiment data were assessed by JB with contribution by SN, who has now taken over the project.

I declare that I have truthfully stated my contribution to these works.

Prague, 2019

Signed: . . . . . .

Mgr. Jan Blecha

Signed: . . . . . .

Supervisor Mgr. Jakub Rohlena, Ph.D.

Here, I would like to express my gratitude to my supervisor Jakub Rohlena for his guidance, encouragement and advice. With his help, I was able to step into the fascinating world of science, for which I will always be grateful. My thanks go also to all my colleagues from Laboratory of Molecular Therapy. More generally, I am thankful to my alma mater, the Charles University, Faculty of Science, where I learned the principles and obtained the support to try to discover a piece of knowledge by my own.

The study was supported by the **Charles University in Prague,** project **GAUK 98215, Czech Science Foundation** and the **BIOCEV European Regional Development Fund CZ.1.05/1.1.00/02.0109**.

Contents

Abstract in English

Mitochondrial electron transport chain (ETC) targeting shows a great promise in cancer therapy. However, why modern ETC-targeted compounds are tolerated on the organismal level and what are the molecular reasons for this tolerance remains unclear. Most somatic cells are in a non-proliferative state, and features associated with the ETC in quiescence might therefore contribute to specificity. Thus, we investigated the ETC status and the role of two major consequences of ETC blockade, reactive oxygen species (ROS) generation and inhibition of ATP production, in cell death induction in breast cancer cells and in proliferating and quiescent non-transformed cells.

First, we characterised the effect of a newly developed ETC inhibitor mitochondria-targeted tamoxifen (MitoTam) in *in vitro* and *in vivo* tumour models of breast cancer with varying status of the Her2 oncogene. We document that $Her2^{high}$ cells and tumours have increased assembly of respiratory supercomplexes (SCs) and increased complex I-driven respiration *in vitro* and *in vivo*. They are also highly sensitive to MitoTam. Unlike the parental compound tamoxifen, MitoTam efficiently suppressed experimental $Her2^{high}$ tumours without systemic toxicity. Mechanistically, MitoTam inhibits complex I-driven respiration and disrupts respiratory SCs in $Her2^{high}$ background *in vitro* and *in vivo*, leading to elevated reactive oxygen species production and cell death. This suggests that in cancer settings increased respiration sensitizes to ETC inhibition by stimulating ROS generation.

Next, we investigated if differences in mitochondrial respiration between proliferating and quiescent cells, representing cancerous and normal tissue, could explain the specificity of ETC targeting. Therefore, endothelium-derived (EA.hy926) and epithelium-derived (MCF10A) non-transformed cells capable of contact inhibition were cultured in low (1 g/L) and high glucose (4.5 g/L) media, representing conditions of limited and ample glucose supply, respectively. Both, proliferating and quiescent (contact-inhibited) cells were exposed to direct ROS inducers that do not interact with the ETC, specific inhibitors of the ETC or inhibitors of mitochondrial ATP production. We also performed similar experiments in EA.hy926 cells with depleted mitochondrial DNA featuring defective ETC to clarify ETC's role in the selectivity phenomenon. Cell death and ROS production, as well as various metabolic parameters, particularly mitochondrial respiration, antioxidant defence expression and

activity, glycolysis rate and ATP levels were assessed. The role of several components of the antioxidant defence systems (SOD2- and GPX1-, TRX-reductase- and GSR) was interrogated by shRNA-mediated knockdown. In the end of study, we confirmed the results *in vivo* using FVBn/c-neu mouse model of spontaneous $Her2^{high}$ mammary carcinoma.

Even though quiescent cells, compared to proliferating cells, featured increased SC assembly and a higher rate of respiration, proliferating cells were more susceptible to cell death induced by direct ROS inducers, ETC and ATP synthase inhibitors when cultured in high glucose conditions. All these agents also induced more ROS in proliferating cells. Interestingly, in low glucose conditions the pattern of cell death sensitivity was reversed for ETC and ATP synthase inhibitors, but not for direct ROS inducers. The amount of cell death in this situation correlated with significant ATP depletion in quiescent cells, rather than with ROS production. This was related to the inability of quiescent cells to compensate for the loss of mitochondrial ATP production by the upregulation of glucose uptake. Regardless of glucose availability, quiescent cells featured increased protein levels and activity of antioxidant enzymes (SOD2, TRX2, PRX3 and GPX). However, silencing of SOD2 or TRX-reductase 2 by RNA interference increased ETC inhibition-induced cell death and ROS production exclusively in quiescent cells under high glucose conditions. Experiments with ETC-deficient cells then revealed that functional ETC paradoxically complements the protective role of antioxidant defence in quiescent cells. This interesting aspect will be investigated in follow-up research.

In conclusion, our data suggest that lack of ATP is the major factor for cell death induction when ETC is blocked in a situation of glucose limitation, while the amplitude of ROS generation becomes dominant when glucose is not limiting. The combination of antioxidant defence and glucose availability therefore co-determines the specificity of ETC-inhibition-induced cell death and explains why ETC inhibition can effectively suppress cancer without considerable collateral damage to normal tissue.

Abstrakt česky

Látky cílené na mitochondriální elektron transportní řetězec (ETC) vykazují dobrý potenciál v protinádorové terapii, ale molekulární podstata jejich specificity stále není zcela objasněná. S přihlédnutím k tomu, že většina somatických buněk je v klidovém neproliferujícím stavu a je vůči těmto látkám inertní, změny mitochondriálního metabolismu spojené se vstupem do klidového stavu by mohli objasnit resistenci. Z tohoto důvodu jsme v předložené práci analyzovali stav ETC spolu s hlavními důsledky jeho inhibice jako je zvýšená produkce reaktivních kyslíkatých radikálů (ROS) a snížená produkce ATP na pozadí indukce programované buněčné smrt v modelech nádoru prsu a v proliferujících a klidových netransformovaných buňkách.

V první řadě jsme charakterizovali efekt nově vyvinuté protirakovinné látky, mitochondriálně cíleného tamoxifenu (MitoTam), *in vitro* a *in vivo* v modelech nádoru prsu s rozdílnou expresí onkogenu Her2. Ukázali jsme, že podstatou protinádorového účinku látky MitoTAM je efektivní inhibice respiračního komplexu I provázená vysokou mírou produkce ROS a to zejména v nádorech se zvýšenou hladinou Her2, které vykazují vyšší míru uspořádanosti ETC do superkomplexů spojenou s vyšší mírou respirace. Tyto výsledky naznačily, že nádory s vyšší mitochondriální respirací jsou citlivější k eliminaci inhibitory ETC v důsledku zvýšené produkce ROS a následném rozpadu vyšších respiračních struktur.

Dále jsme zjišťovali, zda bioenergetické rozdíly mezi proliferujícími a klidovými buňkami, které reprezentují nádorové, respektive somatické buňky, mohou vysvětlit specificitu látek cílených na ETC. Endoteliální (EA.hy926) a epiteliální (MCF10A) buněčné linie byly vystaveny činidlům působících oxidační stres nezávisle na ETC, inhibitorům ETC či inhibitorům mitochondriální produkce ATP. Jedním z testovaných parametrů byla dostupnost glukózy v médiu. Koncentrace 4.5 g/L představovala dostatek a 1 g/L nedostatek tohoto sacharidu. Význam ETC ve studovaném jevu jsme ověřili na linii zbavené mtDNA s defektním ETC. Sledovali důležité metabolické parametry spojené s bioenergetikou, zejména buněčnou respiraci, antioxidační ochranu, ale též úroveň glykolýzy a syntézy ATP. Výsledky jsme poté ověřili na modelu FVB/c-neu myšího spontánního nádoru prsu.

Překvapivě jsme zjistili, že navzdory zvýšené míře uspořádanosti ETC a respirace v klidových buňkách, tyto buňky byly v případě dostatku glukózy méně citlivé k buněčné smrti indukované všemi testovanými látkami, což bylo provázeno nižší produkcí ROS. Klidové buňky měly zvýšenou proteinovou i aktivitní úroveň antioxidační ochrany (SOD2, TRX2, PRX3 a GPX) a genové utlumení SOD2 a TRX2 bylo provázeno zvýšenou mírou buněčné smrti specificky v klidových buňkách. Tyto výsledky naznačují, že zvýšená schopnost detoxifikovat ROS určuje citlivost klidových buněk k inhibici ETC v situaci, kdy glukóza není limitující. Oproti tomu nedostatek glukózy signifikantně zvýšil citlivost klidových buněk vůči inhibitorům ETC a mitochondriální syntézy ATP, zatímco citlivost vůči induktorům ROS nezávislým na ETC zůstala nezměněna. V případě inhibitorů ETC a ATP syntézy jsme zaznamenali souvislost s letálním úbytkem ATP, což bylo umocněno neschopností klidových buněk zvýšit příjem glukózy a doplnit tak ztrátu ATP v glykolýze. Pokusy s buňkami deficientním na ETC ukázaly, že funkční ETC doplňuje ochrannou úlohu antioxidantů v klidových buňkách. Tento zajímavý aspekt bude dále detailněji prošetřen v navazujícím projektu.

Závěrem naše data naznačují, že inhibice ETC s následným vyčerpáním ATP je spouštěcím faktorem buněčné smrti v situaci nedostatečné glukózy, zatímco ROS indukované blokádou ETC iniciují buněčnou smrt, když je glukóza v dostatku. Kombinace antioxidační ochrany a dostupnosti glukózy proto spolu-určuje molekulární specificitu buněčné smrti vyvolané inhibicí ETC. V důsledku toto vysvětluje, jak inhibice ETC může účinně zamezit rakovinné proliferaci bez významného vedlejšího poškození normální tkáně.

Objective

The objective of this study was to investigate why ETC inhibitors suppress tumour growth while maintaining specificity. Particular attention was given to the link between ETC activity and sensitivity to cell death, and to evaluating the relevance of specific outcomes of ETC inhibition, such as ROS generation and ATP production, for cell death induction. This general objective was sub-divided into several specific steps:

- To investigate the efficacy of cell death induction by mitochondria-targeted tamoxifen *in vitro* and *in vivo* in breast cancer models with different Her2 status and establish a possible link between effectivity of cell death induction and the level of respiration.
- To investigate the specificity of ETC targeting and determine if it is governed by the level of respiration using a model system of proliferating and quiescent cells.
- To clarify the relevance of ROS production and ATP generation for ETC-inhibition-induced cell death using pharmacological treatments of proliferating/quiescent cells cultured in high/low glucose conditions and determine how this relates to treatment specificity.
- To investigate the role of antioxidant defence in cell death sensitivity, identify key antioxidant components that determine susceptibility and evaluate the role of functional ETC.
- To verify these results *in vivo* using a mouse model of spontaneous breast carcinoma.

1 Introduction

Most of the somatic cells in an organism are in a differentiated, quiescent state. When required, such as during healing of injury, these quiescent cells are able to re-establish proliferation to maintain organismal haemostasis. When the tight control on proliferation is broken, this gives arise to pathologies such as cancer, a disease of excessive proliferation. Hence, the cancerous phenotype is intrinsically a phenotype of uncontrolled proliferation. With respect to cancer therapy, it is therefore crucial to understand how proliferation and quiescence alter susceptibility to various modes of cell death induction.

A large majority of commonly used anticancer agents supress tumour growth by inhibiting cells proliferation or inducing a programme of self-elimination referred to as apoptosis. Apoptosis is an essential process strictly controlled at multiple levels and is involved in cellular homeostasis and correct development of multicellular organisms. At the same time, apoptosis is a valuable tool to fight cancer, even though the molecular mechanisms that govern sensitivity to treatment are not yet fully resolved. A considerable effort has been invested into understanding the mechanism of sensitivity and to identification of relevant factors responsible for apoptotic sensitivity and regulation. Given that cancer is a disease of uncontrolled proliferation, the proliferation-linked factors of apoptotic sensitivity might be particularly relevant, and their characterization may advance the design of novel, more specific anticancer drugs as well as supress the side effects of the existing one.

1.1 Hallmarks of cancer and cell proliferation

Cancer is a major healthcare burden worldwide. Each year, tens of millions of people around the world are diagnosed with cancer, and more than half of the patients eventually die from the disease. Developments in genomic techniques have shown that solid tumours may comprise subpopulations of cells with distinct genomic alterations within the same tumour. This phenomenon is likely to have implications for cancer therapeutics and biomarker discovery, particularly in the era of targeted treatment. [1-3]

Despite their daunting genetic diversity, cancer cells share several common features (Figure 1). These include defects in proliferation and energetics, as well as altered metabolism. Several hallmarks of cancer have been described and provide a logical framework to unify the remarkable diversity of neoplastic diseases and its biology [3, 4]. Importantly, the most notable feature included within these hallmarks is the ability to maintain chronic proliferation. Cancer cells acquire the ability to sustain proliferative signalling in a number of alternative ways: they may produce growth factor ligands to stimulate stroma cells for growth-stimuli production for cancer growth [5], became growth factor-independent or upregulate their receptors to become hyper-responsive. In addition, prominent part of cancer cells sustain mutations that enhance downstream proliferating signalling [6] or suppress negative-feedback signalling as well as signalling by suppressors of proliferation, giving them proliferative independence. In contrast, normal tissues carefully control the production and release growth factors to balance homeostasis. [4] Other cancer cells hallmarks relevant to this dissertation include the resistance to cell death usually via

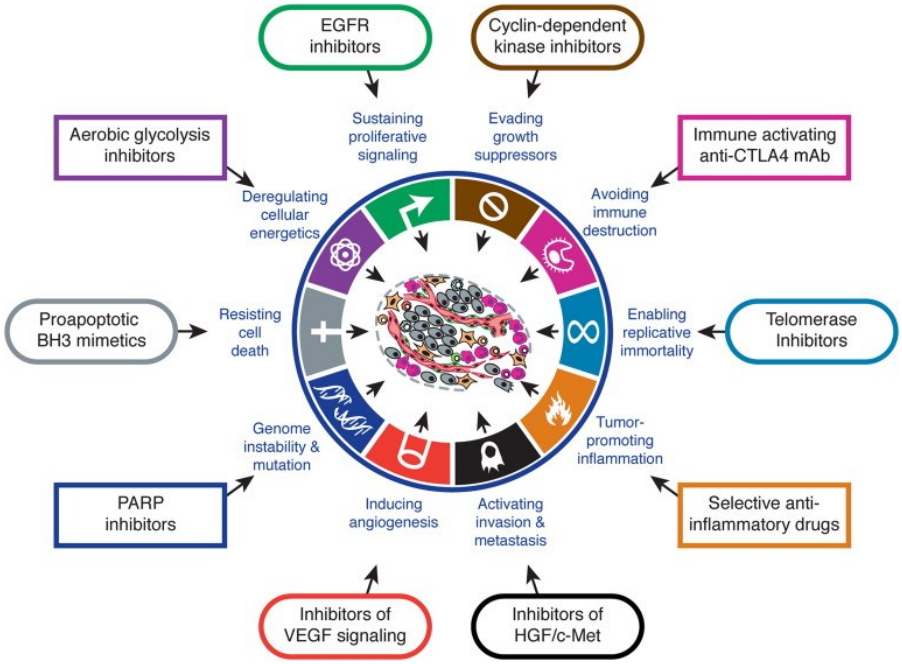

Figure 1 **Therapeutic targeting of the cancer hallmarks.** Drugs that interfere with each of the acquired capabilities necessary for tumour growth and progression have been developed and are in clinical trials or in some cases approved for clinical use in treating certain forms of human cancer. This thesis argues that also drugs targeted at deregulated cellular energetics, in particular the ETC, are affective and selective anticancer agents. Adapted from [4]

defects in cellular damage sensor function as well as faulty functioning of the ageing sensors at the level of telomerases. [7] Furthermore, cancer cells are able to effectively induce angiogenesis, to be well supplied by nutrients and are invasive and metastatic. [8]

1.1.1 Cancer-associated metabolic shift - Warburg effect

Rapid and persistent growth and division of cancer cells involves adjustment in energy metabolism in order to fuel cell proliferation. In many human tumour types, it was documented that tumour cells (similarly to the proliferating somatic cells) have higher rate of glycolysis but decreased oxidative phosphorylation irrespective of oxygen availability. This so-called Warburg effect provides the rapidly proliferating cancer cells with glycolysis-derived metabolic building blocks for biosynthesis of proteins, lipids and nucleic acids, but also generates ample ATP from the enzymatic conversion of glucose to pyruvate and further to lactate within the glycolytic pathway (Figure 2). Lactate production ensures that the NAD^+ pool is continuously regenerated and the anabolic intermediates are produced in a sufficiently fast rate. [9] Indeed, NADPH rather than ATP is limiting for the biosynthesis of amino and fatty acids as well as nucleotides. Thus, even though Warburg shift provides just two molecules of ATP compared to 36 molecules that could be earned by complete oxidization of a molecule of glucose by oxidative phosphorylation under aerobic conditions, glycolysis is kinetically superior and provides enough ATP to satisfy the energy needs of a proliferating cancer cell. In contrast, in non-proliferating cells that do not need that much NADPH or other glycolysis-derived intermediates, most glucose-derived pyruvate is diverted into mitochondria to form acetyl-CoA and produce NADH in the tricarboxylic acid cycle (TCA) in the mitochondrial matrix as well as to synthesize citrate. [10, 11] Citrate is then exported from mitochondria and reduces the rate of glycolysis in non-proliferating cells. While citrate is also exported from mitochondria in the proliferating cells, it is used for cytosolic acetyl-CoA production and therefore does not inhibit glycolysis. Rather it maintain high glycolysis and high ATP/ADP and $NADH/NAD^+$ ratios in proliferating cells. This specific pro-growth biosynthetic wiring may explain at least in part the selective advantage provided by the Warburg effect. It is clear that for a cell to proliferate, the bulk of the glucose cannot be committed to carbon catabolism for ATP production. If this were the case, the resulting rise in the ATP/ADP ratio would severely impair the flux through glycolytic intermediates,

limiting the production of the acetyl-CoA and NADPH required for macromolecular synthesis. [12]

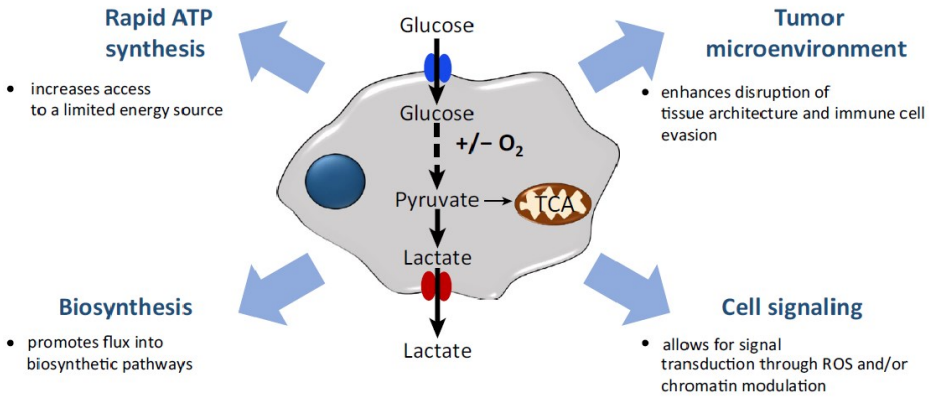

Figure 2 **Proposed Functions of the Warburg Effect**. The Warburg Effect is defined as an increase in the rate of glucose uptake and preferential production of lactate, even in the presence of oxygen. Each of these functions has been hypothesized to be the function of the Warburg Effect. Adapted from [13]

Somatic cells are usually in nutrient rich environment, although cancer cells need to compensate lower efficiency of ATP production and satisfy huge glycolytic demand via upregulating glucose transporters, notably Glut1, which increases glucose import into the cytoplasm. [14, 15] Surprisingly, in some tumours two metabolically distinct population of cancer cells were found. One subpopulation is glucose-dependent featuring the typical Warburg phenotype with high lactate production, while the second subpopulation utilizes produced lactate in the TCA cycle and maintains active ETC. These two populations evidently support each other. Hypoxic cancer cells energy metabolism depends on glucose and produces lactate as a waste, which is preferentially utilised in their better-oxygenated counterparts, saving available glucose for the more hypoxic neighbours. This gives both populations advantage in the instable and chaotically organized tumour tissue. [16, 17]

In summary, one tenth of pyruvate is used in biosynthesis and minor part is oxidized in TCA when Warburg shift occurs. In the end, this metabolic switch gives rise to two ATP molecules from one molecule of glucose [9]. Besides proliferation, disruption and defects of mitochondria, reduction of mitogenesis and changes in oncogene expression can also results in the Warburg shift in metabolism. The metabolic change also allows for the decreased rate of respiration and consequently increased ROS production to stimulate the majority of

proliferating signalling cascades (NF–κB, p53, RAF, HIF–1 etc.) and achieve maximal activity of proliferating kinases (AKT, ERK 1 and 2 etc.) [18].

1.2 Cell cycle and cell proliferation

As mentioned above, one of the prominent hallmarks of cancer is the defective control of cell proliferation, resulting in unrestrained growth of tumour cells. In contrast, the majority of normal somatic cells are in a quiescent state and through their live duration proliferate only infrequently if at all, although they can re-initiate proliferation when properly stimulated. This happens for example when proliferation of endothelial and epithelial cells is required for tissue recovery. Flexible entry and exit of somatic cells into/from the quiescence state is essential for keeping cellular homeostasis and as a potential defence against injury, but this flexibility on the other hand cannot fully prevent tumourigenesis, unlike the irreversible growth arrest called senescence. [19, 20]

All the proliferating cells need to progress through the cell cycle. Cell cycle consists of four main phases (see Figure 3) and is controlled at multiple checkpoints. In mammalian cells, the primary control is maintained by conserved cyclin-dependent kinases, enzymes that exert control over proteins known as cyclins that steer the cells through the various cell cycle phases. [21-23]

After mitotic division of the parental cell in the M phase, daughter cells pass several checkpoints and enter a long G_1 phase, the maturation and vegetative stage. Once they are well established in the G_1 phase and receive a signal for further proliferation, they double the DNA content during DNA replication in the S phase. After the cellular biomass has been accumulated, the cell can progress into the G_2 phase to grow into another mitotic division. At this point, the cycle is completed. As the cells leave the M phase, they can exit the cell cycle by not entering the G_1 phase but sidestepping into the G_0 phase instead, which is considered

the quiescent state. In G_0 phase cells can fulfil their assigned role, yet they do not proliferate and the RNA content is significantly decreased. [19, 24]

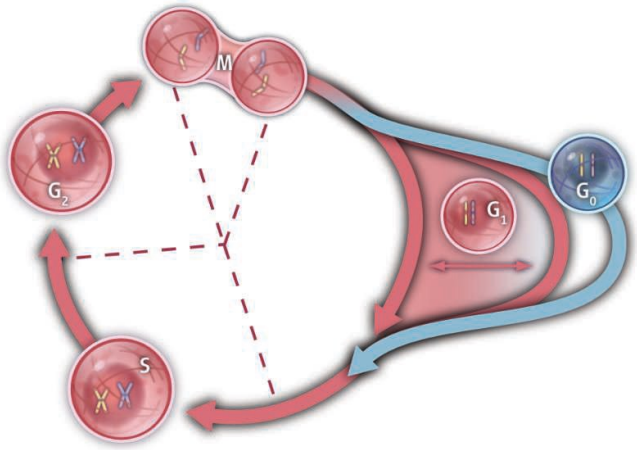

Figure 3 **Scheme of the cell cycle.** The cell division cycle is divided into a growth phase (G_1), a DNA synthesis stage (S), a waiting phase (G_2), and a mitosis (M). Cells that exit this proliferative cycle, but can re-enter later, are quiescent. Whether quiescent cells constitute a distinct state (G_0) (blue) or a continuum of G_1 (red) is debated. Adapted from [19]

Exit from quiescence is often connected with several metabolic changes including upregulation of glycolytic metabolism and mitochondrial respiratory switch referred to as the Warburg effect. This upregulates glycolysis, which is required for generation of glucose-derived biosynthetic intermediates and reducing equivalents in the form of NADPH. This is true for cancer cells, but also for the pro-growth switch of epithelial cells and endothelial cells when the process of wound healing and angiogenesis is initiated. [25, 26]

1.3 Mitochondria: the ultimate multifunctional organelles

Mitochondria are essential multifunctional organelles that contribute to multiple cellular processes, including energy production in the form of ATP, generation of physiological levels of ROS, production of essential metabolites and initiation of cell death. They dynamically react to the changes in the metabolic demand of the cell and integrate multiple metabolic pathways. Importantly, functional mitochondria are crucial in tumourigenesis [27, 28] and targeting of the mitochondrial electron transport chain (ETC) emerges as an effective strategy to suppress and eliminate cancer cells [29-31].

1.3.1 Mitochondrial structure

Mitochondria are bordered by two membranes that delineate two distinct mitochondria compartments (Figure 4): the mitochondrial matrix enclosed within the inner mitochondrial membrane (IMM) and the intermembrane space (IMS) between the IMM and the outer mitochondrial membrane (OMM). OMM forms a border between the organelle and the cytoplasm, and contains a large number of integral membrane proteins, transporters and conductance channels. These proteins mediate active transport of mitochondria-targeted proteins from cytoplasm (for example translocase of the outer mitochondrial membrane, TOM) whereas ion channels such as voltage dependent anion channel (VDAC) contribute to the equilibration of ions such as Ca^{2+}, small metabolites from the TCA cycle and ROS between the IMS and cytoplasm. Notable residents of the OMM are proteins of the regulatory Bcl-2 superfamily that act as critical life-death decision makers within the common pathway of apoptosis (see below for more details).

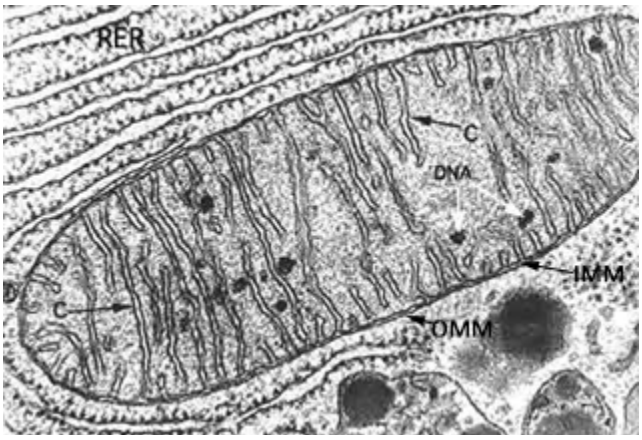

Figure 4 **Electron micrograph of a mitochondrion.** Mitochondrion is bordered by outer mitochondrial membrane (OMM). Dark black spots within mitochondrial matrix portray mtDNA. Inner mitochondrial membrane (IMM) form cristae (C). The rough endoplasmic reticulum (RER) nearby. Adapted from [32]

In contrast to OMM, which is similar to the cytoplasmic membrane, the composition of the IMM is unique. The membrane forms folds referred to as mitochondrial cristae that significantly increase its surface to provide more space for its integral membrane proteins. The IMM contains specific transporters, proteins that regulate metabolite and protein passage into and out of the mitochondrial matrix, proteins component responsible for

mitochondrial dynamics, and especially the large protein complexes of the oxidative phosphorylation (OXPHOS) machinery responsible for mitochondrial respiration.

1.3.1.1 Mitochondrial genome

Unlike other organelles of the mammalian cell, mitochondria contain their own mitochondrial DNA (mtDNA) in the mitochondrial matrix. Human mitochondrial genome consists of multiple copies of double-stranded circular DNA molecule approximately 17 kbp long. However, mitochondria are not self-supporting entities, instead they also rely heavily on imported nuclear gene products. During evolution, mtDNA has developed to carry 37 coding genes. It covers 22 tRNA genes for protein translation, two small ribosomal RNAs and 13 polypeptide subunits of respiratory complexes (seven of complex I, one of complex III, three of complex IV and two of ATP synthase). Mitochondrial DNA is not wound to histone scaffold, hence is higher than nucleic DNA vulnerable to intercalating agents. For this reason, chronical exposure of cells to low concertation of ethidium bromide will cause selective mtDNA loss. All 13 polypeptides encoded by the mtDNA are essential constituents of the enzyme complexes of the oxidative phosphorylation system and mtDNA depletion therefore results in respiratory deficiency [33, 34].

1.3.2 Essential functions of mitochondria

Mitochondria have multiple functions. They participate in the initiation and execution of apoptosis, maintain redox homeostasis, perform fatty acid metabolism, tricarboxylic and urea cycles as well as calcium utilization and signalling. Importantly, mitochondria are where the majority of ATP is produced coupled to the regeneration of NADH in the OXPHOS process (see Figure 5). Hereby, electrochemical proton gradient is generated on the IMM through the proton pumping activity of the ETC. This proton gradient then powers ATP synthase to produce ATP, but also allows delivery of cargo into the mitochondria, including ETC inhibitors linked with cations such as the triphenylphosphonium (TPP^+) group [35, 7]. In addition, ETC is in proliferating cells also important because it facilitates biosynthesis of aspartate and pyrimidine nucleotides. [36, 37]

1.3.3 Electron transport chain and ATP production

ETC is a set of reaction through which the hydrogen and electrons are transfer from reduced cofactors to atomic oxygen obtaining water and releasing energy. This is done so that the energy derived from redox reactions is released little by little without damaging the cell. Electron transport is carried out by a chain of four transmembrane macromolecular protein complexes (referred to as CI, CII, CIII and CIV) and mobile electron carriers cytochrome *c* (cyt *c*) and ubiquinone (CoQ) (Figure 5). All the enzymes further associate into supercomplex assemblies (SCs) for more efficient electron transition, control of ROS and regulation of substrate utilization [38, 39] All the components of ETC cooperate to maintain mitochondrial inner membrane potential. The chain is fuelled by reoxidation of reduced cofactors nicotine amideadenine nucleotide (NADH) by CI at flavin mononucleotide cofactor and flavin adenine dinucleotide ($FADH_2$) in CII. The cofactors may originate from TCA and urea cycle, glycolysis or catabolic oxidation of fatty acids. All the machinery is than referred to as mitochondrial respiration because the final acceptor, oxygen, is spent to form water.

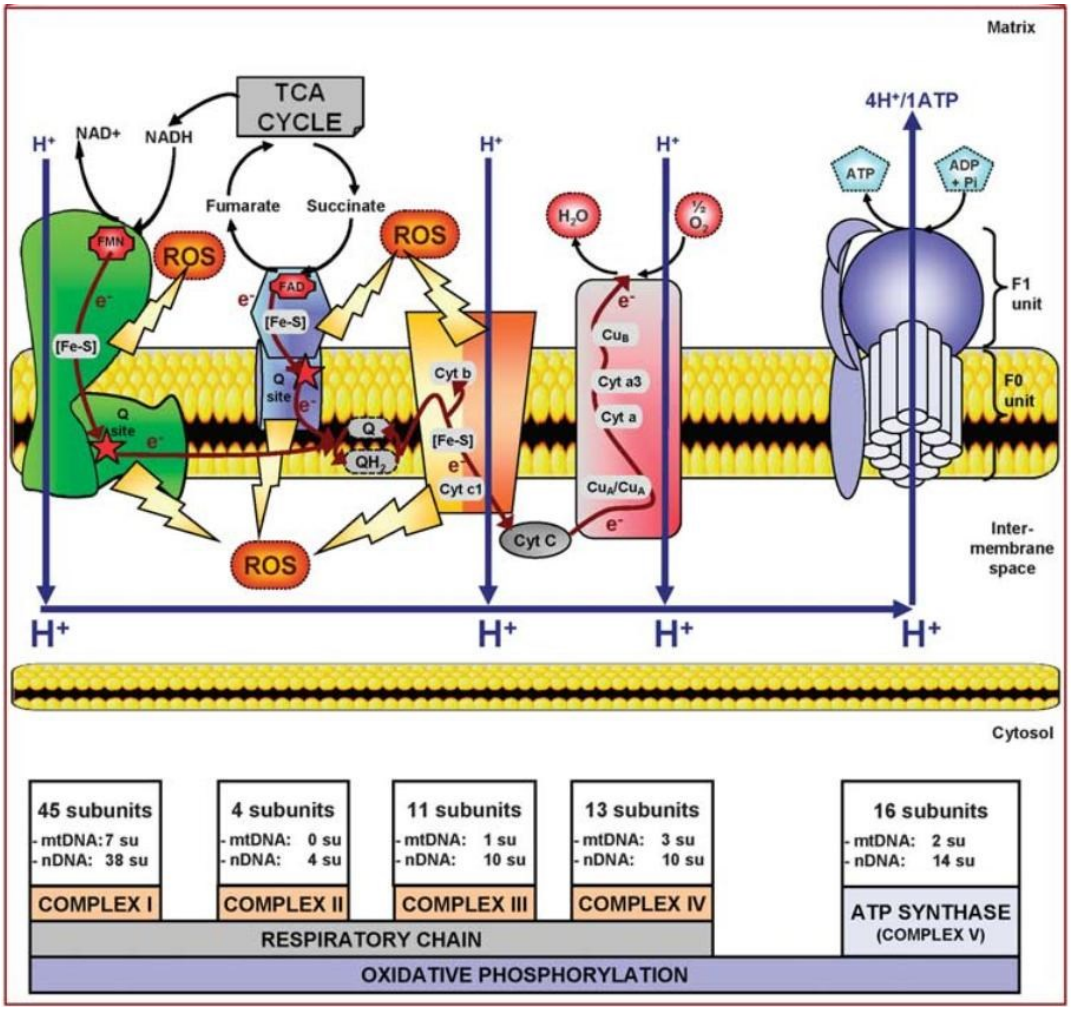

Figure 5 **Illustration of the ETC and OXPHOS**. Four complexes of ETC and the ATP synthase are schematized and the electron/proton pathways along these complexes are indicated. CI (NADH:ubiquinone oxidoreductase) receives electrons from NADH and transfers them from a flavin mononucleotide (FMN) cofactor to the eight C I-embedded iron–sulphur (Fe-S) clusters to eventually reduce ubiquinone (Q) to ubiquinol (QH_2) in the IMM. This reaction is coupled to the translocation of protons across the IMM from the matrix into the intermembrane space (IMS). CII (succinate:ubiquinone oxidoreductase) also contributes to the QH_2 pool via the transfer of electrons from succinate, a tricarboxylic acid (TCA) cycle intermediate, to the complex II-embedded cofactor FAD and then to several Fe-S clusters. QH_2 transfers its electrons to CIII (ubiquinol:cytochrome c oxidoreductase) through two heme centres (cytochromes b and c1) and one Fe-S cluster. The energy generated by the electrons carried by CIII likewise induces a translocation of protons across the IMM. Finally, CIII delivers its electrons to cytochrome c (Cyt C), which transfers them to CIV (cytochrome c oxidase). This terminal complex possesses four redox centres (two copper atoms and two cytochromes a and a3) and uses the energy generated by the electron transfer to translocate protons but also to reduce O_2 in H_2O at the matrix side. [40] All along the ETC, electron leakage can arise and lead to reactive oxygen species (ROS) formation from the main 'hotspots' of CI and CIII, but also CII, as indicated in the figure. The electron transfer is then coupled to the final complex, ATP synthase (complex V), which uses the protonmotive force created by C I, III and IV to generate ATP at the matrix side. This coupling between ETC and ATP synthesis is called oxidative phosphorylation (OXPHOS). The number of mitochondrial DNA (mtDNA)- and nuclear DNA (nDNA)-coded subunits of each complex are also indicated. Adapted from [41]

1.3.3.1 Complex I, NADH: ubiquinone oxidoreductase

Respiratory complex I (NADH: ubiquinone oxidoreductase) is complicated, multi-subunit, membrane-bound assembly of 46 identified subunits in mammals, with a combined molecular mass of 980 kDa. [42] Seven of the protein subunits are coded by mtDNA. In CI redox centre flavin mononucleotide acquire two electrons (one by one) from NADH that are further passed in multistep-redox process through seven [Fe-S] clusters to the I_Q site and used for CoQ reduction to ubiquinols ($CoQH_2$). The transport is accompanied by conformation changes and translocation of four H^+ into IMS, directly contributing to the proton gradient. [41, 43-45]

1.3.3.2 Complex II, succinate: ubiquinone oxidoreductase

Complex II (succinate: ubiquinone oxidoreductase) is the smallest complex of ETC with about 140 kDa and comprises four protein subunits all coded by nucleic DNA. [46-48] CII removes two electrons from succinate during its FAD-mediated reduction to fumarate in the TCA. These electrons are then passed to CoQ, although no protons are simultaneously translocated across IMM.

1.3.3.3 Complex III, ubiquinol: cyt c oxidoreductase

Reduced CoQ generated by CI and CII and other minor cellular dehydrogenases is then utilized by ubiquinol: cyt *c* oxidoreductase (known as CIII). CIII consists of 11 protein subunits, one coded by mtDNA, and has an approximate molecular weight of 300 MDa. Complex III apparatus utilizes four electrons and four protons (two by two) from regeneration of two $CoQH_2$ molecules that are then provided to IMM anchored cyt *c* in complicated multi-step process referred as the "Q cycle". Remaining protons and electrons are spend for re-reduction of CoQ. After the first molecule of $CoQH_2$ is oxidized at the Q_O site, proton is released into IMS while first electron is passed through bound [Fe-S] redox centre to cyt c_1 and subsequently to the electron carrier cyt *c*. Second electron is removed by the bound hem b_L centre, proceeds to b_H hem in site Q_i of CIII and is used for partial reduction of another CoQ to semiquinone. After that, second incoming electron fully reduces the semiquinone to $CoQH_2$, which is normally reoxidized again in Q_O site of CIII later. Proton

gradient is contributed to by four protons during the cycle and two more proton are spent at the matrix site of the IMM supporting the concentration gradient. [49-51]

1.3.3.4 Complex IV, cytochrome c oxidase

The terminal complex IV (cytochrome *c* oxidase) of ETC possesses four redox centres (two copper atoms Cu_A and Cu_B and two cytochromes *a* and *a3*). It uses four reduced molecules of cyt *c* to translocate two protons to IMS but also to reduce O_2 into H_2O at the matrix side. The molecular weight of CIV is 200 kDa and it consists of 13 protein subunits including three coded by mtDNA. Electron transport path starts at Cu_A in COXI subunit that removes an electron from incoming reduced cyt *c* and passes it through cyt *a* to bimetallic centre cyt *a3*/Cu_B, where the electron is used to reduce O_2. [40, 41, 52-54]

1.3.3.5 ATP synthase (Complex V)

The coupling of ATP synthesis to the energy released in the ETC is indirect. The proton-pumping complexes (CI, CIII and CIV) convert energy from a series of electron transfers into a proton electrochemical gradient across the IMM. The proton gradient is used by the ATP synthase (often referred to as CV) for synthesis of ATP. In this biosynthetic reaction, eight protons are translocated across membrane in the direction of proton gradient from IMS to the mitochondrial matrix. Translocation of protons through ATP synthase tunnel consequently spins the ATP synthase rotor (called F1-ATP synthase as opposed to F_O-ATP synthase that forms the proton tunnel) allowing for catalysed phosphorylation of three ADP molecules per the full turn of the enzyme. ATP synthase is 16-subunit (two coded by mtDNA) enzyme of 600 kDa. Its activity can be pharmacologically inhibited by variety of inhibitors, for example oligomycin, which binds the proton channel of the F_O-ATP-synthase. As a consequence, the proton gradient on IMM increases and causes ETC disturbances, oversaturation and electron leak. [55-57]

ATP synthase activity can also be pharmacologically effected by disrupting IMM proton gradient by mitochondrial protonophores FCCP (carbonyl cyanide 4-(trifluoromethoxy)-phenylhydrazone) or CCCP (carbonyl cyanide 3-chlorophenylhydrazone). These two weak acidic agents uncouple oxidative phosphorylation via a decrease in the membrane potential

of IMM [58], as its neutral and charged forms passively diffuse across the lipid bilayer and simultaneously facilitate proton transport. [59] In this way, they stimulate mitochondria respiration, but uncoupling of ETC from ATP production may result in metabolic catastrophe [60]. In addition, when mtDNA is depleted and ATP synthase function is compromised, the residual ATP synthase (minus mtDNA-encoded ATP6 and ATP8) maintains the proton gradient across IMM by hydrolysing ATP in a reverse mode.

1.3.3.6 Supramolecular structures of respiratory complexes

It has been documented that mitochondrial ETC complexes do not operates as separate entities but are mostly organized into so called supercomplexes (SCs) responsible for carrying out cellular respiration. SCs assemblies react to the needs of cellular metabolism and may also respond to substrate availability. [61] While the role of SCs in substrate channelling is controversial [62], they are important for the stability of ETC complexes and for reducing the production of ROS [63, 64]. It is now widely accepted that SCs constitute functional assemblies of respiratory complexes, which is particularly apparent for CI [65, 66]. The level of ETC organization in various subsets of cells is largely unexplored but could be associated with differences in sensitivity to ETC inhibition.

Several architectures of CI-containing SCs were recently identified. [67] The majority of CI is bound with a dimer of CIII and a single CIV in the biggest and most organized SC ($CICIII_2CIV$ also known as the respirasome) (see Figure 6). Respirasome comprises all components required in order to pass electron from NADH to O_2, and occurs in a major 'tight' and a minor 'loose' forms which may represent different stages in SCs assembly or disassembly. Lower supramolecular structures of CIII such as $CICIII_2$ and $CIII_2CIV$ were also documented. [39, 65, 67] The individual complexes form tight interactions that vary between the architectures, with CIV subunit COX7a switching contact from complex III to CI.[68] Studies also report high molecular structures of CII. CII does not have interactions with ETC complexes I, III or IV or the enzymes of the TCA cycle, but instead engages in a specific interaction with the ATP synthase. This so-called ATP synthasome consists of CV associated with adenine nucleotide translocase (ANT) [69] and CII [39, 70], but the exact nature and function of this assembly remains to be elucidated. [71] Moreover, ATP synthase often forms homo-oligomers and especially dimers that contribute to cristae maintenance in the mitochondria. [72] On the

other hand, increased cristae support SC structures in consequence of metabolic demands, IMM compositions and substrates availability. [73]

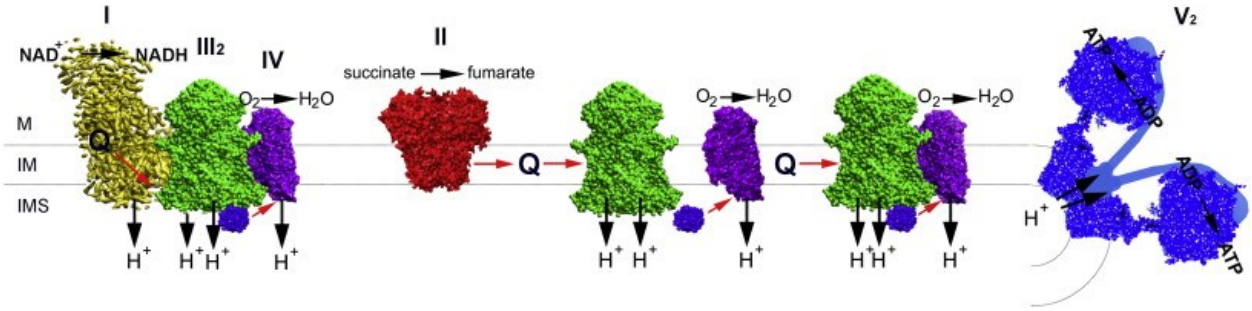

Figure 6 **Plasticity model of mitochondrial supercomplexes.** ETC in which are complexes I–IV partly organised into supercomplexes, except for complex II, which feeds electrons via ubiquinone to complex III non-bound to complex I. Red arrows show electron pathways. In yellow, the complex I, marked as I; in red the complex II, marked as II; in green the complex III_2, marked as III_2; in purple the complex IV, marked as IV; in blue the dimeric ATP synthase, marked as V_2; in violet the cytochrome c; Q, ubiquinol. The positions of the matrix (M), the intermembrane space (IMS) and cristae of inner membrane (IM) are indicated. Adapted from [74]

1.4 Reactive oxygen species generation

Mitochondrial respiratory chain contains many components that may leak electrons. Initially [75, 76], two major superoxide producing sites were identified in mitochondria (CI [77] and CIII [78]), and later also CII was described as an important source of ROS [47]. In addition, several additional sites have also been proposed as potential sources of ROS. To date, dihydrolipoamide dehydrogenase (component of α-ketoglutarate dehydrogenase and pyruvate dehydrogenase) [79, 80], electron transferring flavoprotein (ETF):Q oxidoreductase [81, 82], mitochondrial glycerol-3-phosphate dehydrogenase [83] as well as alternative NADPH oxidases or cyt P450-dependent oxygenases [84, 85] have been identified.

1.5 Inhibition of electron transport chain results in ROS generation

Substances that bind to ETC components block the electron traffic so that before the point of inhibition the electrons accumulate and leak to oxygen or nitric oxide to form ROS and reactive nitrogen oxide species (RNOS), respectively. ETC upstream of the blockade therefore becomes a source of ROS, while ROS formation downstream of the blockade is reduced due to shortage of electrons. [85-87]

Mitochondrial ETC is considered as a major source of ROS in mammalian cells. Superoxide, the ROS species most frequently formed in the ETC, is generated from CI and CII at the matrix side of IMM and from CIII at both, the matrix and IMS side of the IMM (see Figure 7). This happens particularly when the ETC is reduced, i.e. saturated with electrons. Highly saturated state can originate from a high NADH/NAD^+ ratio, a high electrochemical potential across IMM or if an obstacle in the electron flow occurs, for example in a form of an inhibition or an inherited defect. The rate and site of ROS production is also dependent on mitochondrial substrate utilization [85]. It was described that in isolated mitochondria when membrane potential is high and CoQ is highly reduced 1-2 % of oxygen is consumed to form superoxide. However, *in situ* ROS detection is difficult to perform and the percentage of oxygen diverted to ROS formation is probably lower in intact cells. Irrespective of the basal rate, inhibition of the ETC profoundly increases ROS production [88], while at the same time restricts synthesis of ATP by ATP synthase due to the lack of proton-motive force. [89, 90]

While superoxide is the major form of ROS produced by ETC, [91] the reactive oxygen species term covers all partially reduced forms of O_2 – superoxide, hydroxyl, peroxyl, alkoxyl radicals and H_2O_2. [92] Superoxide is formed from a single oxygen, but H_2O_2 is also directly generated by the ETC when electrons leak in pairs. [35, 87]

Superoxide formed in mitochondria turns spontaneously but relatively slowly to H_2O_2, although the conversion rate is greatly accelerated in the presence of mitochondrial superoxide dismutase (SOD2). [85, 86, 93] H_2O_2 than can be released from mitochondria, enzymatically scavenged by thioredoxin (TRX) or glutaredoxin (GRX) antioxidant systems or turned via Fenton reaction to form highly reactive hydroxyl radicals. [84] Superoxide can also react with nitric oxide and form RNOS either spontaneously or in an enzymatic reaction catalysed by one of the three isoforms of cellular NO-synthase. [85]

When levels of superoxide and H_2O_2 rise above scavenging capacity of mitochondrial or cytosolic defence systems, the molecular damage that they cause becomes too great for the cell to repair, triggering a range of different pathologies (ischemia and reperfusion injury, ageing or tumourigenesis). Superoxide and H_2O_2 are also powerful signalling molecules

involved in the regulation of a variety of biological processes such as programmed cell death or autophagy. [84]

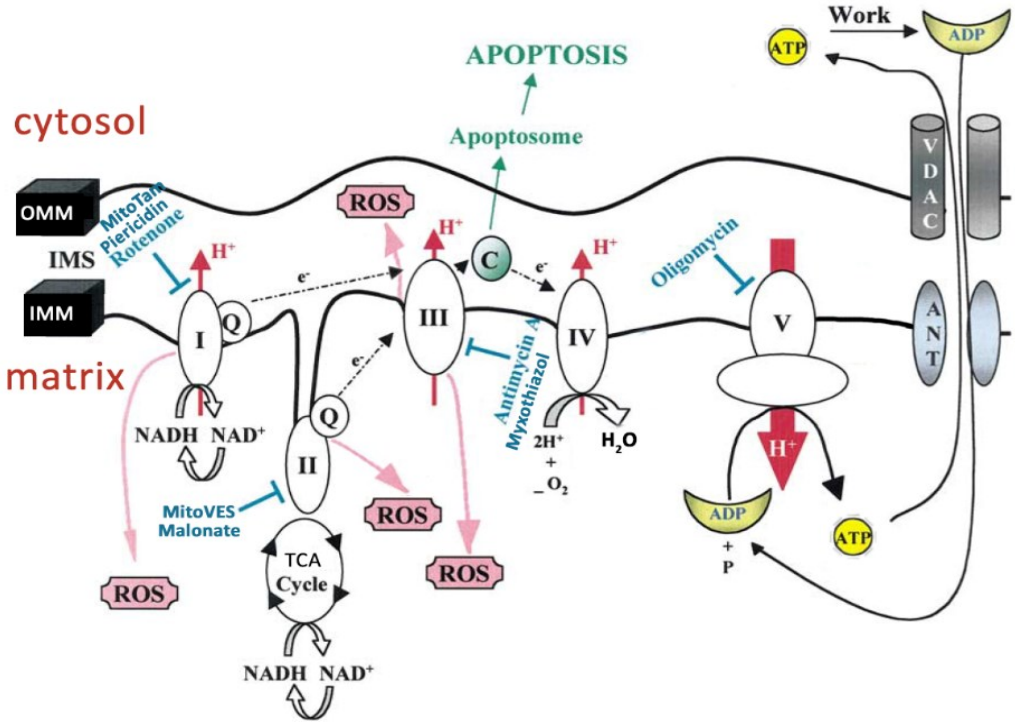

Figure 7 **Electron transport chain with sites of ATP generation and ROS production.** Complexes (I–IV) of the ETC in the inner membrane (IMM) of the mitochondria. Complexes I and II are where electrons enter this chain, via coenzyme Q (Q). Cytochrome c (C) transfers those electrons from complex III to complex IV. On acceptance of an electron, complex IV converts H^+ and O_2 to water. Except for complex II, complexes from I to IV pump protons out of the matrix to the intermembrane space (IMS) to be used by complex V (ATP synthase) to convert ADP into ATP. ATP is then released into the cytosol via the adenine nucleotide transporter (ANT) and the voltage-dependent anion channel (VDAC). Once cytosolic, ATP is converted to ADP during ATP-dependent processes in the cell and re-enters the mitochondrial matrix. ROS that are produced by this process are indicated. Several respiratory inhibitors are represented in blue. Adapted from [94]

The term oxidative stress describes a situation when production rate of ROS and RNOS overcomes the capacity of antioxidant protection. The excess of free radicals then initiates oxidative reactions of proteins, lipids, carbohydrates and nucleic acid resulting in irreversible cellular damage. [91]

1.5.1 ROS production at Complex I

CI is a significant source of ROS, that can be produced when CI functions in both forward and reverse direction (Figure 8). Inhibitors that compete for binding of CoQ (for example rotenone or piericidin A) either promote or inhibit ROS production at CI, depending on whether ROS are produced during the forward or reverse activity of CI. [88, 95]

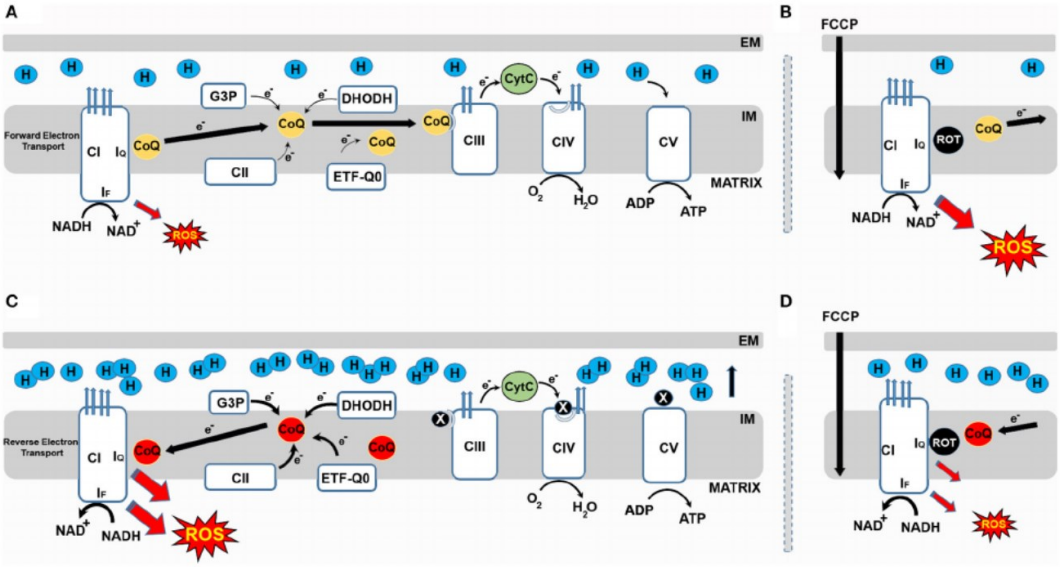

Figure 8 **Respiratory CI produces ROS in both forward and reverse direction**. **(A)** During forward electron transfer (FET), CoQ receives electrons from CI and CII, dihydroorotate dehydrogenase (DHODH), glycerol 3-phosphate dehydrogenase (G3P) and electron-transfer flavoprotein:ubiquinone oxidoreductase (ETF-QO). During this process electrons mainly leak to produce superoxide from the I_F site of CI during the oxidation of NADH to NAD^+. **(B)** In these conditions, if rotenone blocks the I_Q site, electrons cannot be transferred to CoQ, leak and generate ROS. FCCP also increases ROS generation during FET. **(C)** When the CoQ pool becomes over-reduced, a high membrane potential favours the reverse transfer of electrons from ubiquinol to CI in a process called reverse electron transport (RET). During RET electrons leak at either I_F or I_Q generating a significant amount of superoxide. **(D)** Blocking the I_Q site with rotenone during RET prevents CoQ from transferring electrons back to CI and reduces ROS production. Similarly, FCCP reduces ROS by dissipating membrane potential. Taken from [96]

During forward electron transfer, CoQ receives electrons from complexes I and II and several other sources. Electrons mainly leak to produce superoxide from the I_F site of CI during the oxidation of NADH to NAD^+. If rotenone blocks the I_Q site, electrons cannot be transferred to CoQ, electron leak is increased and more ROS are generated at the I_F site. Uncouplers as FCCP also increases ROS generation in this manner. However, when the CoQ pool becomes over-reduced (for example by ETC blockage downstream), a high membrane potential favours the reverse transfer of electrons from $CoQH_2$ to CI in a process called

reverse electron transport. During reverse transport, electrons leak at either I_F or I_Q generating a significant amount of superoxide. Nevertheless, blocking the I_Q site with rotenone during reverse electron flow prevents CoQ from transferring electrons back to CI and reduces ROS production. Similarly, FCCP reduces ROS by dissipating membrane potential and promoting oxidation of CoQ by CIII. [96, 97] In summary, CI produces large amounts of superoxide radicals by two mechanisms: forward, when the matrix NADH/NAD^+ ratio is high, leading to a reduced FMN site, and reverse, when electron donation to the CoQ pool (usually via CII) is coupled with a high membrane potential. [84, 98, 99] Nevertheless, there is agreement that superoxide from CI is generated exclusively on the matrix side of the mitochondrial inner membrane [100, 101], in flavin site I_F or at the CoQ binding site I_Q. [102]

1.5.2 ROS production at Complex II

CII has recently also been recognised as a significant source of ROS (Figure 9) [103]. CII generates ROS in both the forward reaction, from succinate, and the reverse reaction, from the reduced ubiquinone pool. [104] ROS production in the reverse reaction is prevented by inhibition of CII at either the ubiquinone-binding site (by atpenin A5) or at the flavin site (by malonate), whereas ROS production in the forward reaction is prevented by malonate but not by atpenin A5, showing that the ROS arise mainly from the flavin site (site II_F). Superoxide radicals can be produced when the binding site for CoQ is inhibited, for example by MitoVES, but also after reverse electron flow originating from CIII inhibition [47, 105]. ROS producing behaviour is determined by the occupancy and reduction state of the flavin site and is inhibited when succinate concentration is high. [47]

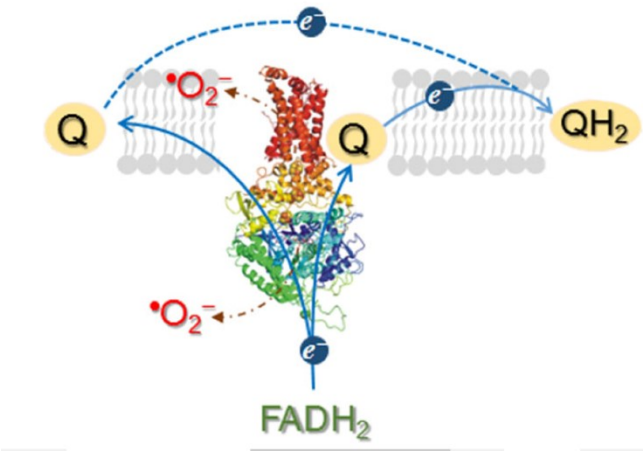

Figure 9 **Schematic of the mechanism of ROS generation mediated by Complex II in the mitochondria.** Blue arrows show the path of electron transport from FADH2 to O_2, or reverse electron flow from $FADH_2$-linked succinate to complex I via Q. Brown dashed arrows indicate the sites mediating ROS (presented as $^{\bullet}O_2^-$) generation. Adapted from [106]

1.5.3 ROS production at Complex III

Within CIII, each of the electron transferring components (FMN, Fe–S centres and ubiquinone) has been proposed [107] to be the major superoxide-producing site by different research groups [108-111]. CIII can produce large amounts of ROS from reaction of oxygen with semi-reduced CoQ bound to the Q_o site [107]. Nevertheless, production of ROS by CIII is normally low, but rapidly increases when the Q_I site is inhibited for example by antimycin. Myxothiazol, inhibitor of Q_o site of CIII supresses this effect. However, myxothiazol can also induce superoxide production at centre Q_o when the CoQ pool is highly reduced, albeit at smaller rates than antimycin [112-114]. Both inhibitors, antimycin A and myxothiazol, strongly effect the Q-cycle (see Figure 10) [115, 116]. Antimycin prevents the formation of the relatively stable semiubiquinon. In the presence of this inhibitor, an additional reduction of the b cytochromes occurs. This paradoxical oxidant-induced reduction occurs because $CoQH_2$ bound at the Q_o site can now transfer an electron downstream and the resulting $Q^{\bullet-}$ can transfer a further electron to any b haems not previously reduced forming unstable semi-reduced state. Myxothiazol blocks events at Q_o site causing upstream ETC oversaturation. [116, 117] Another compound suggested to partially inhibit CIII as a side effect is phenethyl isothiocyanate (PEITC). Thought PEITC primarily depletes glutathione via inhibition of GPXs, it was also proposed to interact with CIII [118]. Both effects may result in massive ROS production. [119]

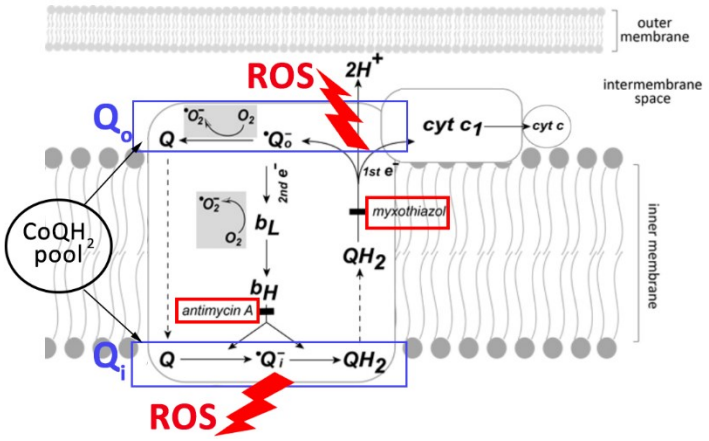

Figure 10 **Superoxide generation mediated by the Q-cycle mechanism in complex III.** Blockade of site Qi by antimycin A promotes ROS production from site Q_o to both sides of the inner membrane. Myxothiazol potently inhibits site Q_o. Adapted from [106]

Q_o is located in the hydrophobic domain on the cytosolic side of the membrane, leading to the prediction that superoxide from this site is most likely to be released to the intermembrane space [120, 121]. Superoxide production from complex III in the presence of antimycin was originally detected on the matrix side (in sub-mitochondrial particles [122]), but also on the cytosolic side of the membrane [100, 123 124] ROS produced by CIII are therefore released to both sides of the IMM. [100, 125]

1.5.4 Complex IV participation in ROS production

Complex IV has not been reported to participate in ROS production, notwithstanding its two-step reduction of molecule of oxygen. Thus CIV seems to be very efficient in preventing premature electron escape [84]. However, inhibition of specific sites in downstream ETC can result in ROS generation from the upstream complexes. For example, when CIII is inhibited it increases ROS generation from CI and CII, and this is the case for CIV as well [78].

1.5.5 ROS production resulting from ATP synthase inhibition

Inhibitors of ATP synthase as oligomycin and its derivatives induce ROS as a secondary effect on the ETC. Once the ATP synthase is blocked, the membrane potential is not utilized for ATP production and increases, which leads to higher ROS production from the ETC complexes and consequently to cell death. [126] However, interference with ATP production can block entry into apoptosis as a consequence of ATP depletion, since apoptosis is ATP-dependent [127, 128].

1.6 Antioxidant defence

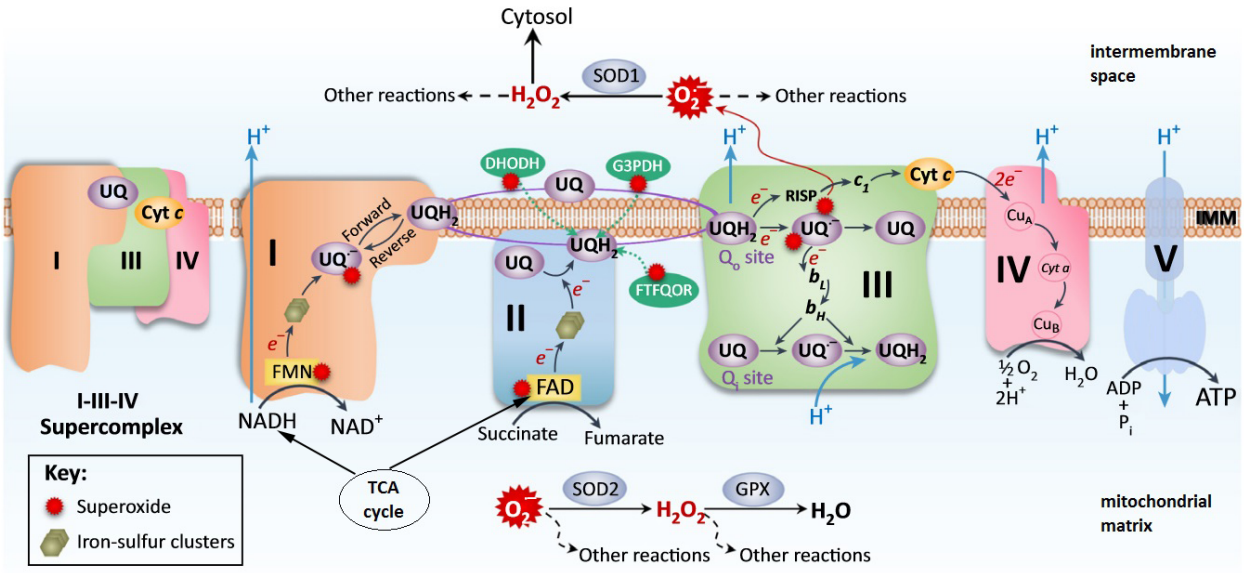

Figure 11 **Simplified illustration of ROS generation sites within ETC in the mitochondria.** As electrons are transported (grey arrows show the path of electron transport from NADH or $FADH_2$ to O_2), they may leak to oxygen, forming superoxide ($O_2^{\cdot-}$). Red stars indicate potential sources of $O_2^{\cdot-}$ production. Superoxide dismutase (SOD) converts $O_2^{\cdot-}$ to H_2O_2)that is reduced to water by glutathione peroxidase (GPX). Both $O_2^{\cdot-}$ and H_2O_2 have been implied in modulating the function of signal transduction pathways ('other reactions' in the figure). UQ also accepts electrons from several non-RC dehydrogenases, including the mitochondrial glycerol-3-phosphate dehydrogenase (G3PDH), dihydroorotate dehydrogenase (DHODH), and electron transfer flavoprotein oxidoreductase (ETFQOQ) . Uphill electron transfer from UQH_2 to NAD+ through complex I is known as reverse electron transport. The I-III-IV supercomplex, which is the most active supramolecular form, is schematically shown on the left of the figure. Black circles show TCA cycle that generates NADH and $FADH_2$ as substrates of electron transport chain and blue arrow represent the proton transport. Rieske iron-sulfur protein (RISP). Adapted from [129]

In addition to the central role in cellular bioenergetics, mitochondria are major producers of ROS, especially when specific ETC inhibitors are used. Under physiological conditions, ROS act as second messengers participating in regulation of various cellular

functions. Their levels in cells therefore need to be tightly controlled and excessive ROS needs to be effectively scavenged to protect the cell from oxidative damage. This is ensured by the antioxidant systems that significantly expedite inactivation of reactive radicals.

Mitochondrial and cytosolic scavenging of superoxide and H_2O_2 are very powerful and regulate the levels of superoxide and H_2O_2 in the mitochondrial matrix and the cytosol and other cellular compartments (see Figure 12). However, they allow small changes in production or consumption to alter steady-state levels of superoxide and H_2O_2 in each compartment to initiate different cellular signalling pathways. [130]

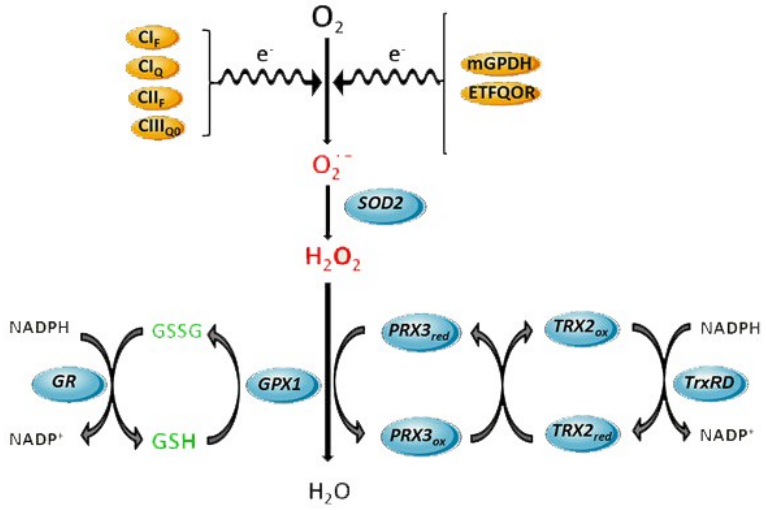

Figure 12 **Mitochondrial ROS generation and antioxidant defence systems**. Complex I flavin site (CI_F), Complex I ubiquinone site (CI_Q), Complex II flavin site (CII_F), and Complex $IIIQ_o$ ($CIII_{Q0}$) are sites of the ETC components shown to generate superoxide anion. Other sources of superoxide can be enzymatic reactions that transfer electrons to the ETC such as mitochondrial glycerol 3-phosphate dehydrogenase (mGPDH), and the last step of β-oxidation, electron-transferring flavoprotein ubiquinone oxidoreductase (ETFQOR). Superoxide generated in the mitochondrial matrix by these sites is dismutated to hydrogen peroxide by SOD2. Hydrogen peroxide is further inactivated using the reducing equivalents of NADPH by mGSH/GPX or PRX3/TRX2 antioxidant systems, yielding water. Mn-dependent superoxide dismutase 2 (SOD2), GSH peroxidase (GPX1), GSSG-reductase (GR), peroxiredoxin 3 (PRX3), thioredoxin-2 (TRX2), thioredoxin reductase (TrxRD). Adapted from [130]

1.6.1 Central role of superoxide dismutases

Reactive oxygen species are scavenged at several levels. First in the antioxidant cascade and one of the most important antioxidant enzymes is superoxide dismutases (SOD). This enzyme catalyses the dismutation (disproportionation) of superoxide anion radical to H_2O_2 and oxygen, which is then utilized by next-step antioxidant systems. In doing so, it protects cells from oxidative damage and regulates the cellular concentration of superoxide radicals and its reactive progeny under both physiological and pathological conditions. [131] Up to date, three different isoforms of the SOD were described: mitochondrial MnSOD (SOD2), that resides in the mitochondrial matrix, cytosolic and lysosomal CuZnSOD (SOD1) and extracellular SOD3 [84]. To control ETC-derived superoxide, mitochondria are equipped with high levels of SOD2. The role of SOD2 in physiology is complex and its gene is regulated by epigenetics and stress response transcription factors (under the regulation of one of the most important stress-responding transcriptional factor FOXO3 [132]). [133] Nevertheless, further research is required to understand the post-translational modifications that regulate SOD2 activity in cancer cells. Moreover, SOD2 influences the activity of transcription factors (such as HIF-1α, AP-1, NF-κB and p53) and affects DNA stability, overexpressed SOD2 in MCF-7 breast cancer cells results in decreased invasiveness [134]. [135, 136]

The H_2O_2 produced from superoxide in mitochondria by SOD2 is then decomposed to water by mitochondria-specific glutathione peroxidases (GPX) [137, 138], as well as by peroxiredoxins (PRX) [139] in the thioredoxin system [140-142], while catalase in peroxisomes may inactivate the remaining H_2O_2 that escapes from mitochondria [143, 144].

1.6.2 Glutathione redox cycling

The primary cellular enzymatic defence systems against H_2O_2 are the glutathione (GSH) redox cycle and catalase (catalases is discussed below). GSH is a cofactor for GPX, which converts H_2O_2 to H_2O at the expense of oxidizing GSH to its disulphide form (GSSG). Glutathione reductase (GSR) regenerates GSH from GSSG, using reducing equivalents from NADPH. The glutathione redox cycle exists in both, the cytosol and mitochondrial compartments of the cell. [145]

Similarly to GPXs, GRXs also utilize the reducing power of glutathione to catalyse disulphide reductions in the presence of NADPH and GSR (the glutaredoxin system).

1.6.2.1 Ubiquitous glutathione

The major intracellular thiol compound glutathione provides strongly reducing thiolic group to maintain the redox balance. Once it is oxidized it binds through disulphide bridge with other molecule of GSH to form oxidized dimeric GSSG. The ratio of GSH/GSSG, high under normal conditions, reflects redox stress inside the cell. Hence the decrease is often connected with unbalanced ROS production and/or ongoing cell apoptotic pathway [146]. Glutathione is distributed in mitochondria, cytosol, nuclei and endoplasmic reticulum. The compartmentations effects its ability to detoxify ROS and scavenge oxidised targets [147]. Mitochondrial GSH is kept in the membranes bound to membrane transporters or in IMS by interactions with Bcl-2 family proteins. Mitochondrial GSH could comprise up to 30 % of all available glutathione and is important to maintenance of mitochondrial lipids and proteins integrity [148]. It was found, that GSH concentration varies in the nuclei and cytosol based on the proliferative status of the cell. It is equally distributed between the two compartments when cell are confluent, but profoundly increases in cytosol during proliferation [149].

1.6.2.2 Glutaredoxins

Glutaredoxins (GRX) operate as dithiol reductants and are involved as alternative pathways in multiple cellular functions. They participate in such processes as formation of deoxyribonucleotides for DNA synthesis, generation of reduced sulphur, signal transduction, and most notably in defence against oxidative stress. [150] GRXs are dependent on the number of active site cysteine residues. Oxidised GRXs are reduced by GSH, and conduct similar functions as the thioredoxin system discussed below. They participate in the regulation of proliferation and differentiation as well as in apoptosis by inhibiting caspase activation and cyt *c* release from mitochondria and levels of H_2O_2 via some peroxiredoxins. [151]

1.6.2.3 Glutathione peroxidases

Detoxifying of H_2O_2 from the cell by glutathione is tightly linked to glutathione-dependent glutathione peroxidases (GPX). These enzymes were shown to catalyse the reduction of H_2O_2 and diverse alkyl hydroperoxides to water or the corresponding alcohol. Once oxidized, GPXs are regenerated to their reduced form by reduced glutathione (GSH). GPXs have been shown to constitute a small multigenic family of eight isoforms in mammals

[152]. Most human GPX contain a Se-Cys residue at its active site. [153] Homotetrameric GPX1 and monomeric GPX4 are the most abundant forms in the mitochondria. While GPX1 is dominant in prevention of oxidative damages, GPX4 has importance in the repair of oxidized membrane lipids [143]. [153]

1.6.2.4 Glutathione reductase

To recover GSH from GSSG, cells employ glutathione reductase, a glutathione recycling enzyme that regenerates glutathione using the NADPH.[154, 155] pool. Glutathione reductase is responsible for the maintenance of GSH/GSSG balance, and consists of a single isoform found throughout the cell.

1.6.3 Thioredoxin system

Together with the glutathione system closely collaborates thioredoxin system that controls the cellular redox environment and can regulate the activity of many redox-sensitive transcription factors as well. [156] Mammalian thioredoxin and glutathione systems have been found to be able to interchange electrons and to serve as a backup system for each other. Thioredoxin system is composed of thioredoxin (TRX) and NADPH-dependent thioredoxin reductases (TRXR). The redox balance of reduced and oxidized thioredoxins (TRX–SH/TRX–SS) is maintained through the activity of TRXR selenoenzymes. [157]

Thioredoxins are ubiquitous small proteins with two cysteine redox active sites for detoxifying ROS. TRX is compartmented into the cytosol (TRX1) which relocates to the nucleus in response to oxidative stress. The mitochondrial redox balance is maintained by the mitochondrial TRX2. [18] On encountering oxidised proteins, TRXs are oxidised to a disulphide form which is then recovered by TRXR, which are also compartmentalised with TRX2 being the specific mitochondrial form (TRXR2). Importantly, TRXs are able to regenerate thiol-dependent peroxidases (peroxiredoxins) which can remove reactive oxygen and nitrogen species at a fast rate [158].

TRXs are also involved in DNA and protein repair, play critical roles in the immune response and cell death via interaction with thioredoxin-interacting protein. TRXs are also essential to sustain other antioxidant protein components. The most prominent TRX-dependent system are mitochondrially localized PRX3 and PRX5 [159]. PRX3 was

described as one of the most abundant mitochondrial proteins and directly inactivates H_2O_2, PRX5 preserve mitochondrial membranes against oxidative damage as it eliminates membrane lipids and proteins damage caused by peroxides [160].

1.6.4 Catalases

For a long time, GPXs were considered the principal antioxidant enzyme responsible for the detoxification of H_2O_2, because catalase has much lower affinity for H_2O_2 than GPX. However, catalase has been found to play a major role in survival. Loss of catalase activity leads to cell death by means of autophagy that involves ROS. [161] Catalase was described as the major site for metabolic branching of H_2O_2 via different antioxidant routes, since it converts H_2O_2 four times faster than GPXs and likewise has one of the highest turnover numbers of all enzymes. [162] However, catalase reactivity is limited by its structural compartmentation in peroxisomes. Catalase is absent in mitochondria of mammalian cells, [163] although it was found in rat heart mitochondria [164]. Importantly, catalase, as opposed to other H_2O_2 converting enzymes, is independent of NADPH. [165]

1.7 Oxidative stress mediated apoptosis

Oxidative stress initiates apoptosis (discussed in the next section, see Figure 13 and Figure 16) by activation MAP Kinases (mitogen–activated protein kinases), JNK or p38–MAPK. Signalling kinase complexes with bound TRX or GRX respond to slight changes in cellular redox balance, for example ratio of GSH/GSSH, and serve as redox switch of apoptotic protein expression or mitochondrial membrane pore opening, an event irreversibly leading to apoptosis [166-168].

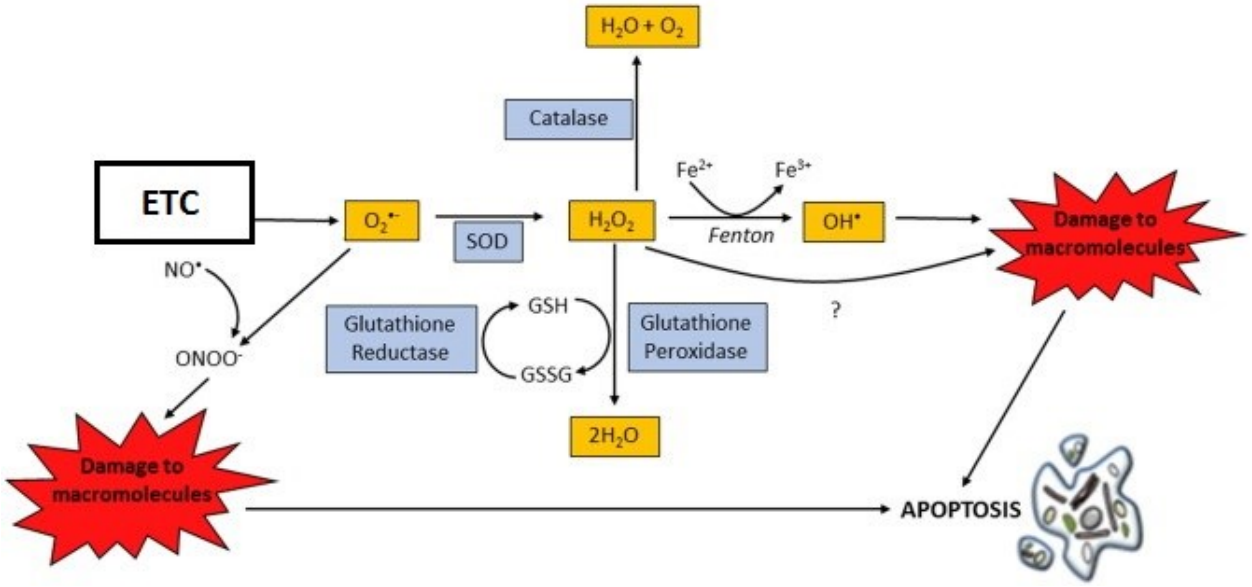

Figure 13 **Oxidative stress of ROS cause cellular damage and apoptosis**. Electron leaks attributed to ETC blockage react rapidly with oxygen to produce superoxide ($O_2^{\bullet -}$), which either reacts with nitric oxide ($NO^{\bullet}$) to produce peroxynitrite ($ONOO^-$), or undergoes dismutation to generate H_2O_2, catalysed by SOD. H_2O_2 can be either detoxified by antioxidants such as catalase and GSH/glutathione peroxidase, or can generate $OH^{\bullet}$ by the metal-catalysed Fenton reaction. $OH^{\bullet}$ and $ONOO^-$ cause damage to cellular proteins, lipids and nucleic acids, which can lead to demise of the cell by apoptosis. Adapted from [169]

1.8 Cell death

Once the cell is defective, going through metabolic stress, irreversible cellular injury from physical/chemical/biological insults or lack of nutrients and growth signals it is being eliminated to maintain organismal homeostasis. Cell death can be either necrotic (passive and unregulated) or apoptotic, i.e. an actively mediated cell suicide process. Regulated cell death is involved in two diametrically opposed scenarios. On the one hand, it may occur in the absence of any exogenous environmental perturbation, hence operating as a built-in effector of physiological programs of development or tissue turnover [170]. On the other hand, it can originate from perturbations of the intracellular or extracellular microenvironment, when such perturbations are too intense or prolonged for adaptive responses to cope with stress and restore cellular homeostasis. [171]

A new nomenclature of cell death was proposed based on the molecular mechanism. Compared to classification from 2009 [172] that describe apoptosis, autophagic cell death, necrosis, cornification and atypical cell death modalities (mitotic catastrophe, anoikis, excitotoxicity, Wallerian degeneration, paraptosis, pyronecrosis, entosis) a variety of new cell death modes were defined and the classification was changed.

Cell death manifests with macroscopic morphological alterations.

Type I cell death or apoptosis, exhibiting cytoplasmic shrinkage, chromatin condensation, nuclear fragmentation, and plasma membrane blebbing, culminating with the formation of apparently intact small vesicles that are efficiently taken up by neighbouring cells with phagocytic activity and degraded within lysosomes;

Type II cell death or autophagy, manifesting with extensive cytoplasmic vacuolization and similarly culminating with phagocytic uptake and consequent lysosomal degradation;

Type III cell death or necrosis, displaying no distinctive features of type I or II cell death and terminating with the disposal of cell corpses in the absence of obvious phagocytic and lysosomal involvement.[173]

Following picture (Figure 14) illustrates recent major cell death modes nomenclature centred on molecular and essential aspects of the process. It present apoptotic and necrotic morphology, although in some modes of cell death molecular mechanisms exhibit considerable overlap.

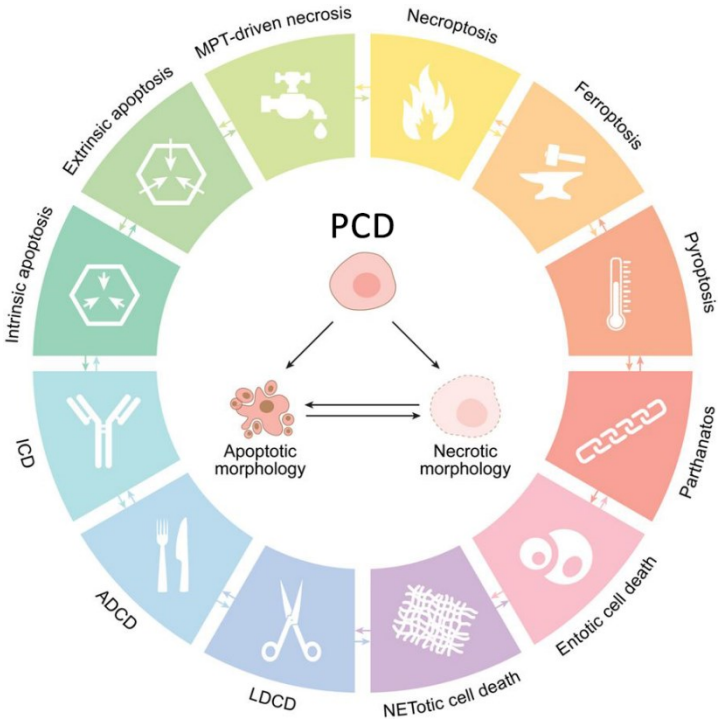

Figure 14 **Major cell death subroutines**. Mammalian cells exposed to unrecoverable perturbations of the intracellular or extracellular microenvironment can activate one of many signal transduction cascades ultimately leading to their demise. Each of such programmed cell death (PCD) modes is initiated and propagated by molecular mechanisms that exhibit a considerable degree of interconnectivity. Moreover, each type of RCD can manifest with an entire spectrum of morphological features ranging from fully necrotic to fully apoptotic, and an immunomodulatory profile ranging from anti-inflammatory and tolerogenic to pro-inflammatory and immunogenic. ADCD: autophagy-dependent cell death, ICD: immunogenic cell death, LDCD: lysosome-dependent cell death, MPT: mitochondrial permeability transition. Adapted from [173]

However, Liu claims [174] that there are only four basic modes of cell death i.e. apoptosis and senescent death, as well as two pathological modes, i.e. necrosis and stress-induced cell death, although there are many ad-hoc variants adapted to different situations.

1.8.1 Programmed cell death modes

Two distinct pathways of programmed cell death are present in the cell. Extrinsic programmed cell death is a specific variant of cell death initiated by perturbations of the extracellular microenvironment detected by plasma membrane receptors. After plasma membrane receptors oligomerization executive caspases are activated directly by receptor domain. In contrast, intrinsic programmed cell death is initiated by perturbations of the extra-cellular or intracellular microenvironment and is characterised by mitochondrial OMM perforation and downstream activation of executioner caspases by apoptotic complex. In this

process mitochondria take the main role. Intrinsic programmed cell death activation may result in markedly caspase-dependent apoptosis or for example in necroptosis - triggered by perturbations of cellular homeostasis (by ROS or rapid depletion of cellular ATP) detected by specific death receptors. Necroptosis has several distinctive characteristics from other types of cell death (apoptosis) and it is a process that critically depends on pseudokinase mixed lineage kinase domain-like (MLKL) and receptor-interacting protein kinases (RIPK3, RIPK1). [175] Moreover, programmed cell death can manifest as anoikis – initiated by the loss of integrin-dependent anchorage or ferroptosis –resulting from intracellular oxidative perturbations under constitutive control by GPX4 and inhibited by iron chelators and lipophilic antioxidants. [173] However, in this dissertation, only intrinsic programmed cell death of apoptosis or necroptosis will be considered.

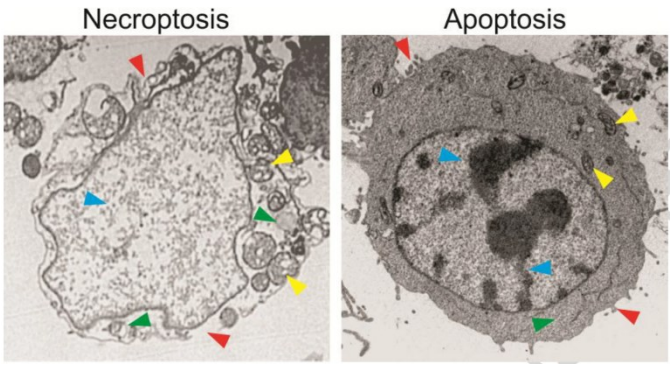

Figure 15 **Necroptosis has several distinctive characteristics compared to other types of cell death, in particular, apoptosis**. Necroptotic cells share several morphological features of necrosis, including early loss of plasma membrane integrity, translucent cytosol, and swelling mitochondria (green arrowheads). In contrast, apoptotic cells lack these features, and are characterised by cell shrinkage, plasma membrane blebbing (red arrowheads), and condensed and fragmented nuclei and organelles (blue arrowheads). Adapted from [176]

Concerning autophagic cell death, basal autophagy is a process that serves to degrade aged and defective cellular organelles and macromolecules for reprocessing, but can also be activated under stress conditions as a mean to provide bioenergetic intermediates and recycle damaged components [177]. This process involves a set of highly conserved autophagy genes (ATGs) and proteins such as LC3B (microtubule-associated protein) that are required for the formation, elongation and maturation of autophagosomes, specialized vesicles that contain proteins and organelles attached to specialized cargo adaptors and deliver them to lysosomes for degradation. Autophagy is regulated by canonical mTOR pathway but it can be

also directly induced by ROS via autophagy-related protein 4 Homolog B (ATG4B) [178] and by NADH redox balance [179]. Autophagy usually plays a protective role, but in excessive stress conditions may also result in cell death referred to as autosis.

The impairment of programmed cell death is a characteristic of many cancers and is recognized as a cancer hallmark. Cell death can be independent of executive proteases (caspases). [172] The most common is apoptotic and necroptotic cell death (both with specific morphological features as shown in Figure 15). At the biochemical level, necroptotic cells show marked depletion of cellular ATP and leakage of intracellular contents, in contrast to apoptosis, which is a more energy-consuming process requiring a relatively higher level of cellular ATP. At the molecular level, necroptosis is caspase-independent and signals through RIP1, RIP3 and MLKL, while apoptosis requires caspase activation and is mediated by interplays of the Bcl-2 family proteins or activation of death receptors. Another key feature of necroptosis is that permeabilization of plasma membrane can lead to release of so-called "Damage Associated Molecular Patterns (DAMPs)", such as high-mobility group box 1 (HMGB1) protein and mtDNA [180], which can trigger a robust immune response and inflammation [176, 181]. [182] Caspase-independent cell death clearly shares similarities to apoptosis (namely mitochondrial permeabilization) but is distinct morphologically, biochemically and kinetically. [183] Dying cells are engaged in a process that is reversible until a first irreversible phase or 'point-of-no-return' is passed. It has been proposed that this step could be represented by massive caspase activation, [184] loss of mitochondrial potential, [185] complete permeabilization of the OMM [186] or exposure of phosphatidylserine residues that emit 'eat me' signals for phagocytosis. [187]

Apoptotic machinery is composed of downstream effectors component and upstream regulators. The regulators could belong either to the extrinsic pathway of apoptosis, involving for example Fas receptor/Fas ligand, TNF–1 receptor/TNFα ligand or Trail cascade, or to the intrinsic pathway that is executed by mitochondria and is induced by variety of signals such as oxidative stress, mitochondrial or nuclear DNA damage or lack of growth factors. [188]

One of the most commonly used tool to initiate apoptosis is a protein kinase inhibitor staurosporin, although its molecular mechanism of action is very complex and still

controversial [189]. As it was documented that staurosporin initiates oxidative stress [190] but this is not responsible for the staurosporin-induced apoptosis [191].

1.8.1.1 Programmed cell death regulation by the Bcl-2 protein superfamily

The intrinsic pathway of apoptosis is regulated by the Bcl-2 protein superfamily (see Figure 16). The physical interactions between members of this family are critical for determination of the cell fate.

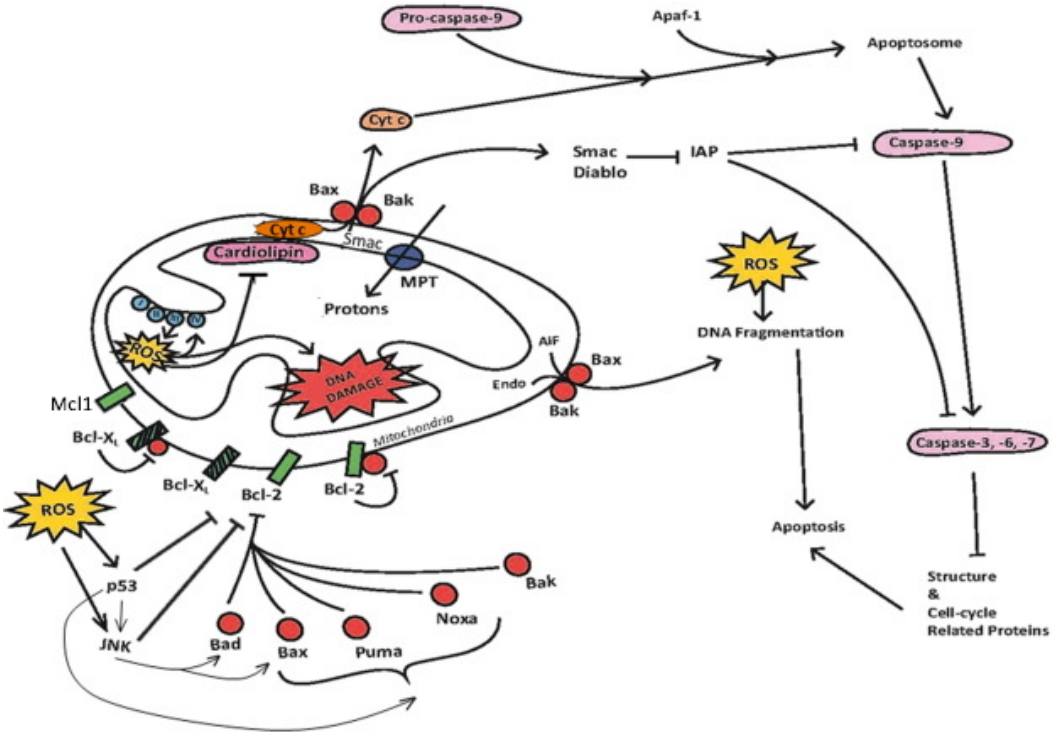

Figure 16 **Activation of the mitochondrial (intrinsic) pathway of apoptosis by ROS is under control of pro- and anti-apoptotic Bcl-2 superfamily proteins.** ROS generated exogenously or endogenously can activate p53 and/or c-Jun N-terminal kinase (JNK), which activate pro-apoptotic Bcl-2 proteins (red circles) that can inhibit the functions of anti-apoptotic proteins (green oblongs). ROS cause oxidation of cardiolipin, which relinquishes cytochrome c (Cyt c), allowing its release into the cytosol. Moreover, ROS cause mitochondrial membrane depolarisation and/or opening of Bax/Bak channels on the OMM, which allows release of AIF, Endo G, cytochrome c and Smac/Diablo into the cytosol. Cyt c then forms the apoptosome complex in the cytosol together with Apaf-1 and procaspase-9, leading to caspase-9 activation. Caspase-9 then activates effector caspases such as caspase-3, resulting in cleavage of cellular proteins and cell demise by apoptosis. AIF and Endo G translocate to the nucleus and appear to be involved in DNA fragmentation. ROS can directly cause damage to nuclear and mitochondrial DNA. Adapted from [169]

The pro-survival members of the family - Bcl-2 itself and its close relatives such as Bcl-xL, Bcl-w and Mcl1 - prevent apoptosis by sequestering pro-apoptotic members of Bcl-2 protein superfamily, such as Bax and Bak. However, damage or stress signals flip on the switch for apoptosis by activating the BH3-only proteins that act to initiate apoptosis, in large part by neutralizing the pro-survival Bcl-2 proteins. When balance of pro- and anti-apoptotic proteins is disturbed, BAK and BAX proteins disrupt OMM integrity by creating large pores that release pro-apoptotic factors into the cytoplasm. Thus, the Bcl-2 family of proteins act as a critical life-death decision point within the common pathway of apoptosis. The interplay of the different Bcl-2 protein members, Ca^{2+} ions with cooperation with other transmembrane proteins especially VDAC in OMM, ANT transporter in IMM, hexokinase, creatinkinase as well as ATP synthase dimers [192-194] is thus of a great importance for inducing the apoptotic permeabilisation of OMM to trigger the release cyt *c* from IMS into the cytosol.

After the release of pro-apoptotic factors into the cytoplasm, cyt *c* activates ATP-dependent assembly of a protein complex named apoptosom. Apoptosom is formed allosterically by seven Apaf-1 molecules that consequently bind and splice caspase 9 (Figure 17). Caspase 9 activation initiates activation of the caspase cascade. [195] Both, extrinsic and intrinsic apoptotic, pathways culminates in cleavage of initiator caspases, such as caspases 8 or 9, which further activates executioner caspases, especially caspase 3, leading to the progressive disassembly and elimination of the cell. [196] Besides cyt *c*, a wide variety of pro-apoptotic proteins is released into the cytosol after OMM permeabilisation. Proteins such as Smac/DIABLO and Omi/HtrA2 neutralise inhibitors of caspases [197] while mitochondrion-specific endonuclease G translocates to the nucleus. Once released from mitochondria, the endonuclease cleaves chromatin DNA into nucleosomal fragments independent of

caspases. [198] Apoptosis inducing factors also escape mitochondria, enter the nucleus and independently of caspases fragment nuclear DNA and condensates chromatins [149].

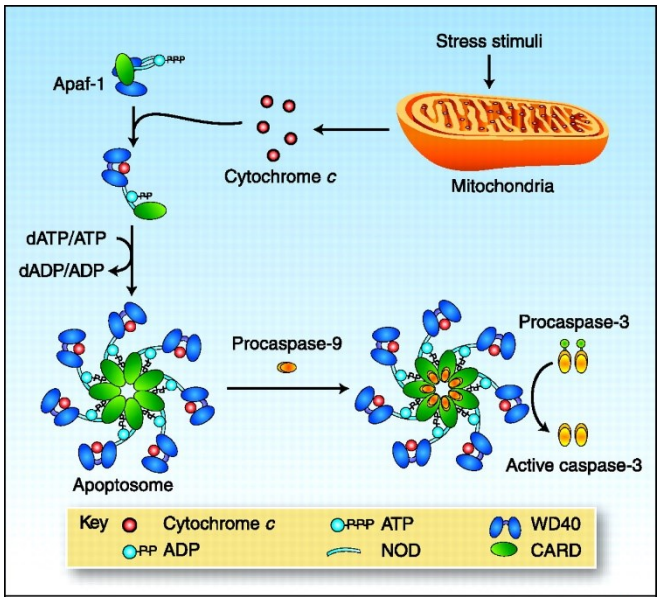

Figure 17 **Cytochrome *c*–induced apoptosome formation and caspase activation**. In healthy cells cytochrome *c* is sequestered in the mitochondrial intermembrane space and Apaf-1 exists as an inactive monomer in the cytosol. In response to stress stimuli (e.g. DNA damage or chemotherapeutic drugs) cytochrome *c* is released from mitochondria to the cytosol where it binds to Apaf-1, triggering a conformational change and hydrolysis of the Apaf-1-bound dATP/ATP. In a process dependent on exchange of dATP/ATP for dADP/ADP, the Apaf-1-cytochrome *c* heterodimers assemble into the apoptosome, which provides a platform for activation of the initiator caspase procaspase-9. Activated caspase-9 then cleaves and activates executioner caspases such as caspase-3. Adapted from [199]

1.8.1.2 Caspases executioners molecules

Programmed cell death that result from apoptosis ends in caspase-mediated dismantling of the cell into packaged cellular fragments. The activation of caspases is tightly controlled by their production as inactive zymogens that are activated by aggregation into dimers or macromolecular complexes when apoptosis is initiated. Activation of apoptotic caspases results in inactivation or activation of substrates, and the generation of a cascade of signalling events leading to the controlled demolition of cellular components.

Caspases are cysteine endoproteases that cleave peptide bonds after aspartic acid residues. Although caspase-mediated processing can result in substrate inactivation, it may also generate active signalling molecules that further promote programmed cell death.

Accordingly, caspases are known to have roles not only in apoptosis (caspase-3, -6, -7, -8, and -9 in mammals), but also in inflammation. Caspases involved in apoptosis have been sub-classified by their mechanism of action and are either initiator caspases (caspase-8 and -9) or executioner caspases (caspase-3, -6, and -7). [200]

Caspase substrates include many proteins as well as other pro-caspases, the limited cleavage of which causes the characteristic morphology of apoptosis. [200, 201] One of the preferred substrates of executive caspases is poly (ADP-ribose) polymerase-1 (PARP-1) that normally functions in routine repair of DNA damage, producing PARP-1 proteolytic fragments that reflect the specific proteases participating in PARP-1 inactivation. [202]

1.8.1.3 Mitochondria as targets for cancer therapy

1.8.1.3.1 Specific targeting of cell death-inducing compounds to mitochondria via the TPP^+ group

Given the pivotal function of mitochondria in ROS generation as well their role in cell death induction, mitochondria may be a promising target for anti-cancer agents. Compounds with anticancer activity acting on mitochondria have been termed "mitocans", and their classification has been proposed by Neužil et. al. [119]. These compounds targeted into mitochondria seem to be more effective than their non-targeted counterparts. In this respect, linking the inhibitors to lipophilic delocalized cation groups presents a promising approach to effectively target and accumulate respiratory inhibitors in mitochondria based on the IMM potential. [203]. In spite of that, detailed molecular mechanism of mitocans' action remains unresolved, but there are indications that selective induction of apoptosis in cancer cells involves considerable reactive oxygen species (ROS) production upon targeted-ETC inhibition, while no such effect is observed in somatic cells [31, 204, 205].

The best studied of these cationic groups is the triphenyl phosphonium (TPP^+), which profoundly accumulates in the mitochondrial matrix up to the several hundred fold. Once it enters mitochondria, the TPP^+ compounds localize into the mitochondrial matrix on the interface of the IMM, where the physiologically active part of the molecule can interact with the ETC [206]. Several classes of compounds use this approach e.g. mitochondrially targeted antioxidants - mitochondria-targeted ubiquinone, mitoquinone (MitoQ) [207], as well as various mitochondria-targeted anticancer agents with strong pro-oxidant properties. First of these

agents, mitochondria-targeted vitamin E succinate (MitoVES) was developed in our laboratory. MitoVES is derived from the redox-silent analogue of vitamin E, α-tocopheryl succinate and was shown to act via binding to CoQ site of CII therefore inhibiting CII-related activity. The interaction results in considerable ROS production and apoptosis activation [29, 104, 105, 208-210]. Secondly, mitochondria-targeted tamoxifen (MitoTam) in much more efficient in inhibiting CI than the untargeted tamoxifen, as demonstrated in this dissertation and in other work from our laboratory. MitoTam, unlike most other anti-cancer agents, not only kills cancer cells without inducing senescence, but also selectively eliminates both malignant and non-cancerous senescent cells. [211, 212] Metformin, a type 2 diabetes mellitus drug, is being avaluted as an agent against pancreatic cancer, although its efficacy is low. Mitochondria-targeted metformin (MitoMet) was found to kill a variety of pancreatic cancer cells 3-4 orders of magnitude more efficiently than found for the parental compound. Experiments from our and other laboratories documented CI as the molecular target for MitoMet. [213-216]

1.8.1.3.2 Mitochondria-targeted agents and the specificity of cell death

As mitochondria play a key role in determination of cellular fate and are the main producers of ROS in most cell, this suggests that understanding the specific differences how mitochondria produce/detoxify ROS in response to ETC inhibition in proliferating cancer cells and non-proliferating somatic cells could provide insight into the mechanism of action/specificity of this new and exciting class of anticancer agents.

Breast cancer is the prevailing type of neoplasia in women, and certain subtypes such as $Her2^{high}$ breast carcinomas are difficult to treat [217-219]. Her2 (also known as ErbB2) is a receptor tyrosine kinase that may regulate metabolism, for example, the pentose phosphate pathway [220] and may translocate into mitochondria to effect bioenergetics [221]. At the same time, $Her2^{high}$ background gives resistance to effective treatment by commonly used therapeutic such as tamoxifen, the first-line therapy in hormone sensitive breast treatment, which also inhibits mitochondrial CI. As tamoxifen at very high doses inhibits CI [212] , its targeting into mitochondria would be expected to result in accumulation adjacent to CI enhancing its inhibitory effects. This accumulation is achieved by the TTP-containing tamoxifen derivative MitoTam. Indeed, expression of the Her2 oncogene in breast cancer is

associated with resistance to treatment, and Her2 may regulate bioenergetics, and in this way determine sensitivity to MitoTam. [222, 223]

Interestingly, the MitoVES compound introduced above, demonstrates not only anti-cancer, but also anti-angiogenic effect. Angiogenesis, the growth and acquisition of new blood vessel, involves substantial proliferation of endothelial cells suggesting that MitoVES might possibly discriminate between quiescent and proliferating cells. Importantly, mitochondria-targeted compounds selectively induce programmed cell death within considerable ROS production arising from ETC in proliferating cells and *in vivo* tumours.[30, 208, 209, 213, 224] At the same time, MitoMet and MitoVES are well tolerated *in vivo* suggesting selectivity to cancer cells [208, 211]. Similar effects as MitoVES in proliferating endothelial cells has 4-(N-(S-glutahiolylacetyl)amino)phenyl arsenide oxide, which causes oxidative stress [225] in proliferating endothelial cells pointing to the different ROS sensitivity in proliferating and quiescent cells. This therefore suggests that modulation in ETC in proliferating and quiescent cells might have different outcomes with respect to cell death induction.

Several different factors could prove decisive in ensuring selectivity of ETC-targeted compounds. First, changes in the organisation of respiratory complexes could result in more effective induction of ROS. Second, enhanced antioxidant defence could desensitize cells to ROS which originate from the inhibited ETC. Third, cell cycle arrest can lead to metabolic changes and inhibition of ETC could thus result in the lack of cellular ATP. Combination of several of these effects could also contributed to altered sensitivity of proliferating and quiescent cells to cell death.

2 Material and methods

2.1 Reagents

All reagents were purchased from Sigma Aldrich (St. Louis, MO, USA), unless stated otherwise.

2.2 Cell culture

The cells used in the study were obtained from ATCC and were authenticated. The EA.hy926 cells were cultured in high glucose (4.5 g/l) (Lonza, Basel, Switzerland, BE12-604F) or low glucose (1 g/l) (Lonza, BE12-707F) DMEM media supplemented with 10% fetal bovine serum (ThermoFisher, Waltham, MA, USA,10270106), HAT supplement 2% (ThermoFisher, 21060017) and 1% antibiotics (penicillin G 100 U/ml and streptomycin 100 µg/ml) and, for low glucose media only, L-glutamine 0.03% in a 5% CO_2, 37°C incubator. Derived ρ^0 subline was cultivated in high glucose media as mentioned supplemented with 50 µg/l uridine (U3003) and 1 mg/l sodium pyruvate (P5280). MCF10A cells were cultured in DMEM:F12 (Lonza, BE12-719f) media supplemented with 5% horse serum (H1138), human insulin 0.1% (I9278), 20 ng/mL epidermal growth factor (ThermoFisher, PHG0311), hydrocortisone 0.5 mg/ml (H0888), cholera toxin 100 ng/mL (C8052). For the experiments the media was changed for low glucose or high glucose DMEM supplemented as DMEM:F12 above. All cell lines were regularly screened for mycoplasma contamination using the MycoAlert kit (Lonza, LT07-318). For experiments requiring pharmacological treatments, equal numbers of cells (6-8 $x10^5$) were exposed to the studied compounds. For quiescent cultures, the cells were seeded into 24-well plates at 80% density, and cultured for 4 days post-confluence. For proliferating cultures, cells were seeded into 6-well plates at $3x10^5$ cells per well two days before the experiment. 1 ml of medium per well were used for both proliferating and quiescent cultures.

Human breast cancer cell lines, MCF7 and MDA-MB-453, were obtained from the ATCC. BT474, MDA-MB-231, MDA-MB-436, SK-BR-3, and T47D human breast cancer cell lines were from J. A. López (Griffith University, Australia). The mouse NeuTL breast cancer cell line was originally derived from spontaneous breast carcinomas of FVBn/c-neu [226]. The cells were cultured in DMEM with 10% FBS and 1% antibiotics in a 5% CO_2, 37°C incubator. The 6-

thioguanine-resistant mouse 4T1 cell line from ATCC was maintained in RPMI1640 (Lonza, 11875093). All cell lines used were authenticated.

2.3 Generation of ρ^0 cells

Endothelial cells EA.hy926 were cultivated for two months in presence of ethidium bromide (0.2 μg/ml) which intercalates into mitochondrial DNA interfering with its replication. mtDNA depletion was confirmed by the absence of mitochondrial oxygen consumption and was confirmed two-monthly using *Oroboros Instruments Oxygraph–2k*.

2.4 Lentiviral production and RNA interference

pLKO1 plasmids containing shRNA sequences against the targeted transcripts were obtained from Sigma-Aldrich. Lentiviral particles were produced in Hek293-FT cells using second generation psPAX and pMD.2G plasmids and calcium phosphate or Lipofectamine 3000 (ThermoFisher, L3000008) transfections. Virus-containing medium was collected after 48 h, centrifuged at 3000 x g for 15 min, and in some cases the viruses were concentrated by overnight incubation with PEG-it (SBI-System Biosciences, Palo Alto, CA, USA, LV825A-1). The supernatants were aliquoted and stored at -80ºC. To induce silencing, the lentivirus-containing supernatants were added to cells grown in normal culture medium overnight. The transduced cells were selected by puromycin, and the level of silencing was assessed by western blotting (WB). The specific shRNA used were as follows: SOD2 - TRCN0000320739, GPX1TRCN0000046231, TRXR2 - TRCN0000433391, GSR -TRCN0000046425.

2.5 Assessment of cellular respiration

Analysis of cellular respiration was performed on instruments that measures oxygen concentration real-time in closed chamber. Respiration is supported or supressed by addition of specific exogenous substrates and inhibitors, respectivelly.

2.5.1 Measurement cellular respiration using Seahorse XF24 analyzer

Cellular respiration was assessed by Seahorse XF24 analyser (Seahorse Biosciences, Santa Clara, CA, USA). For quiescent cultures the cells were seeded at 80% density in the Seahorse XF 24-well microplates and cultured 4 days post-confluence. Proliferating cells were seeded at 20000 per well two days before the experiment. Medium was switched before

the experiment for the base medium (D5030) of pH 7.4, containing 0.2% BSA and 10 mM glucose. Oxygen consumption rate (OCR) was measured in the basal state and after sequential addition of 10 µM oligomycin, 1 and 2 µM FCCP and combined 10 µM rotenone plus 25 µM antimycin. Data were normalized to DNA content measured by the Quant-iT™ PicoGreen® dsDNA reagent (ThermoFisher, P7581).

2.5.2 Cellular respiration analysis via Oroboros Oxygraph 2-K instrument

To determine the efficacy of ETC inhibition by the tested compounds, the respiration of proliferating endothelial EA.hy926 cells under both low glucose (1 g/l) and high glucose (4.5 g/l) conditions was monitored by the Oroboros Oxygraph 2-K instrument (Oroboros Instruments, Innsbruck, Austria) as described [227], using $2x10^6$ of non-permeabilized cells per chamber. Basal routine respiration was established after adding succinate (10 mM) and ADP (3 mM), after that pharmacological agents were added as shown below. For CI- and CII-dependent respiration, digitonin-permeabilized cells suspended in mitochondrial respiration medium MiR05 described in [228] were used in all experiments. The total oxygen concentration and consumption were monitored in the presence of specific inhibitors and substrates of CI (rotenone or glutamate/malate, respectively) or CII (malonate or succinate, respectively) in the presence of increasing concentrations of tamoxifen or MitoTam.

Non-permeabilized respiration was measured after adding: oligomycin (2 µg/ml), FCCP (in 0.5 µM steps, max 2 µM), rotenone (0.5 µM), malonate (5 mM), antimycin A (0.5 µM)

2.6 SDS-PAGE and western blot analysis

SDS-PAGE and WB analysis were performed using standard methods as detailed elsewhere [27] . Antibodies used were: anti-peroxiredoxin III (SantaCruz, Dallas, TX, USA, sc-23973), anti-thioredoxin 2 (Abcam, Cambridge, United Kingdom, ab185544), anti-SOD1 (SantaCruz, sc-11407), anti-catalase (Abcam, ab1877), anti-GPX-1 (Abcam, ab108427), anti-SOD2 (Acris, Herford, Germany, AP03024-PU-N), anti-GSR (Proteintech, Manchester, United Kingdom, 18257-1-AP), anti-TRXR2 (Abcam, ab180493), anti-capase 3 (Enzo, ALX-804-305-C100), anti-PARP-1 cleaved (Cell Signalling, 9541). The anti-β-Actin HRP conjugate (CellSignaling, Danvers, MA, USA, #5125) was used for visualization. Quantification was done in the ImageJ Fiji software [229].

2.7 Blue native electrophoresis (BNE) and high-resolution clear native electrophoresis (hrCNE)

2.7.1 Mitochondria isolation

The cells for mitochondria isolation were scraped into PBS, spun down (400 x *g*, 5 min, 4°C), washed with IBc buffer and spun down again. The supernatant was removed and the cell pellet was kept at -80°C until use. Mitochondria were isolated using a Balch-style homogenizer as detailed elsewhere [29, 105, 230]. The published protocols were modified by using hand-driven 1 ml disposable syringes (Becton Dickinson, Franklin Lakes, NJ, USA, 309628). Mitochondria were isolated by differential centrifugation at 4°C (900 x g, 5 min; 3 000 x g, 5 min; 10 000 x g, 15 min and washed once again) and protein concentration determined by BCA. For BNE all the isolation buffers contained 1 % protease inhibitors (P8340).

The composition of the IBc bufr (described in [231]) was: sacharose (0.2 M), EGTA (2 mM), Tris base (10 mM), pH adjusted to 7.4 (1 M KOH)

2.7.2 Mitochondrial solubilisation

250 ug of mitochondria were centrifuged at 10 000 x *g* at 4°C for 10 min. The pellet was resuspended in 75 µl extraction buffer (EB), solubilised by the addition of 25 µl digitonin (D141) (protein/digitonin ratio ~8 g/g) and incubated for 40 min on ice, mixed by vortex every 10 min. This was followed by centrifugation at 23000 x *g* for 40 min at 4°C. In mitochondrial pellet fraction was protein content determined using the BCA protein assay kit (Thermo Scientific, 23227).

The composition of the extraction buffer was: 6–aminokapronic acid (1.5 M), Bis-tris (50 mM), EDTA (0.5 mM), pH adjusted to 7.0 (1 M KOH)

2.7.3 Blue-native electrophoresis analysis of supercomplex assamblies

BNE was performed using digitonine-solubilised mitochondria as described [232] and followed by immunoblotting. Individual mitochondrial complexes were detected using primary antibodies for EA.hy926 as follows. CI - anti-NDUFB8 (Abcam, ab110242), CII - anti-

SDHA (Abcam, ab14715), CIII - anti-UQCRFS1 (Abcam, ab14746), CIV - anti-MTCO2 (Abcam, ab110258), CV - anti-ATP5A (Abcam, ab110273), mtHSP70 (Abcam, ab2787).

For MCF10A cells we used:- CI - anti-NDUFA9 (Abcam, ab14713), CIII - anti-UQCRC2 (Abcam, ab14745), CIV - anti-COX 5A (Abcam, ab110258), CV - anti-ATP5B (HPA001520), mtHSP60 (Abcam, ab110312). Samples used for native gels were also run on SDS-PAGE/WB to verify equal mitochondrial loading using anti-mtHSP70 antibody (ThermoFisher, MA3-028).

2.7.4 Clear native electrophoresis – In gel activity assays

In gel activity was done by separating the mitochondrial solubilized respiratory complexes via high resolution clear native electrophoresis (Hr-CNE) based on their molecular weight while conserving labile protein-protein interactions. Activity of the complexes was than evaluated as the size and intensity of the specific bands. Activity of CI was determined as NADH:NBT oxidoreductase via reduction of NBT (nitrotetrazolium blue) in the presence of NADH, activity of CII (succinate:NBT oxidoreductase) as reduction of NBT in the presence of succinate. The activity of CIII (DAB: cyt *c* oxidoreductase) was visualized by 3,3'–diaminobenzidintetrahydrochloride (DAB) and cyt *c* and complex IV (cyt *c* oxidase) directly by cyt *c*. Hydrolysis of ATP and reaction of produced phosphate with Pb $(NO_3)_2$ produces a white lead precipitate within the ATP synthase band.

Hr-CNE was performed using digitonine-solubilised mitochondria and followed by in-gel activity assays as decribed followingly and in [233] and modified in [234, 235].

2.7.4.1 COMPLEX I ACTIVITY (NADH:NBT REDUCTASE)

The gel was incubated 20 min in 15 ml of reaction mix (5mM Tris–HCl buffer, pH 7.4, 7 µg/ml NADH, 2.5 µg/ml NBT (N6876)). The reaction was stopped and fixed by 50 % MeOH and 10 % acetic acid in dH_2O and then transferred to 5 mM Tris–HCl (pH 7.4) and evaluated by densitometric measurement via ImageJ Fiji software [229].

2.7.4.2 COMPLEX II ACTIVITY (SUCCINATE:NBT REDUCTASE)

The gel for complex II activity was incubated for 2 hours in 15 ml of reaction mix (5mM Tris–HCl buffer, pH 7.4, 10 mM disodium succinate (W327700), 2.5 µg/ml NBT, 200 µM

phenazin methosulphate (P9625)). The reaction was stopped and fixed by the mix of 50 % MeOH and 10 % acetic acid in dH_2O, transferred to PBS and evaluated by densitometric analysis via ImageJ Fiji software [229].

2.7.4.3 COMPLEX III ACTIVITY (DAB OXIDASE)

Nearly 24-hour incubation of the gel in 15 ml of reaction mixture (50 mM natrium-phosphate buffer (pH 7.2), 2.5 mg/ml 3,3'-Diaminobenzidine (DAB,D8001)) was performed for CIII activity. After bands appeared the gel was transferred to PBS and evaluated by densitometric measurement via ImageJ Fiji software [229].

2.7.4.4 COMPLEX IV ACTIVITY (DAB:CYTOCHROME C REDUCTASE)

The gel was incubated overnight in 15 ml of reaction mixture (50 mM natrium-phosphate buffer, pH 7.2, 2.5 mg/ml DAB, 50 µM cytochrome *c* (C2506)). After bands appeared the gel was transferred to PBS and evaluated by densitometric measurement via ImageJ Fiji software [229].

2.7.4.5 ATP SYNTHASE ACTIVITY (ATP HYDROLASE)

The gel to assess ATP synthase activity was incubated overnight in 15 ml of reaction mixture (35mM Tris/270mM glycin buffer, pH 8.3, 0.2 % $Pb(NO_3)_2$, 14mM $MgSO_4$, 8mM ATP). After white precipitate become apparent the gel was transferred into PBS and evaluated by densitometric measurement via ImageJ Fiji software [229].

2.8 Mitochondrial NAD(P)H measurements

Fluorometry based on intrinsic fluorescence of reduced pyridine nucleotides (NADH and NADPH) can be used to study cellular energy metabolism. After excitation in the UV range, reduced nucleotides emit fluorescence signal which is proportional to the NAD(P)H content.

Mitochondrial NADH was measured by two-photon microscopy using Zeiss LSM880 NLO inverted microscope, equipped with Chameleon Ultra II and Compact OPO MP lasers (Coherent, Santa Clara, CA, USA), internal 32 channel spectral GaAsP detector and two non-descanned BiG-2 GaAsP detectors. We used 63x/1.4 Plan-Apochromat oil immersion objective, 740 nm laser line at 8 mW power (6mW in scanning mode during image acquisition which includes blanking), and emission range 390-480 nm. The NADH emission spectrum

was first confirmed on internal spectral detector, for the final image acquisition we used non-discanned BiG detector. The cells were grown in glass-bottom microscopy plates (In Vitro Scientific, Mountain View, CA, USA, D35-14-1.5-n) in normal culture medium (see the Cell Culture part), pre-treated with 1 nM TMRM for 30 min and examined either untreated, exposed to 5 μM CCCP, or to 1.25 μM rotenone. Mitochondrial NADH was quantified via the Fiji software by segmenting cells using thresholding and averaging signal over mitochondrial ROIs. 3-4 independent experiments were performed, with more than 150 cells per condition imaged in each experiment.

2.9 Detection of cell death

Cell death levels can be detected by Annexin V-FITC/ PI staining. Annexin V is specific marker for early stages of apoptosis as it binds to phosphatidylserine exposed to the cell surface membranes during the apoptotic process. Staining by PI was used to detect necrosis and/or late phases of apoptosis. Both probes can be detected by flow cytometry. For the detection of cell death, cells were seeded before the experiment as described above. If required, the cells were pre-incubated with acetylcysteine 1 mM (NAC, A0150000) or auranofin 0.75 μM (Enzo Life Sciences, Farmingdale, NY, USA, BML-EL206-0100) for 1 or 2 h, respectively. Incubation time with the tested compounds was 22 h, after which cell death was assessed by flow cytometry using Annexin V/propidium iodide (PI) staining as described [105], using BD FACSCalibur or BD LSRFortessa flow cytometers (Becton Dickinson), Annexin V-FITC excitation 488 nm laser/ 530BP30 detection filter, whereas 561 nm laser/ 620BP10 detection filter for PI. Cells positive for Annexin V, PI, or Annexin V/PI were considered dead. The identity of the tested agents was as follows: H_2O_2 (516813), PEITC (253731), rotenone (R8875), piericidin A (Enzo, ALX-380-235-M002), myxothiazol (T5580), oligomycin A (75351), and CCCP (C2759). MitoVES and MitoTam were synthetized in-house [208].

2.10 Detection of intracellular ROS

To evaluate intracellular ROS levels, the cell permeable probes 2′,7′-dichlordihydrofluorescein diacetate (DCF-DA), dihydroethidium (DHE) or MitoSOX were used. DCF-DA is deacetylated by cellular esterases to non-fluorescent non-permeable compound, which is then sensitively oxidized by ROS to fluorescent DCF and can be detected

by flow cytometry. DHE is oxidised by ROS into the fluorescent ethidium, which can be detected by flow cytometry. Signal of both probes is proportional to ROS levels.

For ROS measurements, cell cultured as described were exposed to the tested compounds for one hour. For the last 20 min, the cells were co-incubated with 5 µM DCF-DA (D6883), 5 µM DHE (37291) or 0.5 µ*M* MitoSOX (ThermoFisher, M36008). The level of fluorescence was then assessed by flow cytometry, excitation laser 488 nm and detectors 530BP/30 for DCF-DA and Mitosox and 560BP20 respectively for DHE. Also described in [29].

2.11 Assessment of glucose uptake

Glucose uptake is commonly monitored in live cells using fluorescent analogue compound 2-nitrobenzodeoxyglucose (2-NBDG). This glucose analogue enters the cells at the same rate as normal glucose, although it cannot be metabolised. The signal can be measured by flow cytometry. Glucose uptake was evaluated after 15 min incubation with 50 µM 2-NBDG (ThermoFisher, N13195) by flow cytometry as described [236], on BD FacsCalibur or BD LSRFortessa using 488 nm laser for excitation and 530BP30 filter for detection. In some experiments, cells were pre-treated for 6 hours by 0.5 or 5 µM MitoVES or 7.5 µM myxothiazol.

2.12 Determination of extracellular lactate production

Principle of the method to assess extracellular lactate production is an enzymatic oxidation of present lactate to pyruvate and H_2O_2. Presence of H_2O_2 formed than allows oxidative condensation of chromogen precursors by a peroxidase, which gives rise to detectable coloured dye with an absorption maximum at 540 nm. The absorbance is directly proportional to the lactate concentration in the sample. Lactate concentration in the culture medium was assessed after 19 h of cell cultivation using lactate detection kit (TrinityBiotech, Bray, Ireland, 735-10), following manufacturer's instructions with all volumes scaled down 10 times.

2.13 Estimation of glucose content in culture media

The Amplex® Red Glucose/Glucose Oxidase Assay Kit provides a sensitive and simple method for detecting d-glucose. In the assay, glucose oxidase reacts with D-glucose to form

D-gluconolactone and H_2O_2. In the presence of horseradish peroxidase, H_2O_2 then reacts with the Amplex® Red reagent to generate the red-fluorescent product resorufin with absorption and fluorescence emission maxima of approximately 571 nm and 585 nm. The intensity of fluorescence is then proportional to the glucose concentration in the media. [237]

Glucose content in the cultured media was determined after 6, 16, 24 and 38 h of cultivation under normal experimental conditions (proliferating cells in 6-well format, quiescent cells in 24-well format, both in 1 ml of media) using low and high glucose media and Amplex™ Red Glucose/Glucose oxidase assay kit (ThermoFisher, A22189) following manufacturer's instructions. Fluorescence was measured by Tecan Infinite M200 instrument (Tecan Group Ltd., Switzerland). Data were normalized to glucose content in fresh media.

2.14 Evaluation of intracellular ATP

Intracellular ATP levels were assessed by the CellTiter-Glo kit (Promega, Madison, WI, USA, G7570) following manufacturer's instructions in 96 well format. The resulting luminescence was evaluated using the Tecan Infinite M200 instrument (Tecan Group Ltd.). Data were normalized to the cell number measured by crystal violet in a parallel 96-well plate, and are shown as relative to non-treated controls.

2.15 Measurements of surface exposure of GLUT1

Cells were exposed to the indicated agents and collected by trypsinization, incubated for 30 min in 100 ul PBS with 1:200 Anti-GLUT1 antibody (Abcam, ab15309), sedimented by centrifugation at 300g/4min and gently resuspended in PBS with 1:100 secondary Cy3-stained antibody (C2306). Both incubations were performed at 37°C, 5%CO2 incubator. Fluorescence intensity was determined by flow cytometry using BDFortessa.

2.16 In-gel assessment of antioxidant protein activity

Native in-gel assay is the method used to determine the activity of antioxidant proteins in cells. The SODs convert superoxide radical into H_2O_2 and oxygen, while the catalase and peroxidases convert H_2O_2 into water. This ability to remove oxygen species is used through this method. The gels are saturated by oxidative radicals and necessary substrates and stained by oxidation-dependent dyes. Negative bands appear where the ROS are scavenged.

The size and intensity of colourless bands formed is proportional to the activity of assessed protein. In-gel activity of antioxidant proteins was described in [238].

2.16.1 Sample preparation from cultured cells

Aproximatelly 10^7–10^8 of adherent cells were washed three times of 5 ml of PBS free of Ca^{2+} and Mg^{2+} for 30 s. Majority of the buffer was removed and the cells were scraped from the surface of the tissue culture flask by aid of a rubber policeman. Cells were spun for 5 min at 200*g*, 4 °C, in 1.5 ml microfuge tubes. Cell sediment was re-suspended in three times the pellet volume in 50 mM phosphate buffer (PB, pH 7.8) and sonicated on the Misonix Sonicator 3000 instrument (QSonica, Newtown, CT, USA) at 30% power using microtip ~ 3W, 3x15 s with 25 s pause performed on ice. Cell pellets were collected on the day of use.

2.16.2 Gel preparation

In the stacking gels for the antioxidant activity assays, riboflavin is utilized as a source of free radicals in the presence of light to catalyse the polymerization of the gel. This is used instead of ammonium persulfate (APS) because of the potential enzyme inactivation that APS could cause. This also has the added advantage that the acrylamide does not polymerize until activated by UV light exposure. Under light, polymerization takes 60 min and after polymerization the gels were left in the fridge overnight. Although the riboflavin/sucrose/acrylamide stacking gel is optimal, pre-run in a buffer removing free APS ions and TEMED from the separating gel needs to be performed. The gels were therefore pre-electrophorese before use in pre-electrophoresis buffer for at least 1.5 h, at 40 mA at 4 °C.

Pre-electrophoresis running buffer - 190mM Tris base (T1503), 1 mM of disodium EDTA (E5134) in dH_2O, pH to 8.8 with concentrated HCl. Prepared fresh on the day of use and chill to 4 °C.

Electrophoresis running buffer - 50mM Tris base, 0.3M glycine (G8898) and 1.85 mM disodium EDTA dH_2O, pH to 8.3 with concentrated HCl. Prepared fresh on the day of use and chill to 4 °C.

Sample loading buffer - For 10 ml: 5 ml of Tris stacking buffer (0.5 M, pH 6.8), 5 ml of glycerol (G5516), and 0.05% (w/v) bromophenol blue (B8026) in a 50-ml conical tube. Store at 4 °C for up to 1 year.

Preparing the separating gel - The recipe below is for two gels that are assembled with 1.5 mm spacers. Prepared and poured immediately before use at room temperature. We used 12% gels for SOD and 8% gels for GPX and catalase protein activity determination, respectively.

Reagent	Volume for 8% gel	Volume for 12% gel
dH_2O	10.95 ml	8.48 ml
Acyl-Bis 30% (w/v) (Bio-RAD, 1610156)	4.8 ml	7.28 ml
Tris separating buffer, pH 8.8	2.25 ml	2.25 ml
TEMED	9 µl	9 µl
APS 10% (w/v)	68 µl	68 µl

Preparing the stacking gel - Following recipe is for a 5% (w/vo) acrylamide stacking gel and is used with all native gels. Prepared and poured immediately before use at room temperature.

Reagent	Volume required
Acyl-Bis 30% (w/v)	1.0 ml
Tris stacking buffer, pH 6.8	1.6 ml
Sucrose 40% (w/v) (S0389)	3.2 ml
Riboflavin-5′-phosphate 0.004% (w/v)	800 µl
TEMED	4 µl

2.16.3 SOD activity gel assay

The principle of this assay is based on the ability of $O_2^{\bullet -}$ to interact with NBT, reducing the yellow tetrazolium within the gel to a blue precipitate. Areas where SOD is active develop a clear area (achromatic bands) competing with NBT for the $O_2^{\bullet -}$. SOD1 and SOD2 can be differentiated by the presence of sodium cyanide (NaCN) in the staining solution, which

inhibits SOD1. The SOD activity gel assay uses 12% gels to allow for both visualization of SOD2 (88 kDa) and the smaller SOD1 (32 kDa).

Approximatelly 150 µg was mixed 1:1 with a loading gel buffer and loaded to 12% gel chambers. Next, samples were run in the pre-electrophoresis buffer for 3 h at 40 mA at 4 °C. After 3 h, the buffer were changed for the electrophoresis buffer and run for about 2–3 h more (40 mA, 4 °C), To ensure good separation, once the dye front reaches the bottom of the gel, the gel were run for an additional 1 h. Next, gels were stained in plastic clear transparent container for 7 min in 40 ml of SOD stain solution at room temperature, shaking in the dark or covered by foil. After incubation, gels were gently rinsed twice with dH_2O. Then, gels in sufficient volume of dH_20 were incubated on a fluorescent light box until the gel begun to turn blue/purple and clear bands appear gradually (5min). After bands have appeared, gels were washed three times for 10 min with dH_2O and settled at room temperature for 18–24 h in dH_2O under ambient light to allow for further band development. As last step, the gels were imaged on a computer flat scanner and the band evaluated by densitometry approach in ImageJ Fiji software [229].

SOD gel stain consists of 40 ml of dH_2O with 2.43 mM NBT (N6876), 28mM TEMED (T9281) and 0.14 M riboflavin-5′-phosphate (F1392). Prepared fresh at room temperature.

2.16.4 Analysis of glutathione peroxidase using an in-gel activity assay

The assay is carried out with cumene hydroperoxide as the substrate instead of H_2O_2 to measure total peroxidase activity. Cumene hydroperoxide GPX activity gel (8% gels) is green-blue in color with white broad bands where the enzyme is present (approximately 85–90 kDa). Similar to the catalase assay, the in-gel assay determines GPX levels between samples by removal of the reducing agent, peroxide, needed for potassium ferricyanide to ferrocyanide. Removal of peroxide by GPX inhibits the interaction with ferric chloride and, thus, allows for an achromatic clearing on the gel where GPX is present.

GPX activity assays is performed in 8% native gel. Samples were prepared and the gel electrophoreses run as mentioned in the “2.16.3 SOD activity gel assay” section. After, the gel was pre-washed three times 10 min in plastic container with 1mM GSH (G4251) solution

(50 ml per wash). After that, gels were incubated in 100 ml 0.008% v/v cumene hydroperoxide (F2877) solution for 10 min and after rinsed twice by dH_2O. Gel was stained 1% ferric chloride (157740) (w/v) and 1% potassium ferricyanide (602299) (w/v), separately prepared and then poured on the gel together, both in 30 ml dH_2O containing GSH. When achromatic bands began to form (45 min), gel was rinsed extensively with ddH_2O and evaluated as mentioned above.

2.16.5 Analysis of catalase activity using an in-gel activity assay

Catalase activity gels will be green-blue in colour with white broad bands indicating the position of the enzyme. Following separation of native protein, the catalase enzyme removes the peroxides from the area of the gel it occupies. Removal of peroxide does not allow for the potassium ferricyanide (a yellow substance) to be reduced to potassium ferrocyanide that reacts with ferric chloride to form a Prussian blue precipitate. Catalase gels (8% gels) will have one band (220 kDa) that rarely saturates, getting larger with increasing catalase activity.

Catalase activity assay was performed in 8% (v/v) native gel. Samples were prepared and the gel run as mentioned in "2.16.3 SOD activity gel assay" section. After that, the gels were pre-washed three times 10 min in plastic container with dH_2O. Next, gels were incubated in 100 ml 0.003% v/v H_2O_2 (516813) solution for 10 min and rinsed twice in dH_2O. Gels were stained in 2% ferric chloride (w/v) and 2% potassium ferricyanide (w/v), both in 30 ml dH_2O, prepared separately but poured on the gels together. When achromatic bands began to form (15 min), gel was rinsed extensively with ddH_2O and evaluated as mentioned above.

2.17 NADPH/NADP and GSH/GSSG measurements

Cells were seeded in a 96 well plate and the ratios of GSH/GSSG and $NADPH/NADP^+$ were determined using luminescence assays (GSH/GSSG-Glo™, Promega, V6612 and NADP/NADPH-Glo™, Promega, G9081) according to manufacturer's instructions. The resulting luminescence was measured using the Tecan Infinite M200 instrument.

2.18 Cell cycle evaluation

Cell cycle can be detected using combination of RNA and DNA staining fluorophores as the content of nucleic acids varies through the cell cycle. DNA content is increasing from G1, S, G2/M phases whereas RNA stays constant but decrease upon entering G0 phase. Hoechst 33342 probe which specifically intercalates double strain DNA was used for DNA staining. Pyronin Y specifically stains RNA when DNA is already blocked by Hoechst. Both fluorophores can be detected by flow cytometry using laser 355nm with detection of 450BP50 for Hoechst and laser 461 nm, detector 586BP15 for pyronin Y, and distribution of cells to cell cycle phases can be distinguished based on the RNA/DNA content. [239]

For cell cycle assay, cells were harvested by trypsin, stained by Hoechst 33342 (10 µg/ml, B2261) for 35 min at 37°C, 5% CO_2 in normal culture media. After that pyronin Y (P9172) was added to the final concentration of 0.5 µg/ml for 15 min. $2x10^5$ of stained cells were examined by flow cytometry at a flow rate of 400 cells/s. Hoechst-low/pyronin Y-low cells were assigned to the G_0 phase of the cell cycle.

2.19 Visualization of adherence junctions

For detection of adherence junctions, cells grown on coverslips were permeabilised and blocked with 5% fetal bovine serum, 0.075% Tween-20, 0.075% Triton-X100, 100 mM glycine (Serva, Heidelberg, Germany) in PBS for 1 h, incubated with anti-VE cadherin (Santa Cruz, sc-9989) or anti-E-cadherin (Santa Cruz, sc-21791) primary antibodies (1:100) for 1 h at room temperature, followed by 1 h incubation with anti-mouse Alexa Fluor 647-conjugated antibody (Thermo Fisher, A21236, 1:1000). Samples were embedded in DAPI-containing mowiol and imaged by the Leica TCS SP8 confocal microscope (Leica Microsystems, Wetzlar, Germany) equipped with a white light laser and pulsed UV laser using a 63x lens and sequential scanning at 400 hz. Excitation was at 405 and 640 nm and detection at 420-490 and 655-730 nm using HyD detectors. Images were deconvoluted in Huygens Professional software and processed in the ImageJ Fiji software [229].

2.20 Mouse studies

All experiments were approved by the Czech academy of Sciences or Griffith University Ethics Committee and performed according to the Czech or the Australian and New Zealand Council guidelines for the Care and Use of Animals in Research and Teaching.

2.20.1 Mouse tumour model

Balb-c nu/nu mice were implanted with a slow-release estradiol pellet (60-day release of 12 μg per day; Innovative Research of America, Sarasota, FL) and injected subcutaneously (s.c.) with MCF7 mock or MCF7 Her2^{high} cells at 2×10^6 cells/animal. When tumours reached the volume of 30–50 mm^3 (quantified by ultrasound imaging, USI), mice were treated with either tamoxifen (2 μmol/mouse/dose), MitoTam (0.25 μmol/mouse/dose), or solvent control (4% ethanol in corn oil, 100 μl per dose) given intraperitoneally (i.p.) twice per week.

For *in vivo* studies we used transgenic FVBn (Friend Virus B) mouse strain carrying proto-oncogene *neu* (rat Her2) under the transcriptional control of the mouse mammary tumour virus promoter/enhancer (FVBn/c-neu mice) [226]. When spontaneous breast tumours reached the volume of 200–800 mm^3 , mice were treated with 3 doses (every 4 days) with MitoTam (0.05 mg per mouse) in physiological solution (0.9%) or solvent given intraperitoneally and tumour volume was monitored by the USI instrument Vevo770 (VisualSonics, Toronto, Canada). Mice were sacrificed within two hours of the last MitoTam application.

Tumour, breast tissue, liver and kidney samples were collected for protein isolation. Tissue were homogenized 3x20s, 5000 rpm with 2 min cooling the sample on ice at tissue homogenizer Precellys 24 (Bertin Technologies, Montigny-le-Bretonneux, France) in prefilled lysing kits (Bertin, KT03961-1-203.05) in RIPA buffer containing 1% protease (LOT) and 1% phosphatase inhibitors (P2850).

2.20.2 DNA constructs and cell transfections

MCF7 cells with silenced expression of Her2 oncogene were prepared by stable transfection with shRNA vectors (KH00209N; SA Biosciences, Frederick, MD). Full-length human Her2 construct was produced by PCR amplification of cDNA isolated from MDA-MB-

453 cells using proofreading PFU DNA polymerase (Fermentas, Waltham, MA) and primers 5′-ATA AAG CTA GCC TCG AGC ACC ATG GAG CTG GCG G-3′ (forward) and 5′-ATA AAT CTA GAG AAT TCT CAC ACT GGC ACG TCC AGA C-3′ (reverse). The PCR product was gel-purified, digested with XhoI/XbaI (Takara, Mountain View, CA), repurified, and ligated between the XhoI and XbaI sites of pEF/IRES/Puro plasmid. MCF7 and MDA-MB-231 cells overexpressing Her2 were prepared by electroporation. Empty vectors were used as a control (mock transfection). Stable clones were selected by puromycin and verified by WB. Transient transfections with modified Her2-containing vectors were done using Lipofectamine 3000 (Thermo Scientific).

2.20.3 Assessment of respiration of tissue

Tissue respiration was assessed in an analogous manner as mentioned above in chapter Assessment of cellular respiration using freshly excised tumour or liver homogenized in a dedicated tissue shredder. Respiration was monitored within 1 h after mice were sacrificed to avoid deterioration of the tissue.

2.20.4 Enzymatic assays

Isolated mitochondria were used after freeze–thaw treatment and hypotonic lysis. For NADH-cytochrome c oxidoreductase (CI-CIII) activity, 20 µg of mitochondria were incubated with 50 mM Tris (pH 8.0), 1 mM KCN, 2.5 mg/ml BSA, and 1 mM NADH at 30°C. Reaction (1 ml volume) was started by the addition of 40 µM cytochrome c, absorbance at 550 nm was followed for 90 s, and rotenone (5 µg/ml) was added for another 90 s. Rotenone insensitive rate was subtracted. Succinate-cytochrome c (CII-CIII) oxidoreductase activity was measured similarly, only NADH was replaced by 10 mM succinate and rotenone by 3 µM antimycin. Citrate synthase was measured as described [240], but the reaction was scaled down into a 96-well plate format (200 µl volume).

2.20.5 Cellular and subcellular fractionation

Cells were washed twice with PBS, harvested by scrapping, and suspended in STE buffer (250 mM sucrose, 10 mM Tris, 1 mM EDTA) containing protease inhibitors. Suspension was homogenized on ice using a glass–Teflon homogenizer; mitochondrial fraction was isolated by differential centrifugation as detailed before [27]. For preparation of mitoplasts, isolated

mitochondria were recentrifuged at 10000 g, the pellet resuspended in the hypotonic buffer (10 mM MOPS-KOH, pH 7.2, 1 mM EDTA), and incubated on ice for 30 min with occasional pipetting. The efficiency of the swelling reaction was confirmed by WB for selected IMM, IMS, and matrix proteins with parallel reaction of intact mitochondria incubated in the SEM buffer (10 mM MOPS-KOH, pH 7.2, 250 mM sucrose, 1 mM EDTA).

2.21 Statistical analysis

Data were analysed using the GraphPad Prism 5.04 software using unpaired Student's t-test analysis or two-way ANNOVA for comparisons of more than two parameters. Data are presented as mean values ± SEM of at least three independent experiments, unless indicated otherwise. Statistical significance was determined using unpaired Student's *t*-test or ANOVA when suitable; $p < 0.05$ was considered statistically significant

3 Results

3.1 Sensitivity to electron transport chain-induced cell death in cancer cells

In the first part of this study, we primarily focused on the factors which could sensitize cancer cells to the cell death. Considering the previously described effects of cancer metabolism on mitochondria and the encouraging improvements in anti-cancer efficacy resulting from mitochondria targeting of MitoVES and MitoMet, we investigated the properties of a weak CI inhibitor tamoxifen and its mitochondria-targeted counterpart MitoTam, which accumulates in mitochondria thanks to the attached TPP^+ group. Although it was expected that MitoTam, unlike tamoxifen, would mainly target the ETC, whether its sensitivity would depend on the level of ETC organization and the degree of mitochondrial respiration was unexplored. In fact, the sensitivity to the drug could be also associated with elevated oxidative stress or differences in cellular metabolism as well as with alternated capacities of antioxidant defence or ATP and NAD(P)H production machinery.

For these reasons, we therefore first examined sensitivity of breast cancer models *in vitro* and *in vivo* to tamoxifen and MitoTam and characterized the mechanism of action of the MitoTam compound.

3.1.1 Selective elimination of breast cancer cell lines via MitoTam

First, we tested the efficiency of tamoxifen and its mitochondria-targeted analogue in killing breast cancer cells. IC50 values derived from these experiments are presented in Table 1 and show that targeting of tamoxifen into mitochondria increases its effectivity more than tenfold for BT474, MCF7,MDA-MB-231/436/454 and other breast cancer cell lines. Importantly, this was specific to cancer cell lines, as non-transformed cells such as endothelial-derived EA.hy926 were more resistant. Next, we used the estrogen-dependent MCF7 breast cancer cell line with genetically manipulated Her2 expression as mentioned in methods (2.20.2 DNA constructs and cell transfections). As a result (Figure 18 and Table 1) we present that MitoTam acts markedly more efficiently than the non-targeted counterpart in all situations. Importantly, the efficacy of MitoTam clearly correlated with the presence of the Her2 oncogene overexpression.

Cell line	IC_{50} (tamoxifen)	IC_{50} (MitoTam)
BT474	29.8	2.4
MCF7	15.2	1.25
MCF7 $Her2^{high}$	21.6	0.65
MCF7 $Her2^{low}$	14.1	1.45
MDA-MB-231	35.8	6.2
MDA-MB-436	12.6	3.4
MDA-MB-453	17.5	2.5
SK-BR-3	28.3	3.5
T547D	17.3	3.4
ZR75-1	16.9	2.7
NeuTL	35.6	4.5
EA.hy926[d]	40.3	10.9

Table 1 **Table of IC50 values – MitoTam kills cancer cell lines more effectively than tamoxifen.** Table shows effectivity of both compounds *in vitro* on human breast cancer cell lines and on non-transformed confluent endothelial cells. The effectivity is much higher for MitoTam compared to tamoxifen. Data by Rohlenova K.

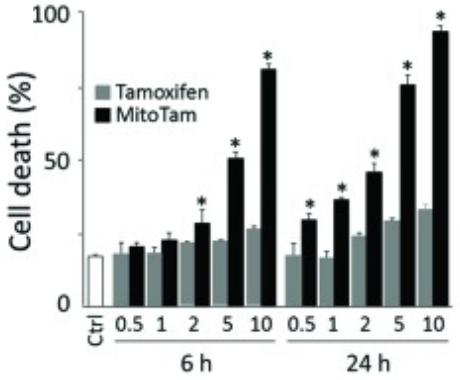

Figure 18 **MitoTam efficiently kills breast cancer cells.** MCF7 cells were exposed to tamoxifen and MitoTam at the concentrations (μM) and time points shown, and cell death was evaluated using the Annexin V-FITC/PI method by flow cytometry. Breast cancer cells are more effectively killed by MitoTAM after 6 and more significantly after 24 hours Data are mean values ($n \geq 3$) ± SEM. * indicates statistically significant difference between tamoxifen and MitoTam efficiency ($p < 0.05$). Data by Rohlenova K.

3.1.2 Suppression of tumour growth *in vivo* by MitoTam

To support the relevance of our data, we tested the effect of Her2 expression *in vivo*. Using immunocompromised Balb-c nude mice we demonstrate that while tamoxifen has an anti-tumour effect, its application resulted only in partial suppression of tumour growth and Her2 expression rendered partial resistance. On the other hand, MitoTam in much lower concentrations effectively inhibited tumour growth of both MCF7 mock and Her2^{high}-derived tumours, and Her2 expression sensitised towards the agent. In fact, in several of the MitoTam-treated experimental animals the Her2^{high} tumours fully regressed without detectable systemic toxicity (Figure 19).

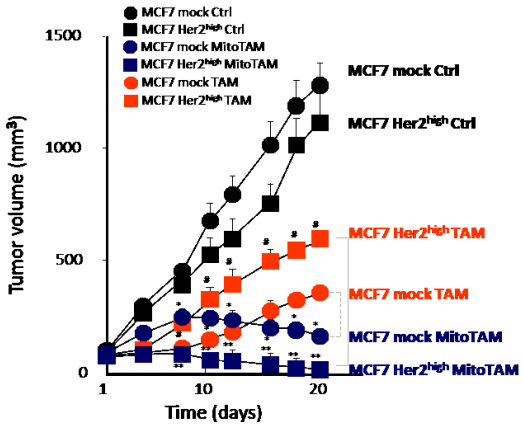

Figure 19 **MitoTam efficiently suppresses Her2^{high} breast carcinomas.** Balb-c nu/nu mice were implanted with a slow-release estradiol pellet and injected s.c. with 2 × 10^6 MCF7 mock or MCF7 Her2^{high} cells per animal. As soon as USI-detectable tumours appeared (~50 mm3), the mice were treated with i.p. injection with 100 µl of tamoxifen (2 µmol/mouse/dose) or MitoTam (0.25 µmol/mouse/dose) dissolved in 4% EtOH in corn oil twice a week. Tumour volume was visualized and evaluated using USI. Data are mean values (n = 6) ± SEM *, **, and #, indicate statistically significant differences ($p < 0.05$) to control group. Data by Rohlenova K.

3.1.3 MitoTam induces ROS, particularly in the Her2^{high} situation

To understand the molecular basis of the observed phenomena we evaluated metabolic parameters and tracked their changes during the course of treatment. Inhibition of ETC is often associated with elevated ROS. In our MCF7 model cell lines we documented that after treatment by MitoTam the ROS levels (Figure 20A) were much more increased compared to tamoxifen (Figure 20B). The effect of MitoTam was more profound again in cells with Her2^{high} background, particularly when mitochondrial-specific probe MitoSOX was used to detect ROS (Figure 20C).

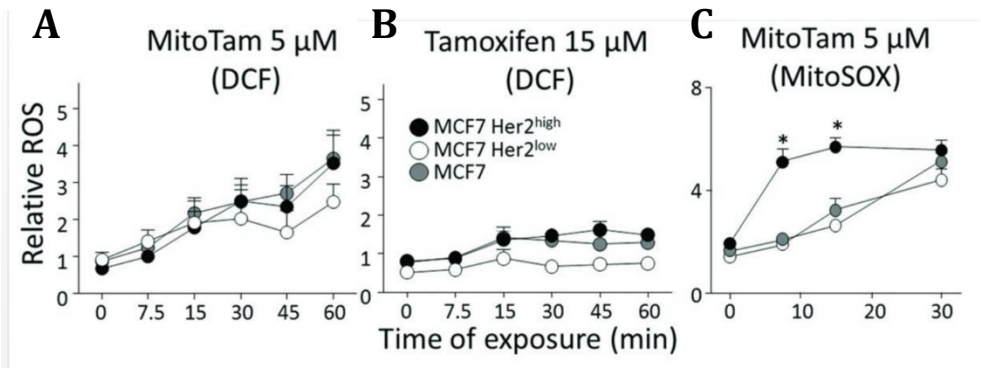

Figure 20 **MitoTam induces generation of ROS.** MCF7, MCF7 Her2^{low}, and MCF7 Her2^{high} cells exposed to **(A)** 5 µM MitoTam and **(B)** 15 µM tamoxifen were assessed for ROS using DCF or **(C)** MitoSOX. The symbol, *, indicates statistically significant differences ($p < 0.05$) between MCF7 Her2^{high} and MCF7/MCF7 Her2^{low} cells/tumours. ROS, reactive oxygen species. Data by Rohlenova K.

3.1.4 MitoTam inhibits respiration in breast cancer model

To see if ROS induced by MitoTam originated from the ETC, we measured the effect of the compound on mitochondrial respiration. MitoTam supressed CI-dependent respiration more effectively than CII-dependent respiration (Figure 21, Figure 22A). As expected, the suppression of respiration by tamoxifen was much weaker (Figure 22B). This was supported by enzymatic assays, where we detected efficient suppression of CI-III but not CII-III activity (Figure 22CD). Interestingly, MCF7 Her2^{high} cells featured higher CI-mediated respiration than mock MCF7 cells (Figure 21) as well as increased CI-III activity (Figure 22C). Also MitoTam-mediated suppression of CI-driven respiration and CI-CIII activity was much more profound in Her2^{high} situation (Figure 21 and Figure 22C), but no effect was observed on CII-III respiration (Figure 22D).

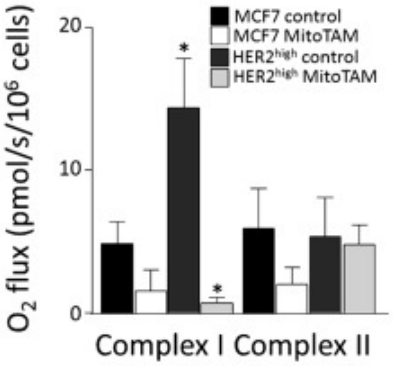

Figure 21 **MitoTam supressed CI-dependent respiration more effectively than tamoxifen, more profoundly in MCF7 cells with Her2 high levels.** MCF7 and MCF7 Her2^{high} cells were treated with 2.5 µ*M* MitoTam for 1 h, harvested, and evaluated for respiration *via* CI and CII. * indicates statistically significant differences ($p < 0.05$) to MCF7 control cells.

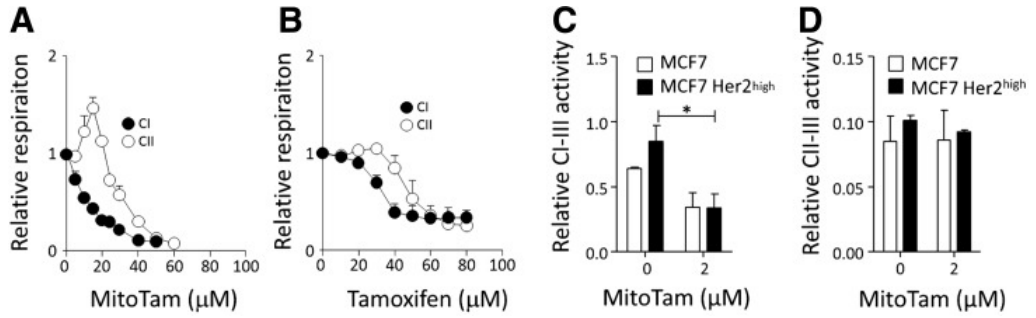

Figure 22 **Complex I-derived respiration is efficiently suppressed by MitoTam more profoundly in Her2^{high} cells.** MCF7 cell respiration (10^6 cells/ml) was evaluated in the presence of CI (glutamate/malate) and CII substrate (succinate) with titrated **(A)** MitoTam or **(B)** tamoxifen. **(C)** NADH-cytochrome c (CI-CIII) and **(D)** succinate-cytochrome c (CII-CIII) oxidoreductase activity was measured in mitochondria isolated from MCF7 and MCF7 Her2high cells and corrected for citrate synthase. * indicate statistically significant differences ($p < 0.05$).

3.1.5 Inhibition of mitochondrial respiration *in vivo* by MitoTam

To confirm the inhibition of mitochondrial respiration effect by MitoTam on *in vivo,* we investigated the effect of MitoTam administration in mice on the respiratory rate in tumour and non-malignant tissues. In line with the *in vitro* results, tumours derived from Her2^{high} MCF7 cells had much higher maximal ETC capacity (Figure 23A), CI-dependent and CII-dependent respiration (Figure 23B). CI-dependent respiration was effectively supressed by MitoTam treatment. In contrast, the respiratory rate of tissue excised from parental MCF7-derieved tumour was lower (Figure 23B), and its suppression by MitoTam was less pronounced. Importantly, administration of MitoTam to mice had no observable effect on the respiration of non-malignant liver tissue (Figure 23C).

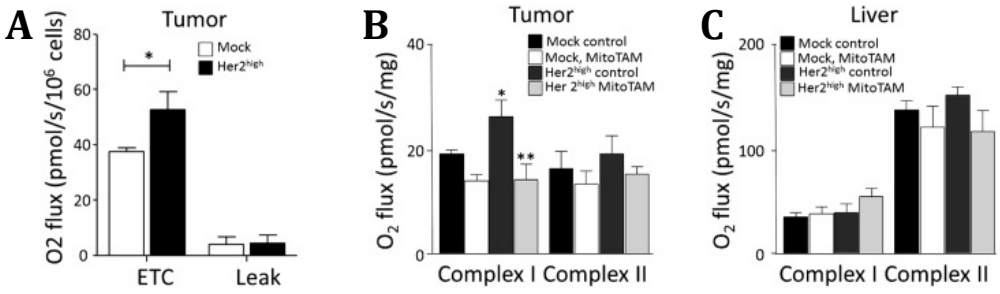

Figure 23 **Highly respiring tumour cells are more susceptible to the effect of MitoTam than non-cancer cells. (A)** MCF7 mock and MCF7 Her2^{high} tumours were evaluated for ETC and leak respiration and **(B)** CI and CII respiration. **(C)** Liver from the same control and MitoTam-treated mice were evaluated for CI and CII respiration. * and **, indicate statistically significant differences ($p < 0.05$) from control. Data by Rohlenova K.

3.1.6 MitoTam disrupts supercomplexes and increase ROS

Based on the previous results, we examined why MCF7 Her2^{high} cells have increased oxygen consumption particularly via CI. For this reason, we determined the organization of the ETC into SCs in Her2^{high} and mock MCF7 cells using BNE-PAGE analysis. This analysis revealed increased respiratory SC assemblies in Her2^{high} cells, compared to the control situation (Figure 24A). Interestingly, MitoTam treatment disrupted the SC particularly in the Her2^{high} background, whereas it had little or no effect in Her2 mock cells (Figure 24B).

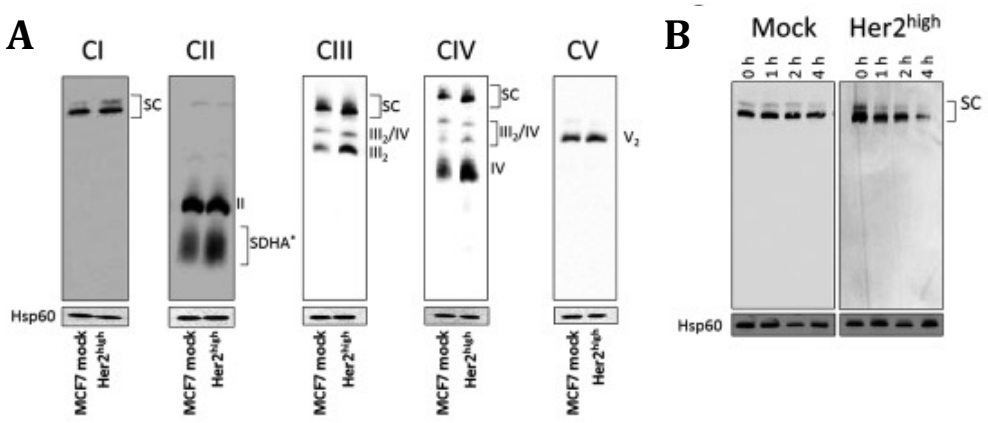

Figure 24 **Increased supercomplex assembly in Her2^{high} cells is disrupted by MitoTam. (A)** Mitochondrial fraction was probed for respiratory complexes and SCs by WB following NBGE with the following antibodies: CI, NDUFA9; CII, SDHA; CIII, Core I; CIV, Cox5a; and CV, ATPβ; Hsp60 was used as loading control. **(B)** MCF7 mock and MCF7 Her2^{high} cells were exposed to 2.5 µM MitoTam for the time periods indicated, and isolated mitochondrial fractions were evaluated for CI and SC by WB following BNGE. Data by Rohlenova K.

In summary, data suggest that MitoTam disrupts SCs particularly when the respiration rate is high and ETC is better organised into SCs. This is connected with efficient ROS production in response to MitoTam treatment in Her2^{high} situation, resulting in oxidative damage to the cell. This renders Her2^{high} cells and tumours particularly sensitive to ETC inhibition by MitoTam. Accordingly, a direct correlation exists in this scenario between the respiratory competence of the cell and the susceptibility to ETC disruption by MitoTam.

3.2 The issue of selectivity: susceptibility to ETC-induced cell death in proliferating and quiescent non-transformed cells

3.2.1 Characterization of experimental model

As described above, inhibition of cellular respiration acts selectively on cancer cells and suppress tumours in experimental animals without systemic toxicity. Therefore, to clarify why ETC-inhibition is specific to cancer cells we examined two different commercially available human cell lines derived from endothelium and epithelium, EA.hy926 and MCF10A, respectively, in proliferating and confluent state. Proliferating cells preserve some hallmarks of cancer cells, although when they reach confluence they present features of quiescent somatic cells. Important practical aspect was that both cell lines form attached monolayer and can reach the confluence-dependent cell cycle arrest. However, proliferating cells grow at lower density than quiescent cells (Figure 25). For this reason we had to optimize experimental conditions to ensure that the same amount of cells were exposed to experimental treatments. Therefore, we used 6well and 24well format to seed proliferating and quiescent cells, respectively. The amount of cells was then approximately 640 thousands for quiescent and 510 thousands for proliferating cultures, corresponding to 960 μg and 1020 μg of protein per well for EA.hy926 cells. For MCF10A cells these counts were 735 thousands/ 335 μg of protein for quiescent cultures and 505 thousands/ 450 μg of protein per well of proliferating cultures. This ensured that comparable number of cells was exposed to the same amount of tested compounds.

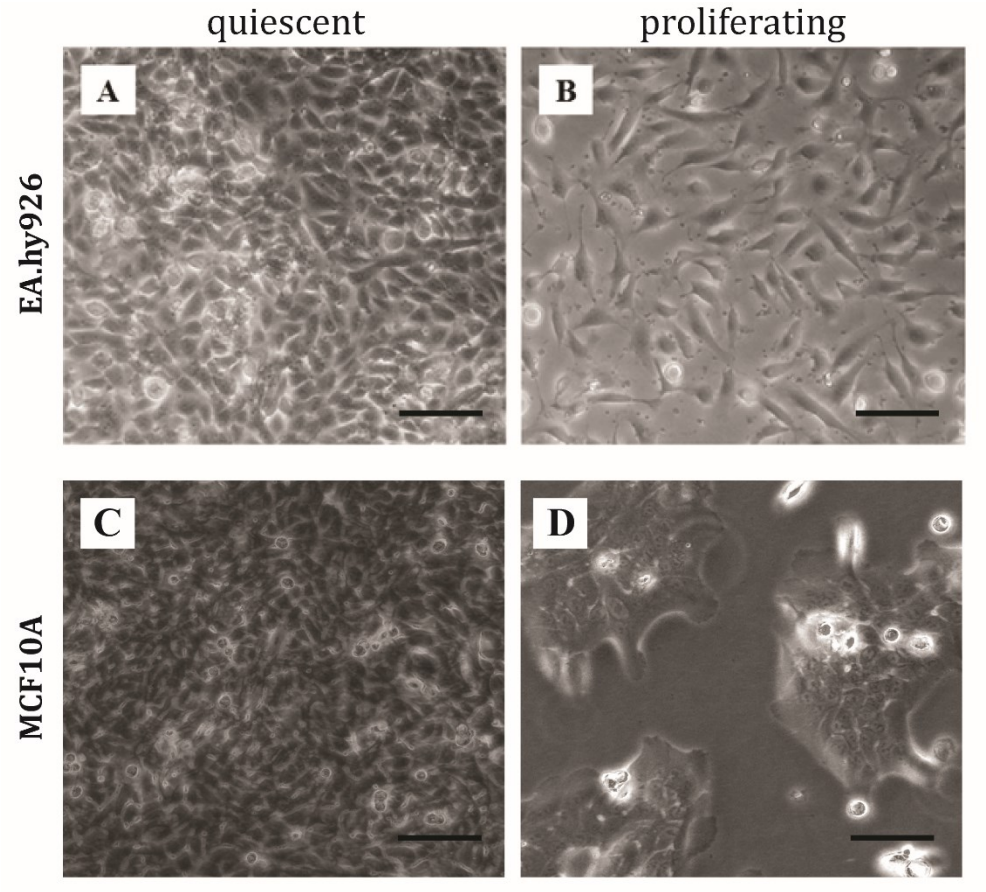

Figure 25 **Morphology of quiescent and proliferating cell.** Representative images of **(A)** quiescent and **(B)** proliferating EA.hy926 and **(C)** quiescent and **(D)** proliferating MCF10A cultures. Pictures captured at light microscope at bright field with 100x magnification. Scale bar represents 100 μm

The cells were cultured in different concentrations of glucose to simulate situations in native organism and in tumour tissues. On one hand, we cultivated cells in high glucose conditions (HighGLC; 4.5 g/l – 25 mM) representing the situation when the cell is well supplied with nutrients and glucose is available in sufficient amounts. Importantly, in this situation the glucose concentrations remains at or above the physiological level (5 mM) throughout the course of the whole experiment (Figure 26). On the other hand, when the cells were grown in low glucose conditions (LowGLC; 1 g/l, 5mM), glucose concentration drops significantly below the physiological level early in the experiment (Figure 26) and may represent a limiting factor. LowGLC situation is expected to occur in badly perfused tumours.

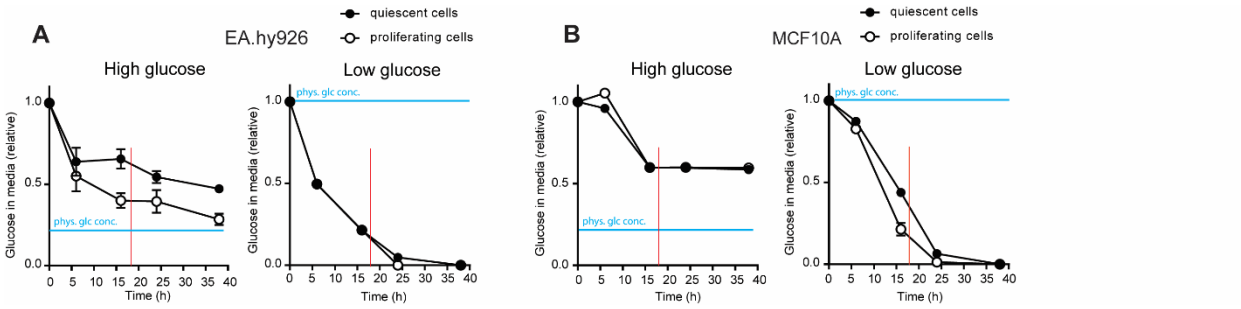

Figure 26 **In HighGLC is glucose concentration maintained around physiological level during experiment.** During the time course of the experiment, the level of glucose is maintained at or above the physiological value at HighGLC conditions, but drops significantly below the physiological level in LowGLC conditions. Cells **(A)** EA.hy926 and **(B)** MCF10A were cultivated as described above. Glucose concentration in cell-conditioned media was determined after 6, 16, 24 and 38 hours of cultivation using Amplex red-based assay. Experimental treatments start at 18 hour time point (red line). Blue line represents physiological glucose concentration. Data are correlated to fresh media and presented as the means ± SEM, n=3.

3.2.2 Contact-inhibited quiescent cells establish cell junctions

To validate the experimental model we confirmed that cells undergo cell cycle arrest and enter quiescent state after reaching confluence. Upon entering confluence cells establish adherence junctions that stimulate cell cycle arrest via contact growth inhibition. Immunostaining for VE-cadherin in endothelial and E-cadherin in epithelial cells followed by confocal microscope imaging revealed that in both EA.hy926 (also in ρ^0 cell line discussed below) and MCF10A cells the cell junctions were well established 5 days post-confluence in quiescent cells in both glucose concentrations, but are not present in proliferating state (Figure 27).

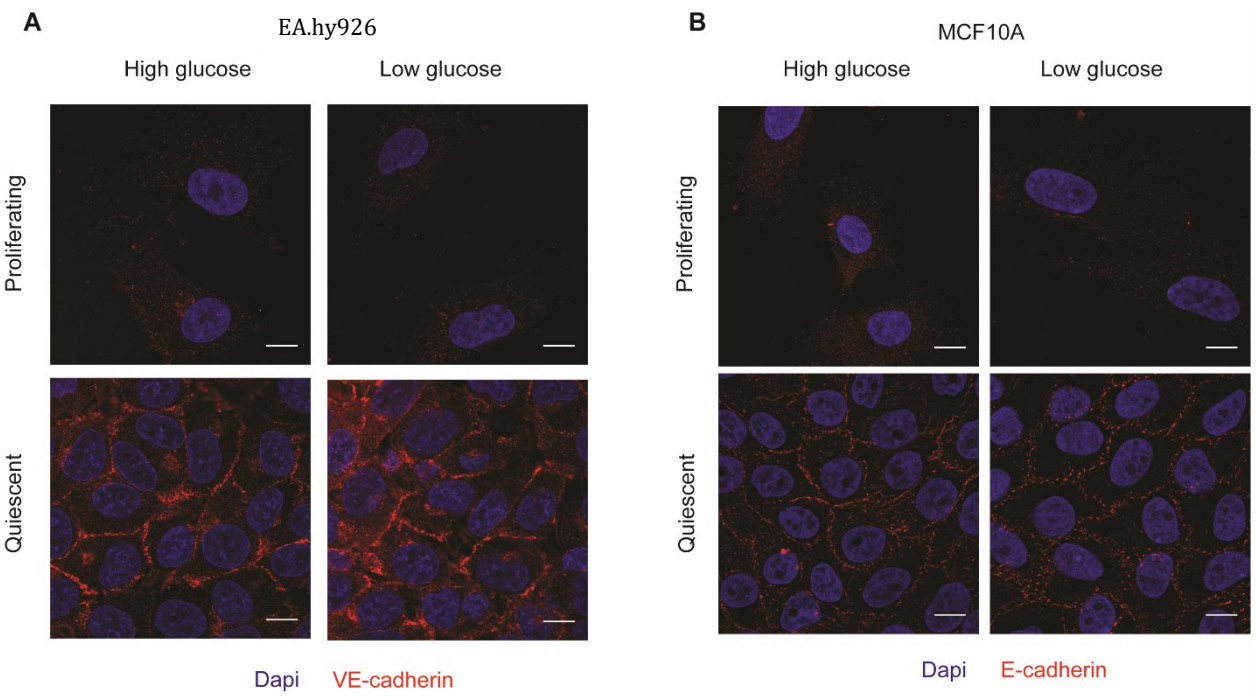

Figure 27 **Confluent cells correctly establish adherence junctions**. Adherence junctions in **(A)** EA.hy926 and **(B)** MCF10A cells were detected by immunostaning for VE-cadherin and E-cadherin, respectively, and analysed by confocal microscopy. Scale bars indicate 10 μm Representative images are shown from 3 independendent experiments

3.2.3 Non-dividing G_0 population is enriched upon entering quiescence

After reaching confluence-induced quiescence, cells are expected to reversibly enter G_0 phase of the cell cycle if they are arrested properly. For this reason, we determined the distribution of the cells within the cell cycle using double staining of both RNA and DNA content by florescent probes Hoechst 33342/Pyronin Y. Flow cytometry analysis revealed significant enrichment of cell population in G_0 phase in quiescent EA.hy926 (also ρ^0 variant - Figure 55) and MCF10A cultures in both glucose conditions compared to proliferating cultures (Figure 28). Similarly, the fraction of cells in G_2/M and S phase, indicative of cell proliferation, were reduced in quiescent cell cultures. Collectively, these results demonstrate that we are in a possession of a plausible experimental model to study molecular changes linked to entering quiescence.

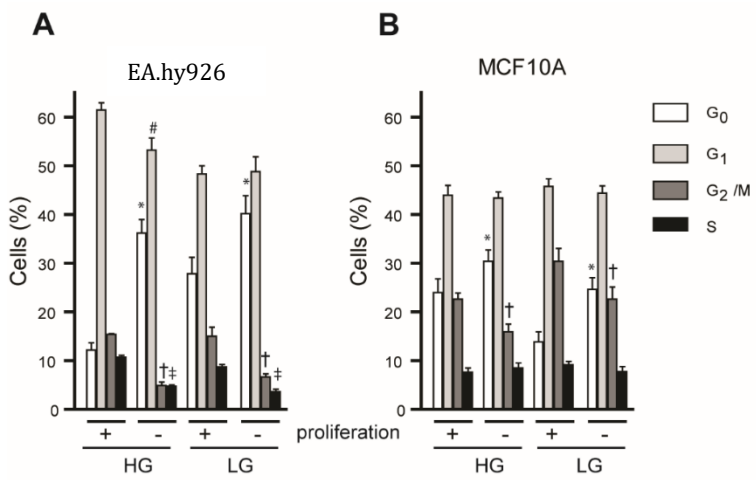

Figure 28 **Confluent cells undergo cell cycle arrest**. Analysis of cell cycle distribution of **(A)** EA.hy926 and **(B)** MCF10A cells was performed by double staining for Hoechst 33342 and Pyronin Y. Flow cytometry was used to assign cells to $G_0/G_1/S/G_2M$ phase of the cell cycle based on the level of Hoechst 33342 and Pyronin Y staining. The symbol * indicates, compared to proliferating cells, significantly increased G_0 phase, the symbol # significantly decreased G_1 phase, the symbol † significantly decreased G_2/M phase, the symbol ‡ significantly decreased S phase. Data are shown as means ± S.E.M. of at least 5 independent experiments.

3.2.4 Estimation of ETC activity and characterization of cellular metabolism

In previous result in chapter "3.1 Sensitivity to electron transport chain-induced cell death in cancer cells" we show that cancer cells are sensitised to ETC inhibition when their respiration rate is higher and they have increased ETC assembly. To investigate whether this link is maintained in non-transformed cell we examined the ETC, including the rate of respiration and the supramolecular assembly into SCs as well as its enzymatic activity.

Respiration analysis of both endothelial-derived EA.hy926 and breast epithelia-derived MCF10A cells revealed that oxygen consumption rate (OCR) was increased in quiescent cells of both cell types (Figure 29) compared to cells proliferating, suggesting that ETC activity is elevated when cells become quiescent.

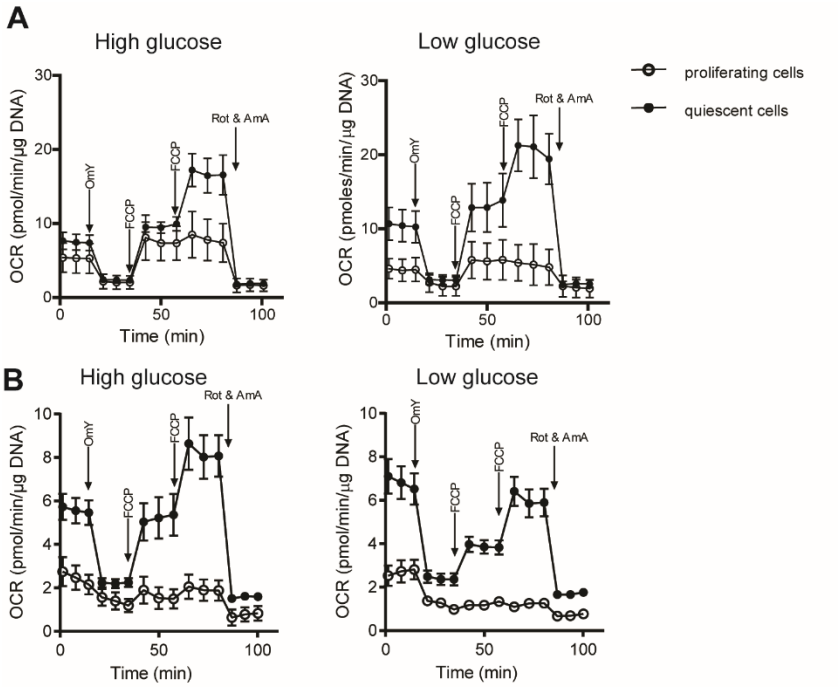

Figure 29 **Respiration is enhanced in quiescent cells.** Oxygen consumption rate (OCR, pMoles/min) profiles in **(A)** EA.hy926 and **(B)** MCF10A cells in both low glucose (1 g/L) and high glucose (4.5 g/l) conditions was measured using Seahorse Bioscience XF24 extracellular flux analyser. Data were correlated to the DNA content and presented as the mean value ± SEM from at least three independent experiments.

3.2.4.1 Protein levels of ETC complexes subunits

Considering the differences in oxygen consumption between proliferating and confluent cells, the protein expression levels of individual protein subunits of ETC complexes were determined by WB. The results (Figure 30) indicate that increased oxygen consumption is reflected by increased expression of CI (NDUFA9 and 3, NDUFB6, NDUFA8), CIII (UQCRC2), IV (COXIV) subunits in quiescent compared to proliferating cells. However, SDHA subunit of CII is more expressed in proliferating cells. These data points to the enrichment of ETC proteins in quiescent cells, irrespective of glucose availability.

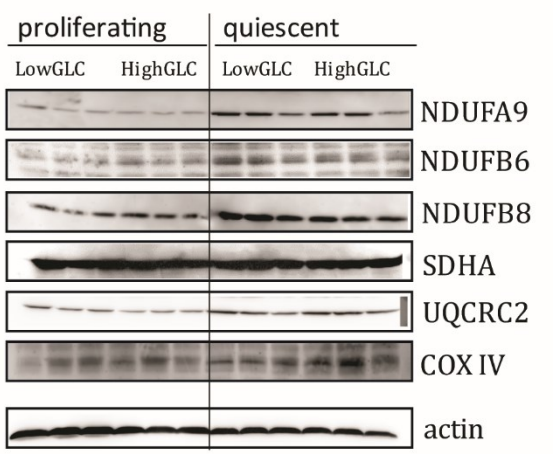

Figure 30 **Complexes I, III and IV are more expressed in quiescent cells.** Expression of individual subunits of ETC complexes in EA.hy926 cells. Primary antibodies for CI (NDUFA9 and 3, NDUFB6, NDUFA8), CII (SDHA), CIII (UQCRC2), CIV (COX IV). Samples represent 3 independent biological replicates.

3.2.4.2 Analysis of respiratory supercomplexes by blue native electrophoresis

As respiration is increased in quiescent cells and the expression of protein subunits of the ECT is higher, this suggests that elevated ETC activity could be linked to more efficient assembly of ETC complexes into SCs. We therefore performed BNE-PAGE using isolated mitochondria and verified that upon entering the quiescence the level of SC is increased in both EA.hy926 and MCF10A cells irrespective of glucose conditions (Figure 31), compared to proliferating cells.

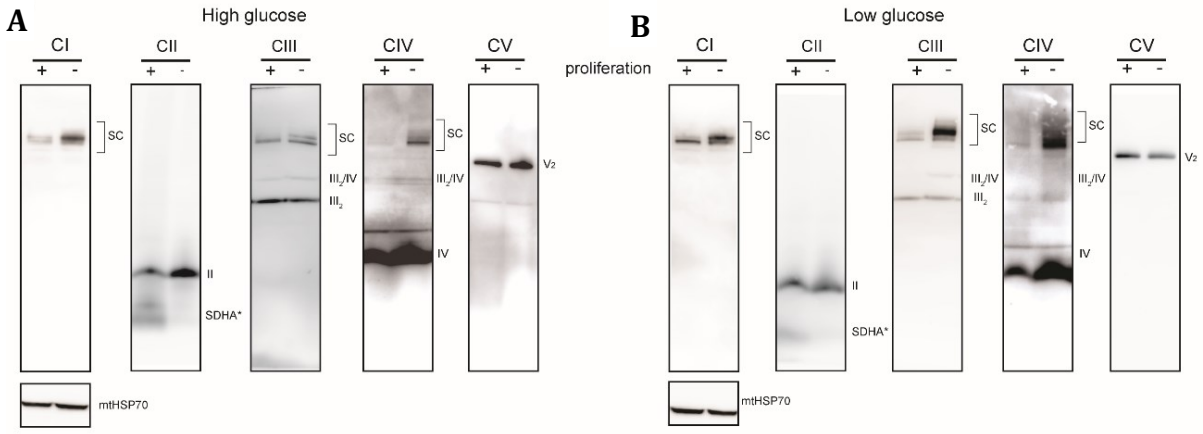

Figure 31 **Electron transport chain assembly is enhanced in quiescent cells**. Isolated mitochondrial fractions from **(A)** high glucose and **(B)** low glucose cultivated EA.hy926 were probed for the presence of SCs by WB following BNE with the following antibodies: CI, NDUFB8; CII, SDHA; CIII, MTCO2; CIV, UQCRFS1; and CV, ATP5A; mtHSP70 was used as loading control. A representative experiment is shown, n=3.

3.2.4.3 Activity of ETC complexes measured by clear native electrophoresis

As we detected increased assembly of the ETC into SCs in quiescent cells, we investigated if these structures are functional and if the enzymatic activity is also enhanced using clear native electrophoresis. The results support our previous data and show that increased SCs assembly results in elevated enzymatic activities of ETC in the quiescent state in all conditions (Figure 32). In summary, the data suggest that the ETC in quiescent cells is more active and primed for increased performance.

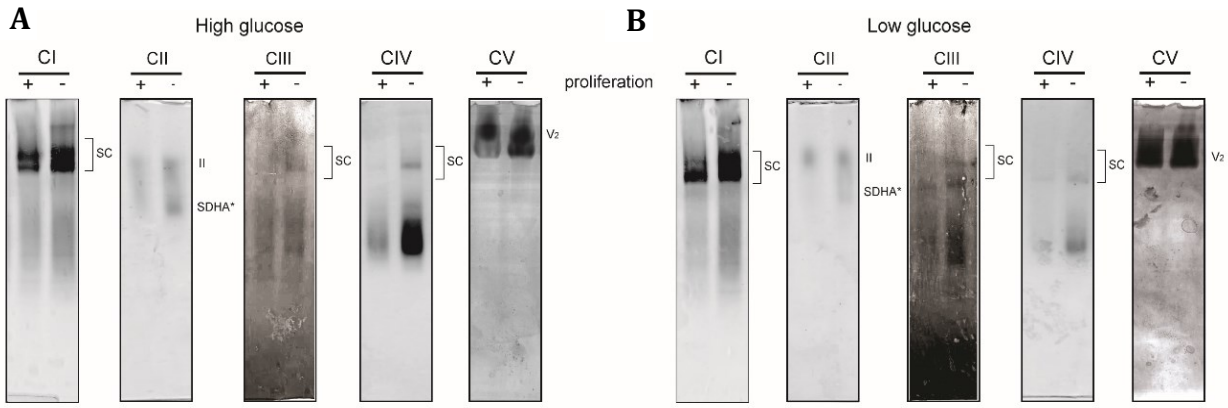

Figure 32 **Quiescent cells have higher activity of respiratory supercomplex assemblies.** In-gel assessment of enzymatic activity of respiratory SCs was performed following hrCNE in isolated mitochondrial fraction from EA.hy926 cells grown in **(A)** HighGCL and **(B)** LowGLC conditions. OXPHOS complexes activity determined as follows: CI - NADH:NBT reductase, CII - succinate:NBT reductase, CIII - DAB oxidase, CIV- DAB:cytochrome c reductase, CV- ATP hydrolase. A representative experiment is shown, n=3.

3.2.5 Mitochondrial NAD(P)H

Having established that quiescent cells feature increased respiration and increased SC assembly, we next performed *in situ* examination of mitochondrial NAD(P)H by two-photon microscopy. This assay determines the balance of the major ETC substrate NADH, providing a readout for ETC activity in mitochondria undisturbed by experimental handling. These measurements documented significantly elevated NADH(P)H signal upon addition of the CI inhibitor rotenone in quiescent but not proliferating cells (Figure 33) in both high and low glucose conditions. This points to increased mitochondrial NAD(P)H production in quiescent cells, which is at baseline avidly consumed by the ETC, but is substantially elevated when CI activity is suppressed by rotenone. In summary, these results demonstrate that ETC gains prominence in quiescence. Consequently, we would expect a higher impact of ETC blockade

in quiescent compared to proliferating (*i.e.* cancer) cells, these non-transformed cells behave analogically to previously discussed breast cancer cells.

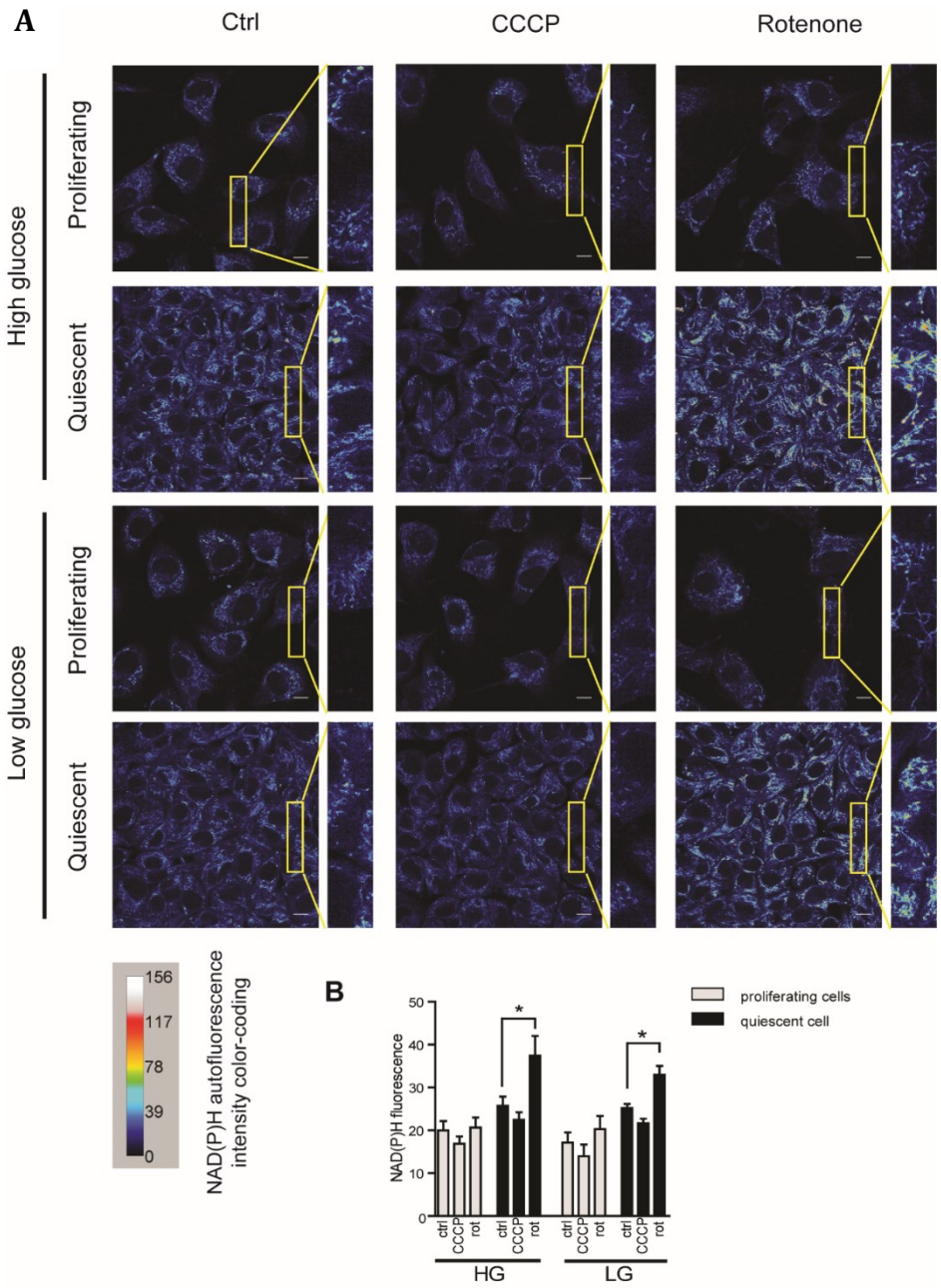

Figure 33 **In-situ measurements of mitochondrial NAD(P)H indicate increased NADH utilization by the ETC in quiescent cells. (A)** Mitochondrial NAD(P)H signal was measured by two-photon microscopy in control, CCCP (5μM) or rotenone (1.25 μM)-treated EA.hy926 cells. Representative images are shown. **(B)** Average values of NAD(P)H signal quantified in Fiji as described in chapter "2 Material and methods". Data represent the means ± SEM of 4 independent experiments. Scale bars indicate10 μm. Data by Rohlena J.

3.2.6 Glycolytic pathway activity and lactate production analysis

Because of a relationship between glycolysis and respiration [9], we determined activity of glycolytic pathway in quiescent and proliferating cells in by measuring glucose uptake and extracellular lactate production rate. Consistently with the increased oxidative phosphorylation in quiescent cells, both glucose uptake and lactate production were suppressed in this situation, while they were elevated in proliferating cells (Figure 34). This indicates a higher glycolytic rate in proliferating cells, in agreement with previously-reported data [26, 241].

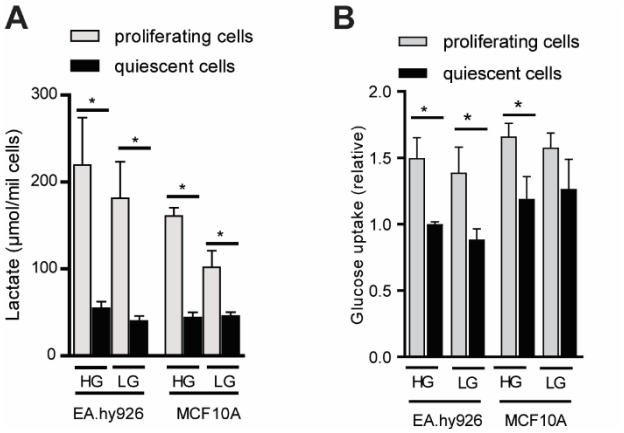

Figure 34 **Proliferating cells shows higher glycolytic activity irrespective of glucose concentration. (A)** Excreted lactate from EA.hy926 and MCF10A cells was measured in the culture medium after 19 hours cultivation. Data represent the means ± SEM of 3-4 independent experiments, and are correlated to cell number. **(B)** Glucose consumption of EA.hy926 and MCF10A cells was measured upon 24h pre-incubation in low glucose media (1 g/L glucose) by flow cytometry using 2-NBDG. Data of EA.hy926 correlated to quiescent in high glucose condition, MCF10A data relative to average high glucose proliferating EA.hy926 signal. Data represent the means ± SEM, n≥3.

3.2.7 Cell death measurements

While in cancer the dependence on oxidative phosphorylation and higher ETC SCs assembly correlate with sensitivity to ETC inhibition, in non-transformed cells this relationship has not been rigorously tested. For this reason, we assessed cell death sensitivity in proliferating and quiescent cells. We exposed cultured cells to different pharmacological compounds consisting of three groups and determined the cell death using double Annexin-FITC/PI staining followed by flow cytometry analysis. First group of agents was represented by H_2O_2 and phenethilisothiocyanate (PEITC), both of which induce ROS and oxidative stress without effecting ETC activity and are expected to induce cell purely in

a ROS-dependent manner. The second group consisted of specific ETC inhibitors (rotenone, MitoTam, MitoVES, myxothiazol) that induce ROS production upon acute ETC inhibition. Agents in the last group interfered with mitochondrial ATP production (oligomycin and mitochondrial uncoupler - CCCP). It should be noted that suppression of ATP production may modulate ROS production from the ETC.

Data presented in Figure 35A-C,G-I demonstrate that proliferating EA.hy926 and MCF10A cells in high glucose conditions are more sensitive to all tested agents than quiescent cells. This suggest that proliferating cells are susceptible to cell death when glucose is not limiting. Interestingly, in low glucose conditions (Figure 35D-F,J-L) when the glucose is significantly below physiological levels, the results are different. While the same pattern is maintained for ROS inducers (Figure 35DJ), for inhibitors of the ETC or ATP synthesis we observe higher sensitivity in quiescent cells. This suggest that under conditions of glucose limitation the ETC-driven production of ATP may become the dominant factor that determines cell survival, while proliferating cells appear more sensitive to ROS irrespective of glucose concentration.

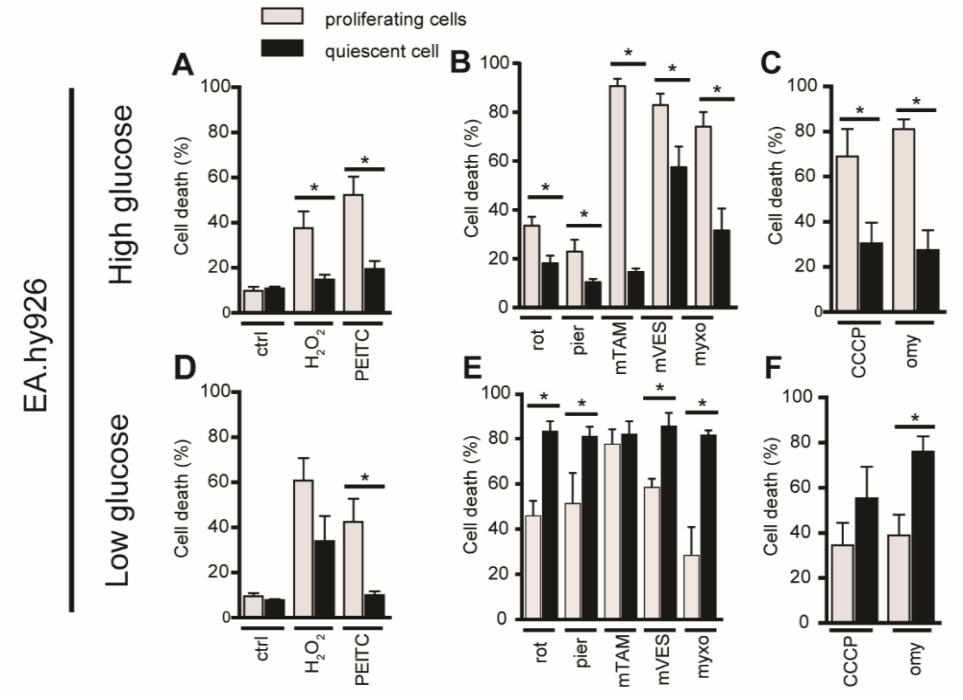

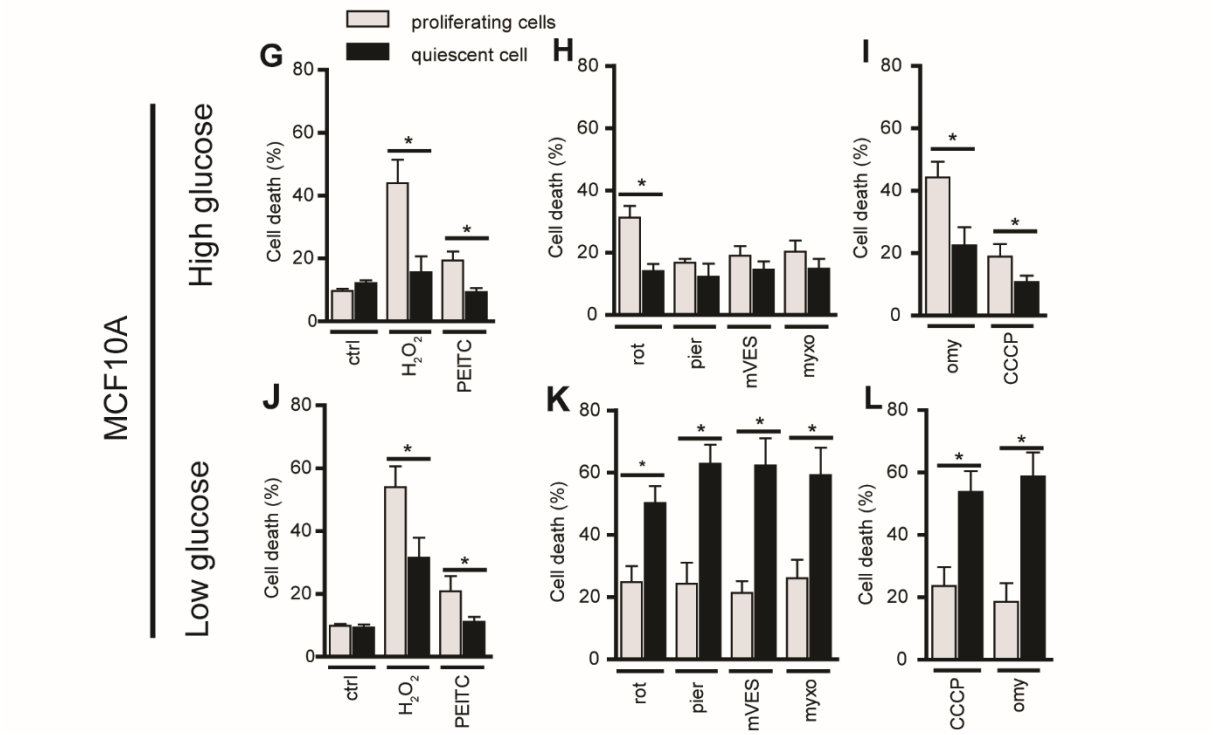

Figure 35 **ETC inhibition induced cell death is increased in proliferating cells cultured in high glucose conditions, while in low glucose conditions the quiescent cells became more sensitive.** EA.hy926 **(A-F)** and MCF10A **(G-H)** cells cultivated in high glucose (4.5 g/L glucose, **A-C**, **G-I**) or low glucose (1 g/L glucose, **D-F**, **J-L**) media, respectively, were treated with H_2O_2 800 mM, PEITC 10 µM, rotenone 2 µM, piericidin 80/0.05 µM, MitoTam 4/2 µM, MitoVES 10 µM, myxothiazol 15/0.1 µM, CCCP 75/10 µM, oligomycin 25/0.5 µM for 22 hours. Concentrations used are given for high/low glucose media. The cells were stained with Annexin V-FITC and propidium iodide, and evaluated by flow cytometry as described in 'Materials and methods'. Data represent the means ± SEM of minimum 4 independent experiments.

3.2.8 Effect of tested compound on mitochondrial respiration

To verify the expected effect of the tested compounds on the mitochondrial respiration, we performed respirometry measurements in the Oroboros Oxygraph Instrument. Data in Figure 36 show that H_2O_2 and PEITC at concentrations used in the cell death experiments had no effect on oxygen consumption, indicating no effect on ETC in our experimental model. As expected, specific ETC inhibitors (Figure 36C-G) of CI – piericidin, rotenone, MitoTam, CII – MitoVES, CIII – myxothiazol significantly decreased respiration in both high and low glucose conditions. The third group of compound effected respiration in an opposite and expected way, decreased (oligomycin) or increased (CCCP) oxygen consumption (Figure 36HI).

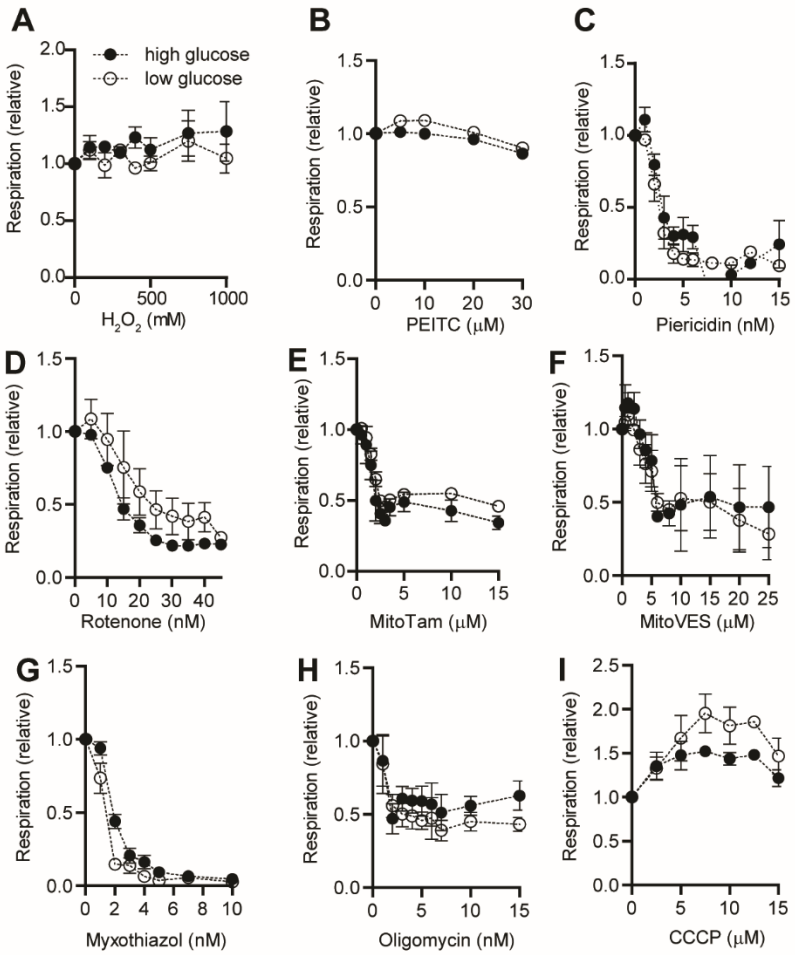

Figure 36 **The inhibiting effect of investigated agents on cellular respiration.** Oxygen consumption by proliferating EA.hy926 cultured in both low glucose (1 g/l) and high glucose (4.5 g/l) media was monitored by the Oroboros Oxygraph instrument. Basal respiration was established after adding succinate (10 mM) and ADP (3 mM), and was followed by the titration of pharmacological agents indicated in **A-I**. Data shown as means ± SEM of minimum 3 independent experiments

3.2.9 Intracellular ROS production

Inhibition of ETC can results in increased ROS production or/ and in ATP deficiency. To investigate the effect on ROS, we exposed the cells to the tested agents and determined cellular ROS levels using DCF-DA fluorescent probe and flow cytometry analysis. The data show that proliferating cells in high glucose conditions consistently generated more ROS upon treatment by all tested compounds than quiescent cells (Figure 37A-C, G-I). This correlates with the higher cell death rate in proliferating cells discussed above.

In contrast, when glucose was limiting the observed pattern of ROS production changed. Correlation between increased ROS levels and the sensitivity to cell death in proliferating cells was maintained for ROS inducers, but for the ETC inhibitors the motif of ROS production was not consistent and did not correlate with increased sensitivity to cell death in quiescent low glucose-cultured cells Figure 37 D-F, J-L. This suggest that while sensitivity to ROS may determine the cell death rate when glucose is not limiting, under glucose limitation another mechanism may come into play and determine sensitivity to cell death, as discussed later.

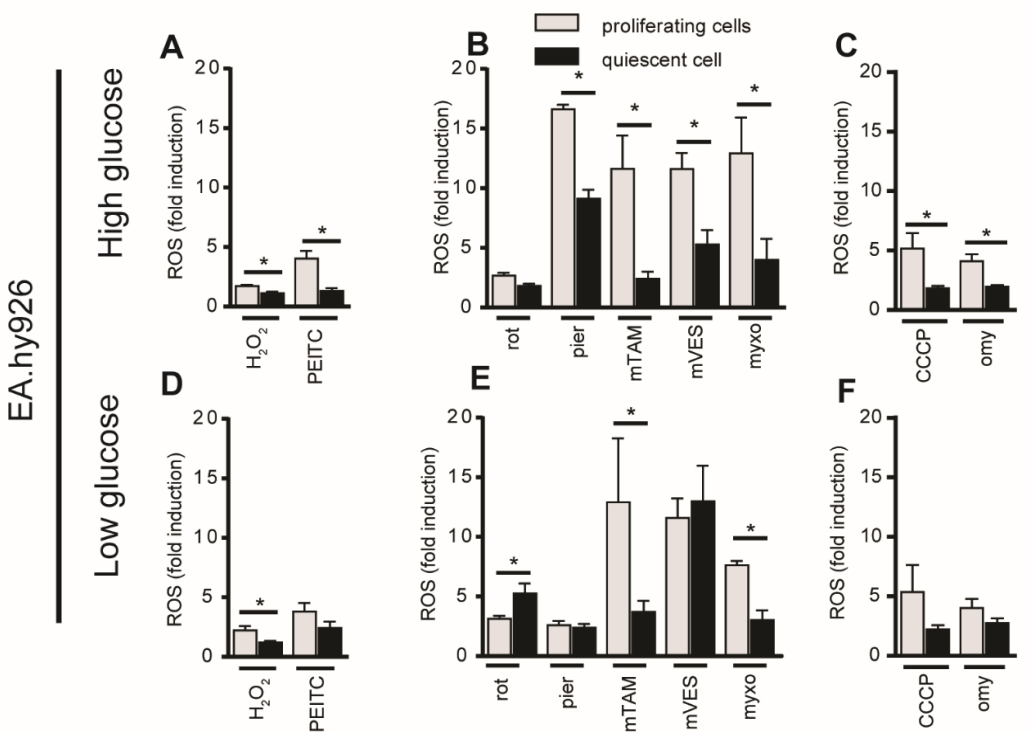

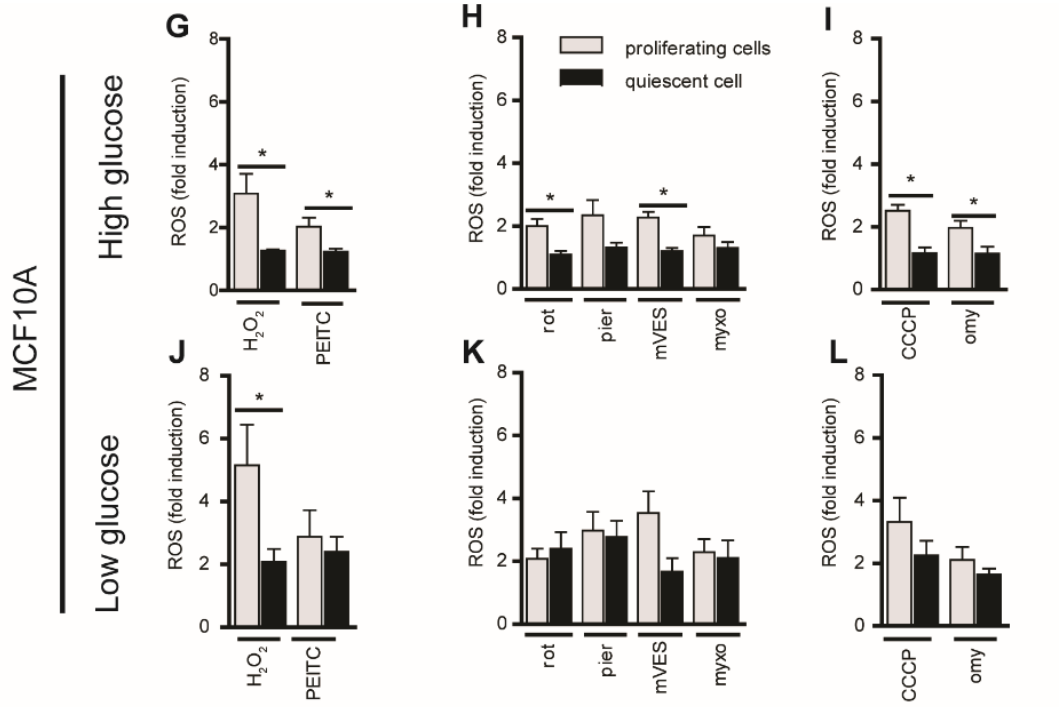

Figure 37 **ROS production upon treatment by oxidant agents and oxidative phosphorylation inhibitors is reduced in quiescent cells. (A-F)** EA.hy926 cells cultivated in high glucose (4.5 g/L glucose, **A-C**) or in low glucose (1 g/L glucose, **D-F**) media were treated with H_2O_2 800 µM, PEITC 3 µM, rotenone 20 µM, piericidin 50/10 µM, MitoTam 7.5 µM mVES 10 µM, myxothiazol 15 µM, CCCP 75 µM, and oligomycin 2.5 µM for 1 hour, followed by staining with the DCF fluorescent probe. **(G-L)** MCF10A cells cultivated in high glucose (4.5 g/L glucose, **G-I**) or in low glucose (1 g/L glucose, **J-L**) media were treated with H_2O_2 800 µM, PEITC 10 µM, rotenone 2 µM, piericidin 50 µM, mVES 10 µM, myxothiazol 25 µM, CCCP 75 µM, oligomycin 2.5 µM for 1 hour and then stained using the DCF fluorescent probe. Data are expressed relative to the non-treated controls and represent the mean ± SEM of 4-6 independent experiments.

3.2.9.1 Antioxidant treatment by N-acetyl cysteine prevents cell death in proliferating cells

To verify our hypothesis that proliferating cells are more sensitive to ROS induction upon ETC inhibition than quiescent cells, we used N-acetyl-cysteine (NAC) to boost the antioxidant capacity of the cells prior to cell death measurements in EA.hy926 cells. Data presented in Figure 38 demonstrate that pre-treatment with NAC improved resistance of proliferating cells to cell death, while little or no effect was observed for quiescent cells. This suggests that antioxidant defence is weak in proliferating cells, while it is strong in quiescent cells at baseline and application of NAC does not improve it any further.

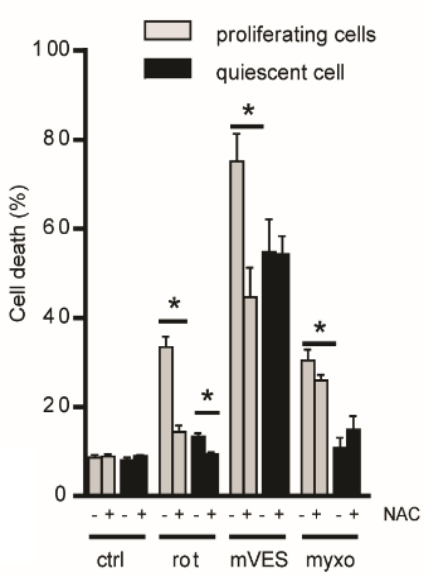

Figure 38 **Pre-treatment by antioxidant NAC decreases cell death sensitivity in proliferating cells.** Cells were pre-treated with NAC for 1 hour, followed by rotenone 5 µM, mitoVES 10 µM and myxothiazol 15 µM treatment. After 22 hours, cell death was assessed using Annexin V-FITC/ PI staining. Data shown are means ± SEM, n≤5.

3.2.9.2 Antioxidant defence protein expression

To establish the level of antioxidant defence in proliferating and quiescent cells, we first assessed the expression of antioxidant proteins by WB. In Figure 39 we demonstrate that the mitochondrial antioxidant proteins are enriched in quiescent EA.hy926 cells, irrespective of glucose availability. This was particularly apparent for SOD2, glutathione peroxidase 1 (GPX1) and to some degree also for peroxiredoxin 3 (PRX3) and thioredoxin 2 (TRX2). On the other hand, cytosolic SOD1 and catalase were marginally higher expressed in proliferating cells irrespective of glucose availability. However, in proliferating and quiescent MCF10A cells (Figure 39B) we detected similar protein levels, again independent of glucose availability.

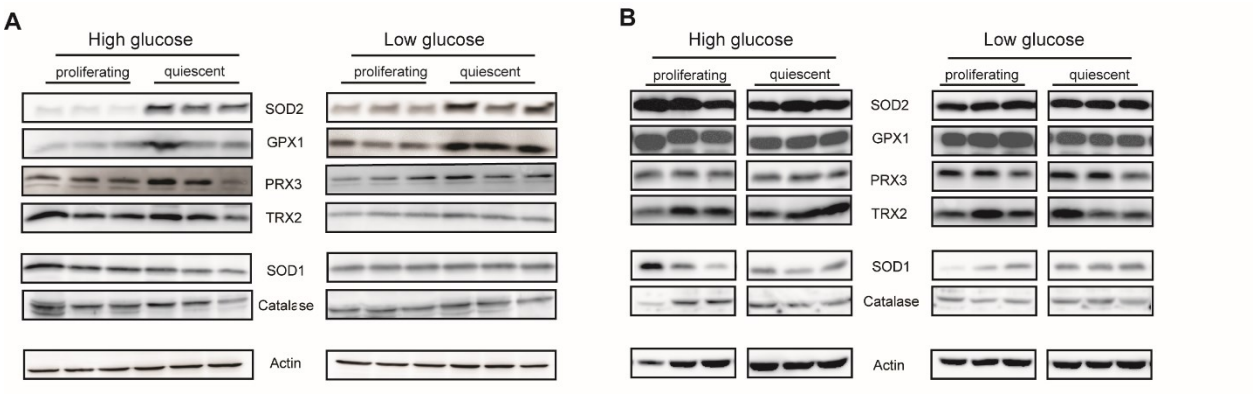

Figure 39 **Antioxidant defence protein expression is increased in quiescent cells EA.hy926 cells.** Whole cell lysates from **(A)** EA.hy926 and **(B)** MCF10A cultured in high and low glucose media were assessed by WB for expression of the indicated antioxidant proteins. Data represent 3 independent experiments.

3.2.9.3 Antioxidant defence native in-gel activity

As protein expression may not mirror activity, and to reconcile the apparent discrepancy between EA.hy926 and MCF10A cells, we performed in-gel activity assays for superoxide dismutase, glutathione peroxidase and catalase (Figure 40AB, quantified in C). This analysis revealed that the enzymatic activity of SOD2 and glutathione peroxidase was significantly increased in EA.hy926 quiescent cells (Figure 40A). For MCF10A quiescent cells

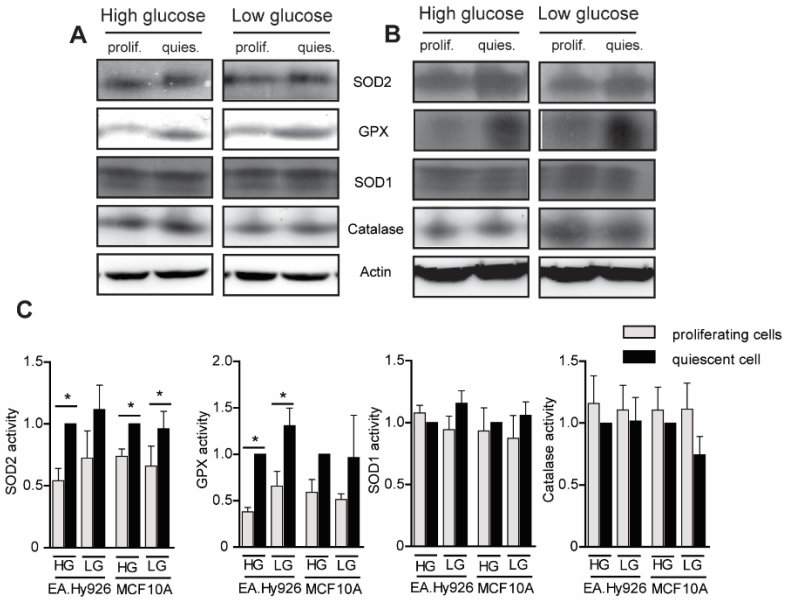

Figure 40 **Activity of antioxidant defence is increased in quiescent cells.** In-gel activities of indicated antioxidant enzymes were assessed in **(A)** EA.hy926 and **(B)** MCF10A cells in high and low glucose media. Data were quantified by densitometry **(C)**, and correlated to quiescent cells in high glucose media. Data shown are means ± SEM of 4 independent experiments.

the in-gel activity assays also revealed an increased signal for GPX and SOD2, but not for SOD1 or catalase (Figure 40B), suggesting that in quiescent MCF10A cells the activity of antioxidant enzymes is independent of their total level and probably regulated by post-translational modification. Irrespective of the mechanism, the effect of quiescence on the activity of antioxidant systems was conserved between EA.hy926 and MCF10A cells.

To establish that the elevated antioxidant defence components are functionally important, we employed a TRXR inhibitor auranofin. This agent causes depletion of reduced thioredoxin and disables the thioredoxin-dependent antioxidant systems. After auranofin pre-treatment, quiescent cells showed increased cell death sensitivity to ETC inhibitors MitoVES and myxothiazol, while much smaller effect was observed in proliferating cells (Figure 41). These data provide evidence for the relevance of thioredoxin system in cell death protection in quiescent cells in high glucose conditions, and also support the overall conclusion for the importance of the antioxidant defence in protecting the quiescent cells from cell death.

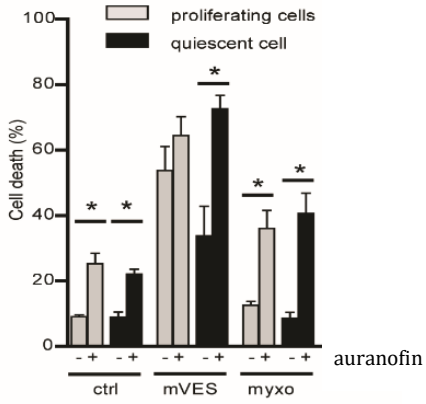

Figure 41 **Inhibition of thioredoxin reductase increases cell death sensitivity in quiescent cells.** Cell were pre-treated by 0.75 µM auranofin for 2 hours, followed by MitoVES 10 µM and myxothiazol 15 µM treatment. After 22 hours, cell death was assessed using Annexin V-FITC/ PI staining. Data are shown are means ± SEM of at least 5 independent experiments.

3.2.9.4 Intracellular pool of NADPH

The ratio of NADPH/NADP may reflect the antioxidant defence capacity of the cells as NADPH is essential for the antioxidant components action, in particular thioredoxin and

glutathione. For this reason, we assessed the NADPH/NADP+ ratio using commercial NADPH/NADP+ luminescent kit in both proliferating and quiescent cells for both EA.hy926 and MCF10A cell. The NADPH/NADP+ ratios was increased in quiescent cells (Figure 42 A) for both cell subtypes and both glucose conditions. On the other hand, ratio of reduced to oxidized glutathione was elevated in proliferating cells (Figure 42 B).

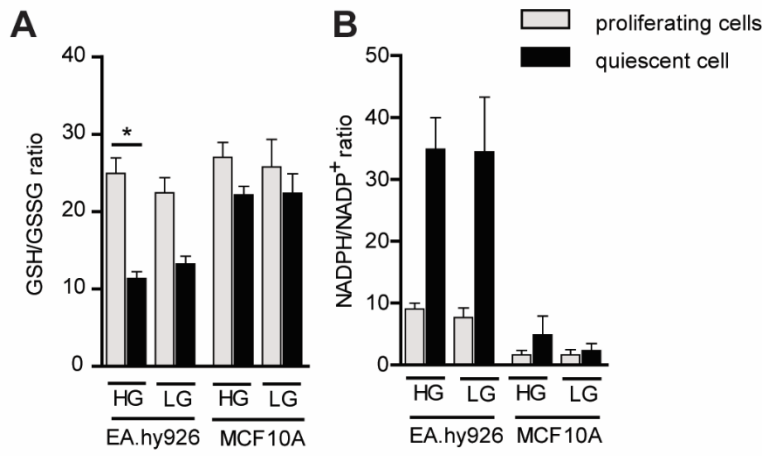

Figure 42 **The ratio of GSH/GSSH is increased in proliferating cells, whereas NADPH/NADP+ quiescent cells irrespective of glucose availability.** GSH/GSSG ratio **(A)** and NADPH/NADP+ ratio **(B)** was determined by luminescence assay in whole cell extracts. Data shown are means ± SEM, n=4

All together suggests that quiescent cells are better able to withstand the oxidative insult but glutathione might be more avidly utilised by the increased antioxidant defence in quiescent cells.

3.2.9.5 Antioxidant defence silencing

To evaluate functional importance of antioxidant defence we suppressed individual protein components by shRNA in EA.hy926 cells in high glucose conditions, treated these cells by inhibitors of the ETC (CI – rotenone, CII – MitoVES, CIII – myxothiazol) and determined the level of cell death and ROS production. First, we knocked down GPX1, which inactivates H_2O_2 in glutathione-dependent manner. However, silencing of GPX1 had only a negligible effect on cell death susceptibility in both proliferating and quiescent cells, even though we observed increased ROS levels in quiescent cells compared to non-silenced control (Figure 43 AB). Similar results were obtained upon silencing of glutathione reductase (Figure 43 CD), the glutathione recycling enzyme. Even though this treatment disables the whole

glutathione system, we observed only a limited effect on cell death induction and ROS in quiescent cells. This suggests that glutathione-dependent system are not primary defence mechanism against ROS-induced cell death in quiescent cells.

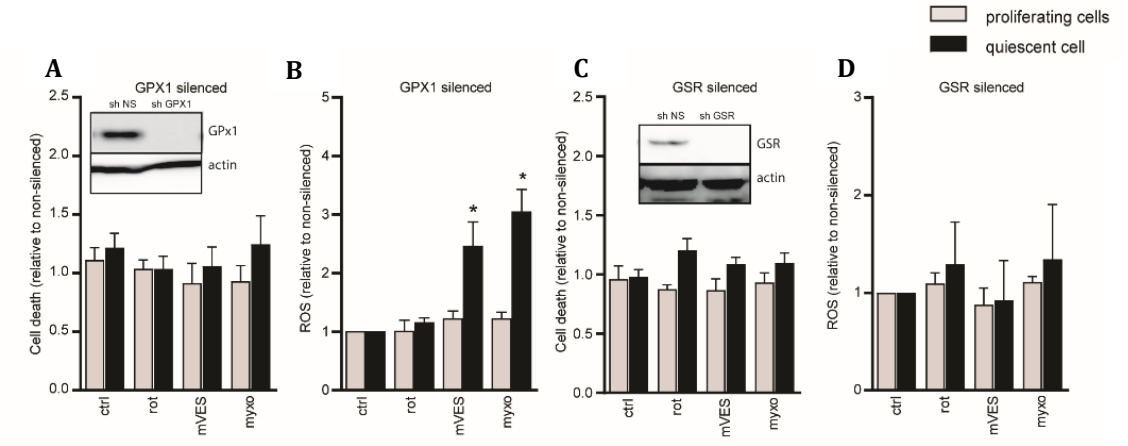

Figure 43 **Interference with the glutathione system does not have a major effect on cell death sensitivity in quiescent cells.** Cells were treated with indicated compounds as describe in Figure 35 and Figure 37 for 22 h and 1 h respectively and (**A,C**) GPX1-silenced cells were assessed for cell death (**A**) and ROS production by DCF (**B**). (**C,D**) GSR silenced cells were assessed for cell death (**C**) and ROS production by DCF (**D**). Data represent the means ± SEM, n≤4., and are expressed relative to non-silencing control.

Given the limited impact of the interference with the glutathione system, we next proceeded to evaluate the relevance of the other parts of the antioxidant defence system. We first disabled SOD2, and this resulted in significantly increased cell death upon ETC inhibition specifically in quiescent cells, and was accompanied by increased ROS production, detected by both DCF-DA and DHE fluorescent probes (Figure 44). Finally, we examined the mitochondrial thioredoxin system. We disabled the thioredoxin reductase 2 (TRXR2), the mitochondrial isoform of the thioredoxin recycling enzyme. Similarly to SOD2 intervention, silencing of TRXR2 led to significantly increased cell death and ROS in quiescent cells (Figure 45).

To conclude, we propose that the thioredoxin branch of antioxidant defence together with mitochondrial SOD2 play an essential role in protecting quiescent cells from ROS-induced cell death and determine sensitivity to ETC inhibition when glucose is not limiting.

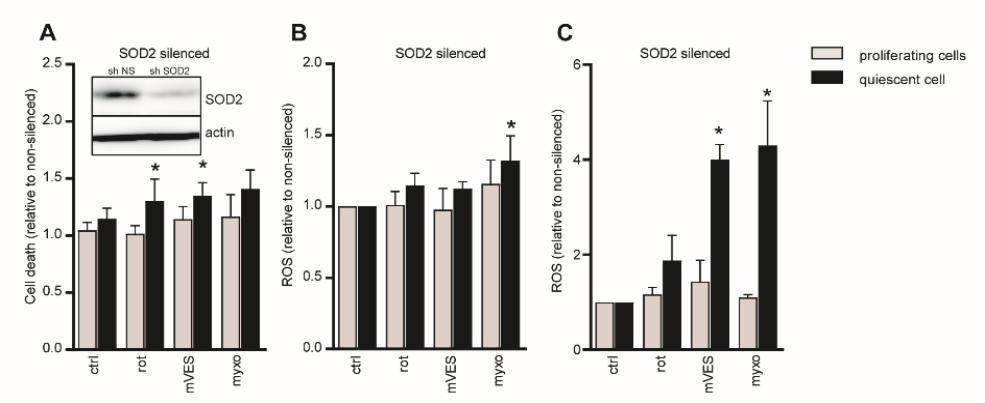

Figure 44 **Silencing of SOD2 increases susceptibility of quiescent cells to ROS-induced cell death.** EA.hy926 cells cultured in high glucose media were silenced for SOD2. The cells were treated with indicated compounds as described in Figure 35 and Figure 37 for 22 h and 1 h respectively and **(A)** cell death was assessed by the Annexin V/PI, while ROS levels by **(B)** DCF or **(C)** DHE method. Data shown are means ± SEM of 4 independent experiments, and are shown relative to non-silencing control.

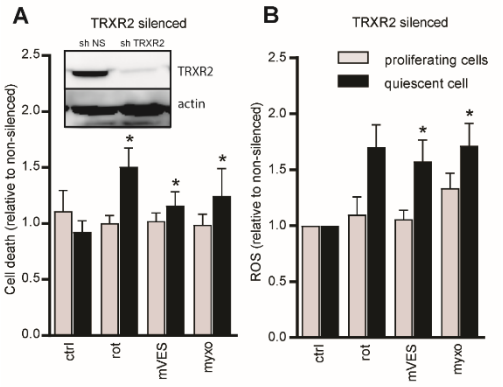

Figure 45 **Silencing of TRXR2 increases susceptibility of quiescent cells to ROS induced cell death.** EA.hy926 cells cultured in high glucose media were silenced for TRXR2. The cells were treated with indicated compounds as describe in Figure 35 and Figure 37 for for 22 h and 1 h respectively and **(A)** cell death was assessed by the Annexin V/PI, while **(B)** ROS levels by DCF method. Data shown are means ± SEM of 4 independent experiments, and are shown relative to non-silencing control.

3.2.9.5.1 Conditions of limiting glucose availability

The previous experiments indicated a limited or no effect of ETC-derived ROS on cell death under conditions of limited glucose availability. To confirm this, we performed equivalent silencing experiments for EA.hy926 cells cultured in low glucose condition. Interestingly, we detected no compelling effect of the silencing neither on cell death sensitivity (Figure 46) nor on ROS production (Figure 47).

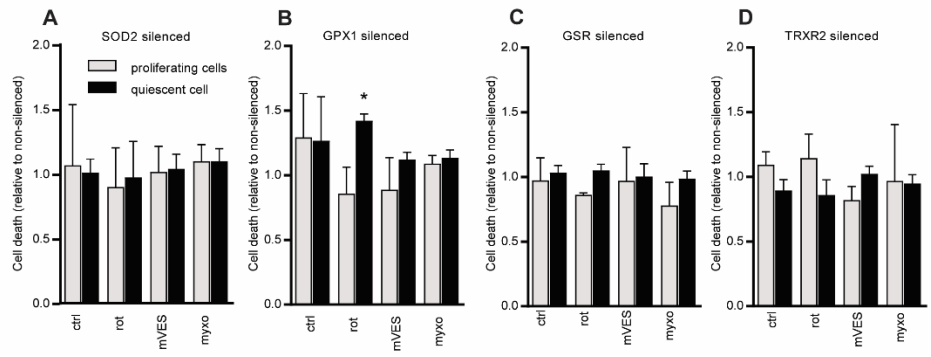

Figure 46 **Antioxidant defence does not protect quiescent cells from cell death when glucose is limiting.** EA.hy926 cells cultured in low glucose media were silenced for **(A)** SOD2, **(B)** GPX1, **(C)** GSR and **(D)** TRXR2. The cells were treated with indicated compounds as describe in Figure 35 for 22 h and cell death was assessed by the Annexin V/PI method. Data shown are means ± SEM of 4 independent experiments, and are shown relative to non-silencing control.

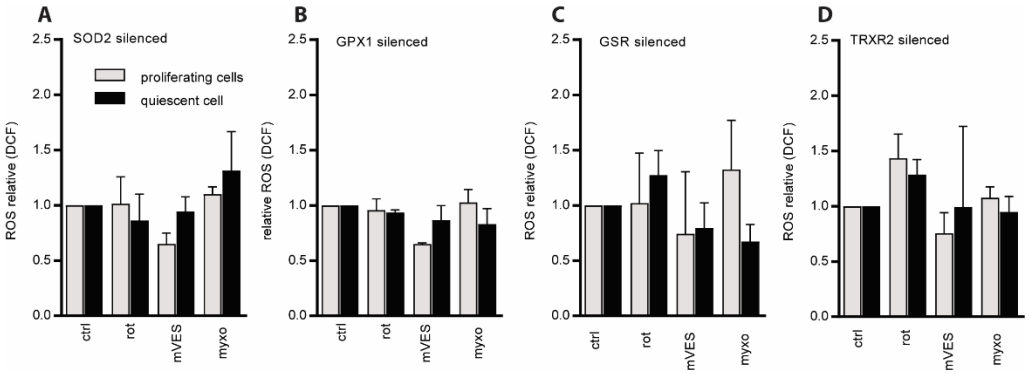

Figure 47 **Silencing of antioxidant components does not affect intracellular ROS levels in low glucose media.** EA.hy926 cells cultured in low glucose media were silenced for **(A)** SOD2, **(B)** GPX1, **(C)** GSR and **(D)** TRXR2. The cells were treated with indicated compounds as describe in Figure 37 for 1 h and ROS levels were assessed by DCF method. Data shown are means ± SEM of 4 independent experiments, and are shown relative to non-silencing control.

This supports our conclusion that under glucose limitation, the differences in the amount of ROS produced from the ETC do not play a major role in the sensitivity to ETC inhibition.

3.3 Intracellular ATP depletion as a mechanism of cell death in conditions of glucose limitation

3.3.1 Cell death and susceptibility to ROS production are changed when glucose is limiting.

The results presented above demonstrate that increased ROS level upon ETC-inhibition cannot explain cell death sensitivity under conditions of glucose limitation. We therefore started to investigate the second possibility, namely that ATP depletion could be responsible for cell death in this situation. We exposed proliferating and quiescent cells in both high and low glucose conditions to the tested agents for 30 minutes. While the treatment did not affect

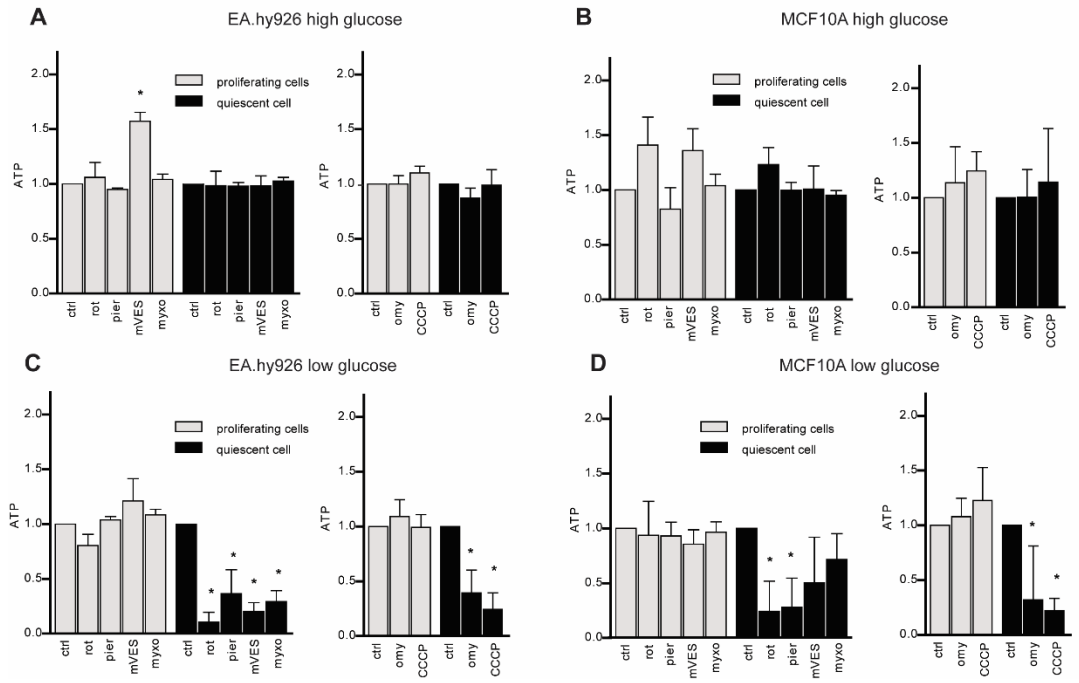

Figure 48 **Cellular ATP is depleted in quiescent cells in sub-physiological glucose levels when ETC is inhibited**. **(A,C)** EA.hy926 or **(B,D)** MCF10A cells in high **(A,B)** and low **(C,D)** glucose media were treated for 0.5 hour with 2 µM rotenone, 5 µM piericidin, 10 µM MitoVES, 15 µM myxothiazol, 25 µM oligomycin, 75µM CCCP and ATP level was assessed using luminescent assay. Results were corrected to cell number measured by crystal violet in a parallel plate. Data presented are the means ± SEM of 3 independent experiments.

ATP levels neither in proliferating nor in quiescent cells when the glucose concentration was

high, we observed a significant reduction in the ATP content in quiescent cells cultured in low glucose media (Figure 48). Importantly, the observed ATP decrease correlated with enhanced cell death (Figure 35).

3.3.2 Quiescent cells at physiological concentration of glucose are resistant to ATP depletion

Glucose in the culture media is metabolised, and in low glucose media its concentration quickly drops below the physiological level (Figure 26). However, if ATP depletion occurred at the physiological glucose concentration, it would render quiescent cells more, not less sensitive to ETC inhibition, and could not explain the observed selectivity of ETC inhibition for tumours. In support of the result above, we performed an experiment where we exposed EA.hy926 to ETC inhibitors in fresh low glucose media of 5.5 mM glucose (the physiological concentration), or to low glucose media cell-conditioned by quiescent cells for 18 hours. While we observed no depletion of ATP in fresh low glucose media, in cell-conditioned media the ATP content was clearly reduced (Figure 49).

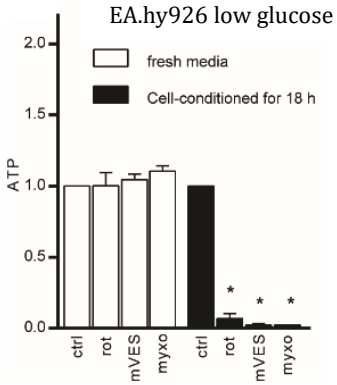

Figure 49 **When ETC is inhibited in physiological level of glucose it does not result in cellular ATP decrease.** Quiescent EA.hy926 cells in fresh low glucose (5.5 mM) media or low glucose media cell-conditioned for 18 hours were exposed to the indicated agents as described above, and the ATP content was determined. Data represent the means ± SEM, n=3.

Together this suggest that depletion of ATP is defining factor for cell death in quiescent cells when glucose is limiting, but not when it is available at the normal physiological concentration.

3.3.2.1 Glucose uptake is deficient in quiescent cells

Once the OXPHOS-derived ATP production is selectively blocked, cell usually compensate by upregulating the glycolytic pathway to cover their energy demands. Therefore, we investigated how efficiently proliferating and quiescent cells are able to increase the uptake of glucose once the ETC is inhibited. Using the same method as in "2.11 Assessment of glucose uptake", we detected a significant increase of glucose uptake after ETC inhibition in proliferating but not in quiescent cells compared to untreated control (Figure 50 AB). Glucose uptake is dependent on the expression of GLUT receptors on the cell surface, while the most important glucose transporter is GLUT1. Immunostaining and flow cytometry analysis of GLUT1 surface expression (Figure 50 CD) revealed that ETC inhibition led to significantly increased GLUT1 expression on the proliferating cell surface compared to non-treated controls, whereas just a minor increased of surface GLUT1 was observed in quiescent cells in both low and high glucose conditions in EA.hy926 cells. All this data suggest

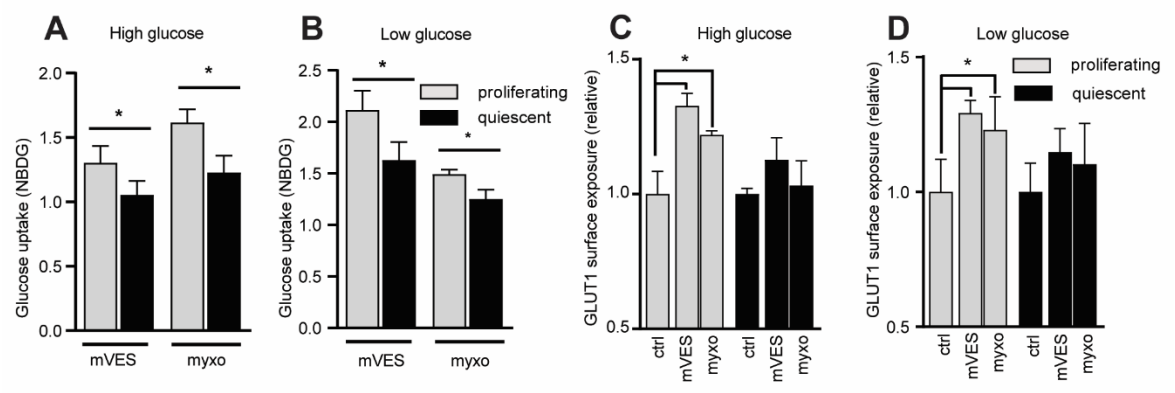

Figure 50 **Proliferating cells, unlike quiescent cells, are able to enhance glycolytic pathway after ETC blockage. (A,B)** Glucose uptake was assessed using 2-NBDG staining and flow cytometry after 6 h treatment with 0.5 µM (low glucose) or 5 µM (high glucose) MitoVES and 7.5 µM myxothiazol. Data shown represent means ± SEM of 4-5 independent experiments, and are expressed relative to the untreated control. **(C,D)** Surface GLUT1 was determined by immunostaining of non-permeabilized cells using primary anti-GLUT1 IgG and secondary Cy3 labelled anti-Rabbit IgG and flow cytometry. Cells were pre-treated for 2 hours by 5 µM MitoVES and 7.5 µM myxothiazol. Data shown represent means ± SEM of 4-6 independent experiments, and are expressed relative to the untreated control.

a lower dependence of proliferating cells on oxidative phosphorylation and better capacity of glycolytic metabolism upon the loss of ETC activity. Importantly, quiescent cells cannot enhance glycolytic pathway upon ETC-inhibition, which leads to a loss of intracellular pool of ATP, metabolic catastrophe and cell death.

3.4 Mode of cell death – caspase activation and PARP-1

Having established the molecular aspects of sensitization to cell death, we further investigated the mechanism of ETC inhibition-induced cell death in proliferating and quiescent cells cultured at high and low glucose media. In order to do this, we performed WB analysis of whole cell lysate after 16 hours incubation with the tested compounds, focusing on the activation of caspase 3 and the cleavage of PARP-1, the preferred downstream substrate for several apoptotic proteases [202]. However, we observed activation of caspase 3 and cleavage of PARP-1 only in high glucose conditions, particularly in proliferating cells, but not in low glucose conditions. Staurosporine was used as an ETC-independent apoptosis-inducing agent. Based on the data reported in Figure 51, we suggest that in high glucose conditions the oxidative stress resulting from the ETC blockage leads to apoptosis, whilst in low glucose depletion of ATP pushes the cell towards necrosis catastrophe or programmed necroptosis.

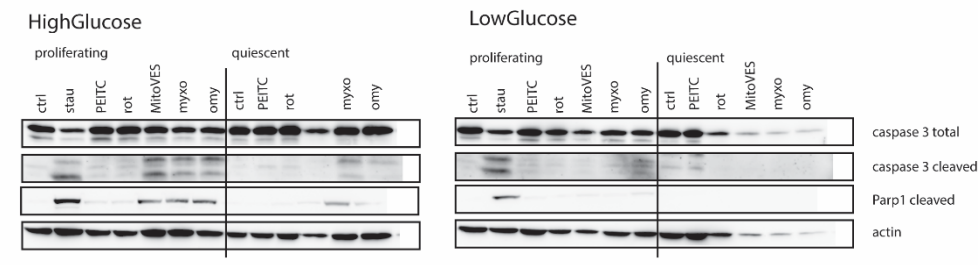

Figure 51 **Caspase-3 is activated and consequently PARP-1 is cleaved upon ETC-inhibition in high glucose conditions.** WB analysis of whole cell lysates of EA.hy926 in high and low glucose conditions. Both proliferating and quiescent cells were exposed for 16 hours to staurosporine 1.5 µM, PEITC 10µM, rotenone 5 µM, MitoVES 10 µM, myxothiazol 15 µM, oligomycin 10 µM, lysates were analysed by SDS-PAGE and probed using antibodies for caspase 3 (total and cleaved) and cleaved PARP-1. Actin was used as a loading control. A representative picture is shown of 3 independent experiments.

3.5 Characterisation of antioxidant defence in spontaneous *in vivo* tumours

3.5.1 Tumour growth

Since we documented enhanced specific anticancer effect of mitochondrially targeted ETC inhibitors and outlined the molecular mechanism which makes rapidly proliferating cells more susceptible to compounds interacting with OXPHOS we applied our proposed model to *in vivo* testing. Indeed, spontaneous FVBn/c-neu mice mammary carcinomas grew in significantly reduced rate when mice were administered *i.p.* with MitoTAM, while this treatment did not affect weight of the animals (Figure 52AB). Interestingly data shows that tumour growth was not only suppressed, but in fact tumours became reduced.

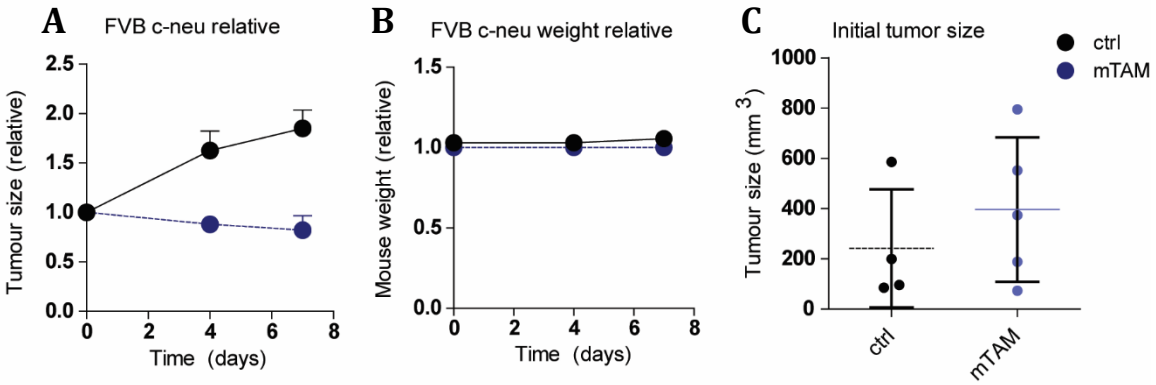

Figure 52 **Tumour growth is effectively supressed by MitoTAM.** FVBn/c-neu mice with spontaneous breast tumours reached the volume of 200–800 mm^3, mice were treated by 3 doses (every 4 days) of MitoTam (0.05 mg per mouse) in physiological solution (0.9 %) or solvent given intraperitoneally. **(A)** Tumour volume was monitored by caliper and expressed as tumour volume relative to the start of treatment. **(B)** Animal weight relative to the start of the treatment. **(C)** Initial tumour volume at the beginning of treatment.

In summary this confirmed that MitoTam effectively suppresses spontaneous tumours without systemic toxicity.

3.5.2 *In vivo* analysis of the antioxidant defence

To evaluate if elevated antioxidant defence contributes to the maintenance of MitoTam specificity *in vivo*, the experimental transgenic FVBn/c-neu mice described above were sacrificed and the level of key antioxidant defence components was determined in FVB/c-neu carcinomas, as well as in normal breast, liver and kidney tissue. We investigated whether antioxidant defence was increased in non-tumour tissue (expected to proliferate more slowly), and if antioxidant defence expression is affected by treatment with MitoTam.

Interestingly, we observed lower antioxidant protein levels in rapidly proliferating tumour tissue compared to non-proliferating somatic tissues (Figure 53). This was apparent for all the antioxidant enzymes tested. The largest differences were observed between the tumours versus kidneys and liver, while the differences with the normal mammary tissues were smaller. Furthermore, is some situations we observed an additional increase in antioxidant proteins in the tissues from animals exposed to MitoTam treatment.

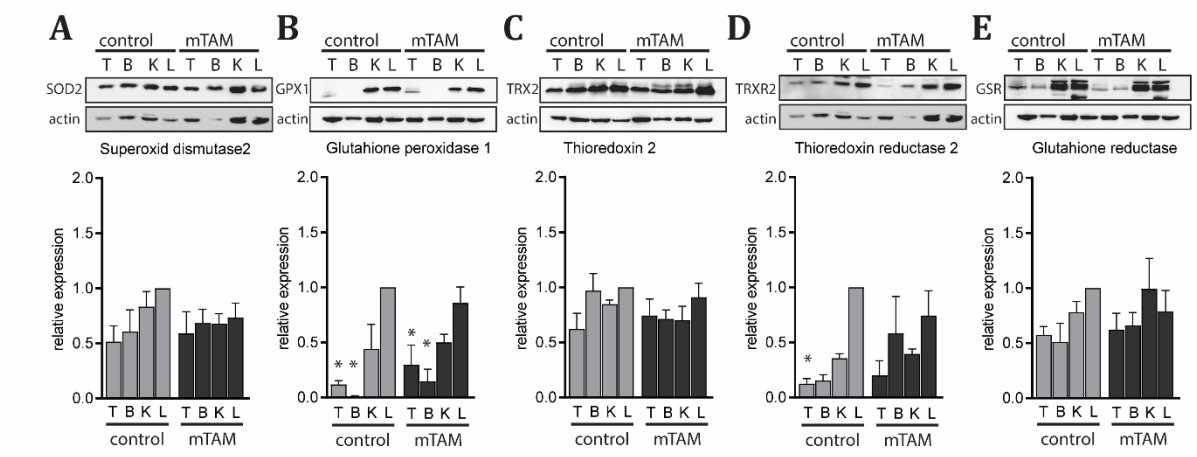

Figure 53 **Antioxidant defence in rapidly proliferating tumour tissue is lower than in non-proliferating tissue.** FVBn/c-neu mice with spontaneous 200–800 mm^3 breast tumours were treated with 3 doses (every 4 days) of MitoTam (0.05 mg per mouse) in physiological solution (0.9 %) or with solvent intraperitoneally. Mice were sacrificed within two hours of the last MitoTam application. Tissue samples were evaluated for protein expresion of **(A)** SOD2 **(B)** GPX1 **(C)** TRX2 **(D)** TRXR2 and **(E)** GSR antioxidant components by WB. Pictures show a representative experiment (n=3) and results evaluated in graphs beneath a relative expression to liver tissue in control non treated cells. * means represents significantly lower compared to liver tissue. T – tumour, B – breast, K – kidney, L – liver tissue, mTAM - MitoTam

To conclude, *in vivo* results point to a lower expression of antioxidant defence proteins in proliferating tumour tissues compared to somatic tissues, suggesting increased sensitivity of tumour tissue to ETC inhibition-induced ROS.

3.6 Cell death in ρ^0 ETC-defective cell line

3.6.1 ETC-defective ρ^0 cell line evaluation

Given the link between cell death sensitivity and the ETC we further clarified the functional role of ETC in the phenomena in ethidium bromide treated ρ^0 cell line, where mitochondrial DNA (mtDNA)-depletion resulted in a defective respiration. This was verified by respiratory measurements using the Oroboros oxygraph instrument. Figure 54 shows that ρ^0 lost ETC activity and do not consume oxygen, unlike parental EA.hy926. We also attempted to prepare MCF10A ρ^0, but this was unsuccessful, as ethidium bromide treatment was toxic to these cells.

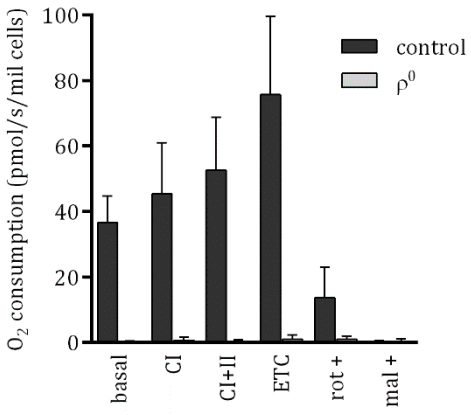

Figure 54 **Depletion of mtDNA leads to defective mitochondrial respiration in ρ^0 cell line**. EA.hy926 were cultured for two months in the presence ethidium bromide prior to measuring the oxygen consumption. After establishing the baseline, cells were permeabilised by digitonin and treated with specific substrates for CI (glutamate, malate, ADP, cyt *c*), CI+II (+ succinate), ETC (+FCCP) and inhibitors using Oroboros Oxygraph Instrument. Data shown are means ± SEM of 4 independent experiments

Despite their defective respiration, ρ^0 cells were able to arrest normally at confluence, as evidenced by the enrichment of the G_0 phase of the cell cycle (Figure 55).

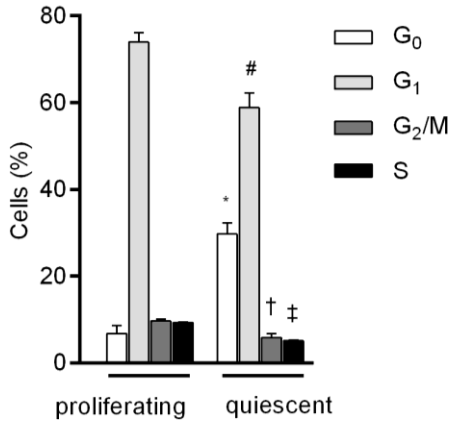

Figure 55 **ETC-defective ρ⁰ cells arrest normally at confluence.** Analysis of cell cycle distribution of EA.hy926 ρ^0 cells was performed by double staining for Hoechst 33342 and Pyronin Y. Flow cytometry was used to assign cells to $G_0/G_1/S/G_2M$ phase of the cell cycle based on the level of Hoechst 33342 and Pyronin Y staining. The symbol * indicates, compared to proliferating cells, significantly increased G_0 phase, the symbol # significantly decreased G_1 phase, the symbol † significantly decreased G_2/M phase, the symbol ‡ significantly decreased S phase. Data are shown as means ± S.E.M. of at least 5 independent experiments.

3.6.2 Cell death and ROS

To investigate the relevance of the functional ETC for cell death sensitivity in proliferating and quiescent cells, we exposed ρ^0 cells in both states to the agents tested above. Unlike in ETC-functional cells (Figure 35), we observed higher sensitivity of quiescent cells to H_2O_2, PEITC, MitoVES and CCCP, and relatively little difference for rotenone, oligomycin, myxothiazol and piericidin (Figure 56A). This points to a role for the functional ETC in the regulation of cell death sensitivity in proliferating and quiescent cells, and suggests that quiescent cells become more sensitive to ROS inducers when the ETC is inactive. Furthermore, ROS were often more increased in quiescent compared to proliferating cells, unlike in ETC-functional cells (Figure 56B). This is clearly apparent for PEITC and CCCP. All together it suggest that functional ETC, together with the antioxidant defence, plays an important role in determining cell death sensitivity.

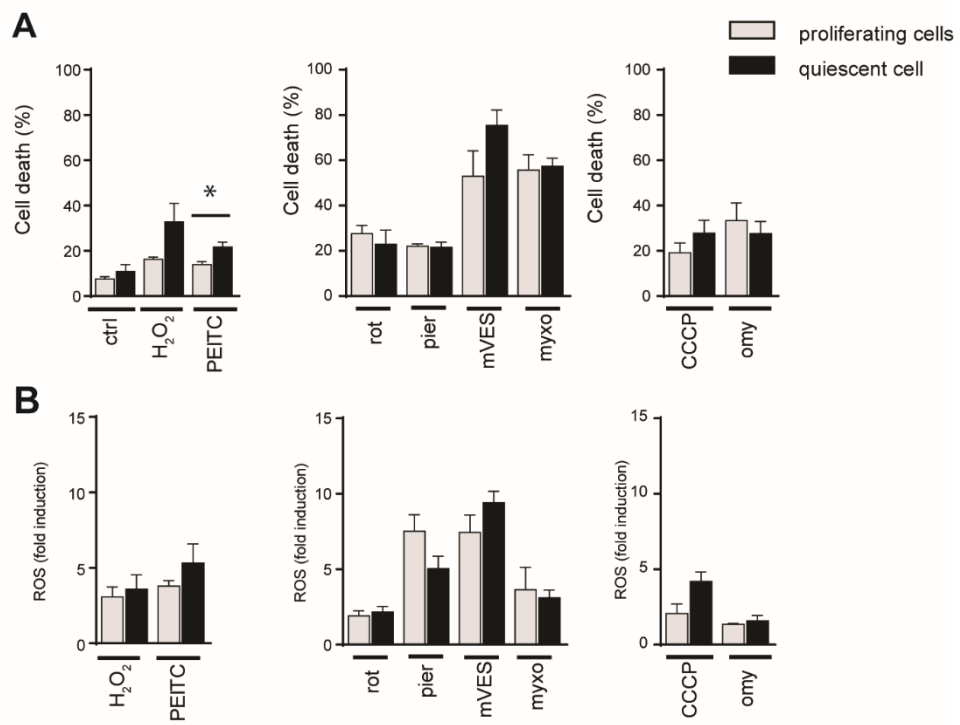

Figure 56 **ETC-defective cells are more sensitive to cell death cause by ETC-inhibitor and oxidant agents but it is not consistent with ROS production.** EA.hy926 ρ^0 cells were treated with H_2O_2 800 mM, PEITC 10 µM, rotenone 2 µM, piericidin 80 µM, MitoVES 10 µM, myxothiazol 15 µM, CCCP 75 µM, oligomycin 0.5 µM for 22 hours or 1 hour respectively. Concentrations used are given for **(A)** cell death and **(B)** ROS level experiments. The cells were stained with Annexin V-FITC/propidium iodide or DCF cytometric method. Data represent the means ± SEM of minimum 4 independent experiments.

3.6.3 Antioxidant defence in ρ^0 cells

To understand the altered cell death sensitivity in ρ^0 cells, we examined their antioxidant defence. The analysis revealed that these ETC-deficient cells closely mirror the ETC-competent EA.hy926 cells. WB shows an obvious enrichment of SOD2, GPX1, PRX3 and TRX2 protein levels in quiescent ρ^0 cells compared to proliferating ones, whereas catalase and SOD1 remained the same. These results correlate with the assessed in-gel activity demonstrating higher SOD2 and GPX activity in quiescent cells. (Figure 57)

Collectively this suggests that functional ETC regulates cell death in quiescent cells independently of the antioxidant defence.

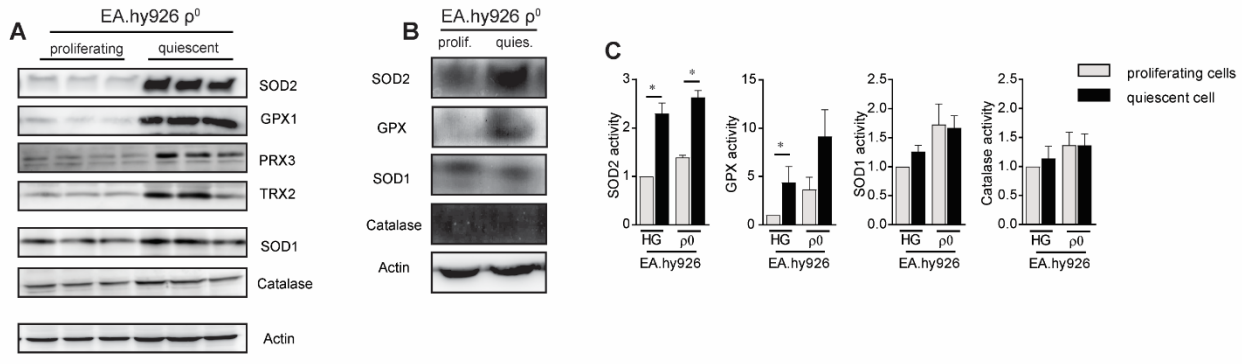

Figure 57 **Antioxidant defence of ρ⁰ cells is higher in quiescent cell when ETC is defective. (A)** Whole cell lysates from EA.hy926 were assessed by WB for expression of the indicated antioxidant proteins. **(B)** In-gel activities of indicated antioxidant enzymes were assessed in ρ⁰ cells. Data were quantified by densitometry **(C)**, and correlated to quiescent cell sample. Data shown are means ± SEM of 4 independent experiments.

3.6.4 ATP levels

We also examined the second metabolic effect of ETC inhibition that we studied, ATP depletion. Clearly, ATP cannot be produced from OXPHOS in ρ⁰ cells, as these cells do not have functional OXPHOS and cannot grow in low glucose condition. However, it is possible that pro-oxidant agents such as H_2O_2 or PEITC could compromise ATP production by glycolysis. We examined this possibility, but we could not detect any discernible effect of these agents on ATP levels (Figure 58). Therefore, an additional mechanism must be responsible for increased cell death sensitivity of quiescent ρ⁰ cells.

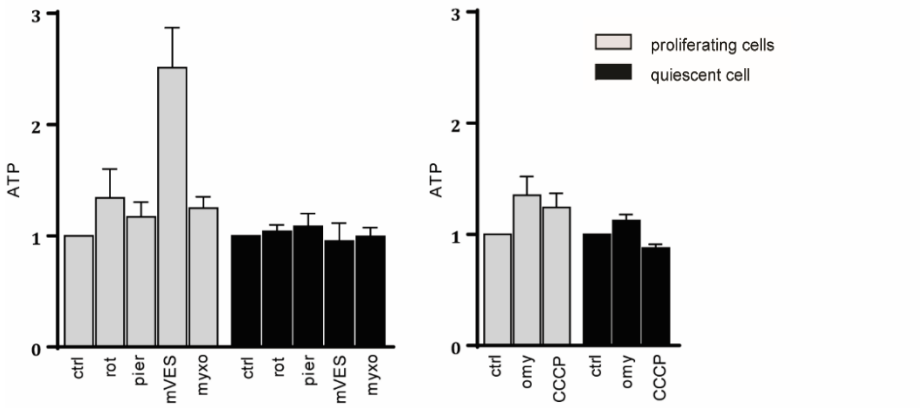

Figure 58 **Cellular ATP are maintained in ρ⁰ cells when ETC is compromised and inhibited.** EA.hy926 ρ⁰ were treated for 0,5 hour with 2 µM rotenone, 5 µM piericidin, 10 µM mVES, 20 µM myxothiazol, 25 µM oligomycin, 75µM CCCP and ATP level was assessed using luminescent assay. Results were corrected to cell number measured by crystal violet in a parallel plate. Data presented are the means ± SEM of 3 independent experiments.

3.6.5 Defective autophagy – a possible explanation for cell death sensitivity in quiescent ρ^0 cells

Autophagy is a process that serves as a mechanism for clearance of disrupted organelles and molecular debris, and can protect the cells in stress conditions. Pilot experiments (Figure 59) show that autophagy, in terms of LC3B protein expression and activation, appears deficient in quiescent ρ^0 cells. This was particularly apparent when we used chloroquine, which blocks autophagosome degradation in the lysosome (autophagosome-lysosome fusion, hence autophagic flux) and therefore amplifies the signature of autophagic defects. While these autophagy-related observations may reflect correlation rather than causality, these results look very promising and will be elaborated in a follow-up research to establish the possible functional relevance of defective autophagy.

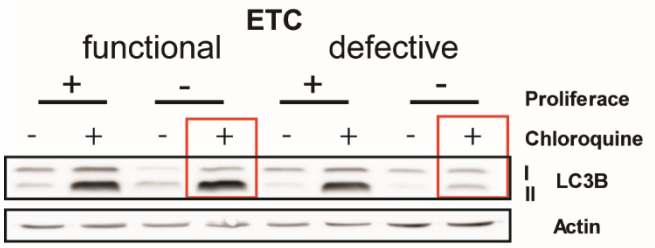

Figure 59 **Defect in ETC is linked to the defect in autophagy**. EA.hy926 whole cell lysates from ETC-defective ρ^0 and parental ETC-functional cells was assessed for protein levels of autophagic protein LC3B by WB method. To inhibit autophagosome degradation 50 μM chloroquine was added to the cells for 16 hours. Red squares mark observed change in autophagy. Representative picture of three is presented.

All the data suggest, that functional ETC may have an important role in the phenomenon of different cell death susceptibility upon ETC inhibition. Entering a quiescence state bring resistance by increased antioxidant defence, but defective ETC may override this effect by compromising autophagy flux, which may prove dominant for the ultimate cell fate.

4 Discussion

In spite of considerable advances in molecular cancer therapy, cancer remains one of the major causes of premature death [242]. Between the most frequent carcinomas, breast cancer is responsible for a high number of deaths and includes subtypes which are very challenging to treat [243]. ETC targeting has been described as a particularly effective approach in cancer treatment. Recently the efficacy and low toxicity has been demonstrated for ETC targeted drugs in multiple pre-clinical cancer models [208, 244]. Notwithstanding the considerable effort that has been invested in uncovering the mechanisms governing susceptibility of cancer cells to ETC inhibition-induced cell death, the molecular mechanisms sensitising cancer cells to this kind of treatment and even those that protect normal cells and significantly contribute to specificity are still unknown.

Modification of existing drugs with available pharmacological and toxicity profiles is a useful way to obtain new therapeutic agents. Among the commonly used anticancer drugs suitable for modification we selected tamoxifen. Tamoxifen is used as a first-line therapy of estrogen receptor-positive breast cancer, although high percentage of patients develop resistance caused by multiple molecular reasons, for example by the overexpression of the *HER2/neu* (also referred to as ErbB2) oncogene. [245] In addition, high number of patients suffers tumour relapse and tamoxifen treatment also has some undesired side effects [217, 218]. At the same time, tamoxifen in supra-pharmacological doses inhibits cellular respiration via CI [246]. This opened an avenue for designing a novel anticancer compound predicted to target CI that could increase effectivity and expand applicability to breast cancer subtypes that are at present resistant to the unmodified tamoxifen.

To overcome the resistance issue, to cope with side-effects as well as to enhance efficacy, several compounds directed at the ETC were recently designed in our laboratory and synthetized by our collaborators [208, 213, 247]. Similarly we modified tamoxifen to produce mitochondria-targeted tamoxifen - MitoTam. MitoTam is a tamoxifen conjugated with the mitochondria-targeting TPP^+ group, which gives to the original tamoxifen moiety substantial potency in accumulation at the matrix/IMM interface close to its intended molecular target, CI.

In the first part of this study we therefore investigated the effect of MitoTam on cancer cells to uncover the mechanisms that sensitize to ETC inhibition. We found that MitoTam kills a variety of breast cancer cells with a much higher efficacy than tamoxifen and is also more efficient in killing Her2^{high} cells and tumours compared to those where Her2 expression was low. Moreover, we observed very efficient suppression of experimental Her2^{high} breast carcinoma growth *in vivo*. Regarding the molecular target, we verified that mitochondria targeting substantially enhanced the weak native inhibitory activity of tamoxifen towards CI [212]. It results in a much more efficient suppression of CI enzymatic activity as well as CI-dependent respiration, and leading to enhanced generation of ROS from the ETC [105, 208]. Rather surprisingly, we also discovered that MitoTam treatment resulted in a disruption of respiratory SCs, which was particularly apparent in the Her2^{high} background where SCs are more assembled, consistent with the increased respiration of Her2^{high} cells and tumours. This is in compliance of the SCs role in facilitating passage of reduced electron carriers such as CoQ within the ETC [64, 248] and prevention of premature escape of electrons, thereby limiting ROS formation. Accordingly, disruption of SCs, possibly by direct MitoTam binding or by initial ROS produced from CI, could amplify the overall rate of ROS generation specifically in Her2^{high} background and push the Her2^{high} cells over the threshold of oxidative stress to cell death.

The results discussed above raise the possibility that higher ETC activity could directly sensitize cells to MitoTam and other ETC inhibitors because of the higher propensity to produce ROS as a consequence of ETC inhibition in such a situation. Therefore, mitochondria-derived oxidative stress could be the initiating factor of cell death after ETC inhibition while resistance of cells could follow from the ability to cope with increased ROS levels by antioxidant scavenging. We therefore addressed the question why our ETC disrupting agents are well tolerated in animals, and if relative differences in respiration level/ROS production/detoxification could account for the specificity observed. This issue is of high importance for efficient and save cancer therapy.

The greatest difference between somatic and cancer cells and main hallmark of cancer cells is the proliferative status. Most of the somatic cells in the organism are in a quiescent, non-proliferative state. There, changes associated with entering quiescence may play an important role in resistance to ETC inhibition, as suggested by previous work [224, 249]. Before we set out on this research, we presumed that maybe quiescent cells might have depressed metabolism, living in a frugal manner not requiring excessive energy or building blocks for biosynthesis. This would result in less ROS being formed upon ETC inhibition, and similarly to the above described differences among different subsets of cancer cells, increased ETC activity in proliferating cells could sensitize to cell death. To our surprise, in the current study focused on ETC inhibitors we found that quiescent cells feature increased respiration, elevated SC assembly and mitochondria that produce more NADH, consistent with fully active TCA cycle in quiescent cells that has been reported previously [26]. Apparently, the ETC gains prominence in quiescence, and quiescent non-transformed cells should be susceptible to cell death induced by ETC inhibition, resulting either from increased ROS generation or mitochondrial ATP loss (discussed below). Furthermore, elevated NADH is expected to stimulate ROS generation from the ETC [88]. Indeed, NADH accumulation is efficiently induced in mitochondria of quiescent cells upon the ETC blockade.

Notwithstanding the above reasoning, inhibition of ETC under ample glucose supply led to reduced ROS production and reduced cell death in quiescent cells when compared to proliferating cells, suggesting that ROS detoxification is increased in quiescent cells as proposed previously [250-252]. It thus seems that the increased antioxidant defence in quiescent cells overrides the possible sensitizing effect of higher respiratory rate/ETC activity. This is not the case in cancer cells and tumours, where the correlation between ETC activity sensitivity is maintained. Indeed, we detected higher expression of antioxidant defence components in somatic versus tumour tissue in a mouse model of spontaneous breast carcinoma. Data presented herein also point to increased ROS, and not to ATP depletion, being the dominant factor in cell death induction upon ETC inhibition in proliferating cells when glucose is not limiting. That also imply that ROS detoxification, not the ETC status or increased ETC-mediated ATP production, determine resistance to cell death in quiescent cells. This is in direct contrast to cancer cells, where correlation between ETC

activity/assembly and the efficacy of ETC inhibitors to induce cell death has been established in multiple studies [105, 213, 253-255]. Furthermore, it is in line with reports showing that redox modulation may be an effective anti-cancer strategy [256, 257].

Pharmacological and genetic manipulations of SOD2 and TRXR2, the mitochondrial thioredoxin reductase [258], revealed that the SOD2 - thioredoxin axis of antioxidant defence plays a principal role in efficient protection of quiescent cells from ETC blockade-induced ROS and cell death. In contrast, interference with the glutathione system (GPX1 and GSR) led to some elevation of ROS upon ETC blockade in quiescent cells without increase in cell death, suggesting that this system plays a less important role in quiescent cells. Moreover, moderate decrease in GPX1 level is not crucial for protection against cell death hence organisms lacking GSR utilise other, similar thiol systems [155].

This is consistent with the notion that superoxide is the primary species of ROS-induced damage, possibly leading to direct oxidation of various mitochondrial components [259-261]. The thioredoxin system may counter this oxidative damage, consistent with its role in the regulation of cell death [262-264]. In agreement, deletion of SOD2, TRX2 or TRXR2 in mice is incompatible with life [265-267], while genetic inactivation of GSR or GPX1 is not associated with lethality [268, 269].

The sensitivities of proliferating versus quiescent cells to ETC inhibition change dramatically in the conditions of glucose limitation. Here, a substantial decrease of cellular ATP upon ETC blockade in quiescent cells was observed, which correlates with increased cell death. Downregulation of antioxidant defence components did not increase cell death any further, suggesting that cell death in this situation is largely ROS-independent, instead relating to acute bioenergetic stress. In contrast to quiescent cells, proliferating cells strongly upregulate glucose uptake upon ETC suppression by increasing the level of glucose transporters, which likely compensates for the loss of ATP production in mitochondria. This effect may be particularly important for scavenging glucose when its availability is low, and may explain why quiescent cells are more sensitive to ETC inhibition when glucose is below its normal physiological range. A similar mechanism has been reported in cancer cells, where

the failure to upregulate glucose transporters and glucose uptake sensitized to ETC inhibition only when glucose availability was limiting [270].

To interpret the results of this study, it is important to realize that the high and low glucose media represent situations of ample and limited glucose supply. In low glucose media, the glucose concentrations found in our system within the time frame of the experiment are much lower than those that are regularly encountered *in vivo* in well perfused tissues [271, 272]. In fact, when ETC inhibitors were applied in fresh low (1 g/l) glucose media corresponding to the physiological 5 mM glucose concentration, no ATP depletion was observed. This means that in normal healthy tissues where perfusion is intact, glucose does not present a limiting factor, and it is expected that effective inactivation of ETC blockade-induced ROS by antioxidant defence will play the primary role in governing sensitivity. On the other hand, in poorly perfused regions, such as hypoxic areas of tumours where the availability of nutrients is low, the application of ETC inhibitors may significantly accelerate cell death in a ROS-independent manner. This is consistent with reports of low glucose availability in tumours [271, 273], and with previous findings showing that ETC inhibition was highly effective in non-perfused hypoxic regions [274]. We therefore propose that the mechanism for the observed selectivity of ETC inhibition in cancer is two-fold. First, elevated antioxidant defence limits ROS production upon ETC inhibition in somatic quiescent cells that do not suffer from glucose limitation, the large majority of cells in an organism. Second, in poorly perfused tumours where glucose is limiting, the application of ETC inhibitors will lead to bioenergetic catastrophe, amplifying the ROS-related effects, and broadening effectivity to cancer cells that might have a 'quiescent'-like phenotype [254].

In stark contrast, preliminary data indicate that quiescent cells without functional ETC are highly susceptible to ROS inducers, suggesting that increased resistance of quiescent cells to oxidative stress is compromised by ETC deficiency. This is despite the fact that results demonstrate high levels of antioxidant defence components also in quiescent cells with deficient ETC. Hence, susceptibility of ETC-deficient quiescent cells to ROS inducers cannot be explained by non-functional mitochondrial antioxidant defence, and other mechanisms must therefore be involved. Moreover, there is strong evidence that quiescent ETC-defective cells no longer show resistance to cell death compared to corresponding proliferating cells

and the reduced levels of ROS upon pro-oxidant treatment so typical for quiescent cells with function ETC could not be established in the ETC-deficient situation. Therefore, the role of stress-response pathways, such as autophagy [275], may be important in this context. Interestingly, we have found that the autophagic flux is compromised in ETC-deficient quiescent cells, whereas it is increased in quiescent cells when the ETC is functional. Basal autophagy is a process that serves to degrade aged and defective cellular organelles and macromolecules for reprocessing, but can also be activated under stress conditions as a mean to provide bioenergetic intermediates and recycle damaged components [177]. It is therefore possible that defective autophagy may sensitize ETC-deficient cells to cell death and be responsible for the increased sensitivity of ETC-deficient quiescent cells to ROS. Functional ETC might be necessary to maintain autophagy in quiescent cells, but this is only a speculation now and this issue will be a subject of further investigation.

To conclude, ETC targeting represent a new, promising approach for treatment of multiple cancer types, including neoplasias that are difficult-to-treat, and resistant populations of cancer cells within tumours [253, 255, 276]. As such, this study is relevant for future development and optimization of very interesting, novel anti-cancer agents that target the ETC and present potential broad-spectrum therapeutics for a range of malignancies.

5 Conclusion

In this dissertation, we focused on resolving the molecular mechanism of sensitivity to mitochondria-targeted anticancer agents that act primarily as inhibitors of mitochondrial respiration. We also resolved the molecular mechanisms that contribute to the specificity of ETC inhibitors in the cancer settings. Finally, we demonstrated the importance of functional ETC in the specificity phenomenon.

First of all, we showed that mitochondrial targeted tamoxifen derivative, referred to as MitoTam, eliminates breast cell lines *in vitro* and mammary carcinoma tumours *in vivo* more effectively than the original tamoxifen via inhibiting CI of the ETC. We found that the presence of the breast cancer oncogene Her2 sensitises to MitoTam treatment and this is linked to higher ETC assembly into SCs and results in higher rate of respiration in the $Her2^{high}$ setting. In this situation, MitoTam treatment leads to superior ROS production as a consequence of SC disruption. The first conclusion of this thesis therefore is that increased respiratory rate and increased assembly of the ETC into SCs in transformed cells sensitizes to ETC inhibition. This has practical implication for the treatment of residual drug-resistant populations of cancer cells that often feature increased respiration and could be potentially eliminated by ETC targeting.

Second, we described the molecular basis for the resistance of somatic cells and sensitivity of proliferating cells to mitochondrial targeted ETC inhibitors. We resolved that when glucose is available in sufficient amount, proliferating cells undergo programmed cell death when ETC is inhibited. Higher susceptibility of proliferating cells can be explained by the increased ETC-derived ROS levels upon ETC inhibition, ATP synthase inhibition or direct ROS mediators treatment. In spite of increased ETC enzymatic activity in quiescent cells and their mitochondrial SC assemblies, their antioxidant defence is set to cope with possible increased ROS levels, making quiescent cells more resilient to effect of OXPHOS inhibitors. The protection is provided specifically by the SOD2 and thioredoxin system. Furthermore, it is possible that while SOD2/thioredoxin system are prominent in quiescent cells, the glutathione system may be more important in proliferating cells (as suggested by the NAC experiments). To conclude, antioxidant defence plays a central role in the protection of

quiescent somatic cells from ETC-derived oxidative insult and cell death, and significantly contributes to the specificity of ETC-targeted anticancer agents.

Third, in the conditions of glucose limitation, expected to occur in badly perfused tumours, quiescent cells showed higher sensitivity to cell death. This was linked to ATP depletion upon ETC-inhibition rather than to ROS, and derived from the inability of quiescent cells to upregulate glucose uptake and compensate for the absence of mitochondrial ATP production by glycolysis. Therefore, we conclude that in condition of glucose deprivation that are unlikely to occur in normal perfused tissues, ATP depletion plays the major role and contributes to the specificity of ETC inhibition.

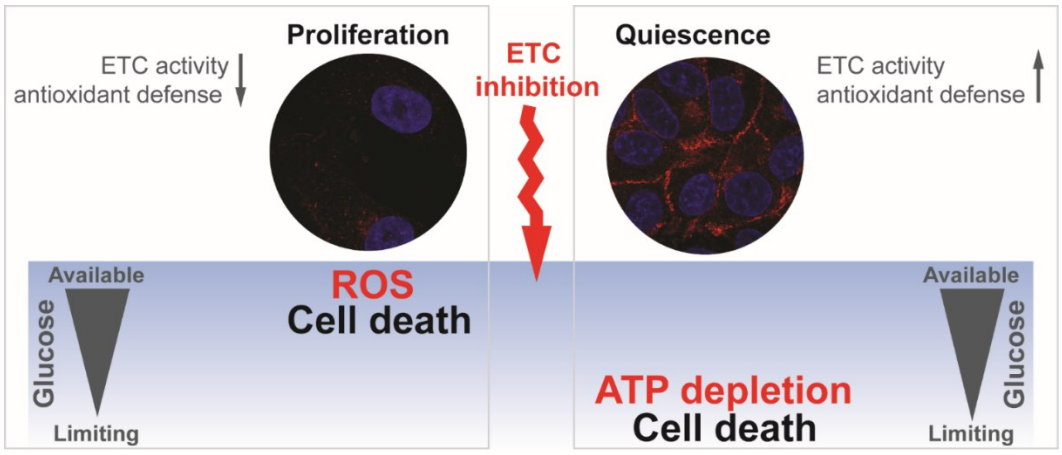

Figure 60 **Molecular bases of sensitivity to electron transport chain inhibition-induced cell death**

At the very end of the study, we evaluated the influence of ETC functionality on the sensitivity to cell death in quiescent cells. Cells without mtDNA and thus lacking mitochondrial respiration had altered sensitivity to cell death in the quiescent state. These ETC-deficient quiescent cells became sensitised to direct ROS inducers. Therefore, when ETC in not functional important stress response pathways such as autophagy may become compromised. We conclude that, surprisingly, functional ETC plays an important role in stress protection in quiescent cells.

In summary, we propose that ETC-specific anticancer treatment represent a promising therapeutic approach. Targeting of ETC inhibitors to mitochondria enhances their activity, and is particularly effective when cancer cells feature increased cellular respiration and increased ETC assembly. The specificity of ETC inhibition in cancer is in part conferred by increased antioxidant defence in non-proliferating non-transformed cells. ROS production from the ETC is the dominant factor that determines susceptibility to cell death induced by ETC disruption in a situation when glucose is not limiting. Hence, ETC inhibitors that induce maximal ROS will kill proliferating cancer cells most efficiently while maintaining specificity. On the other hand, in a situation of glucose limitation characteristic for tumours, ATP depletion upon ETC disruption gains prominence, and non-proliferating cells become highly susceptible to cell death because they are unable to upregulate glucose uptake. This will supplement the ROS-related effects and optimize impact towards cancer, including cancer cells with a dormant-like phenotype.

6 List of abbreviations

ANT	adenine nucleotide translocase
Bcl-2	B-cell lymphoma
BNE	blue native electrophoresis
CCCP	carbonyl cyanide 3-chlorophenylhydrazone
CI, CII, CIII, CIV	respiratory mitochondrial complex I,II, III, IV
CoQ ($CoQH_2$)	coenzyme Q_{10}/ ubiquinone (reduced form ubiquinol)
CV	ATP synthase
cyt *c*	cytochrome c
DCF-DA	2', 7'-dichlorofluorescin diacetate
DHE	dihydroethidium
ETC	electron transport chain
FAD	flavin adenine dinucleotide
FCCP	carbonyl cyanide 4-(trifluoromethoxy)-phenylhydrazone
GPX	glutathione peroxidase
GRX	glutaredoxin
GSH and GSSG	glutathione (oxidized form)
GSR	glutathione reductase
hrCNE	high-resolution clear native electrophoresis
IMM	inner mitochondrial membrane
IMS	inter-membrane space
mtDNA	mitochondrial DNA
NAC	N-acetyl cysteine

NAD(P)H	nicotinamide adenine dinucleotide (phosphate) coenzyme
OMM	outer mitochondrial membrane
OXPHOS	oxidative phosphorylation
PARP	poly (ADP-ribose) polymerase
PEITC	phenethyl isothiocyanate
PRX	peroxiredoxin
RNOS	reactive nitric oxide species
ROS	reactive oxygen species
SCs	supercomplexes
SOD1	superoxide dismutase 1 (CuZnSOD)
SOD2	manganese superoxide dismutase (MnSOD)
TCA cycle	tricarboxylic acid cycle
TOM	translocase of the outer membrane
TPP^+	tetraphenylphosphonium cation
TRX	thioredoxin
TRXR	thioredoxin reductase
VDAC	voltage-dependent anion channel
WB	western blot

7 List of references

[1] Fisher, R., Pusztai, L., and Swanton, C. (2013) Cancer heterogeneity: implications for targeted therapeutics, *Br J Cancer 108*, 479-485.

[2] Ma, X., and Yu, H. (2006) Global burden of cancer, *Yale J Biol Med 79*, 85-94.

[3] Abbott, R. G., Forrest, S., and Pienta, K. J. (2006) Simulating the hallmarks of cancer, *Artificial life 12*, 617-634.

[4] Hanahan, D., and Weinberg, R. A. (2011) Hallmarks of cancer: the next generation, *Cell 144*, 646-674.

[5] Cheng, N., Chytil, A., Shyr, Y., Joly, A., and Moses, H. L. (2008) Transforming growth factor-beta signaling-deficient fibroblasts enhance hepatocyte growth factor signaling in mammary carcinoma cells to promote scattering and invasion, *Mol Cancer Res 6*, 1521-1533.

[6] Davies, M. A., and Samuels, Y. (2010) Analysis of the genome to personalize therapy for melanoma, *Oncogene 29*, 5545-5555.

[7] Jafri, M. A., Ansari, S. A., Alqahtani, M. H., and Shay, J. W. (2016) Roles of telomeres and telomerase in cancer, and advances in telomerase-targeted therapies, *Genome Med 8*, 69.

[8] Nishida, N., Yano, H., Nishida, T., Kamura, T., and Kojiro, M. (2006) Angiogenesis in cancer, *Vasc Health Risk Manag 2*, 213-219.

[9] Vander Heiden, M. G., Cantley, L. C., and Thompson, C. B. (2009) Understanding the Warburg effect: the metabolic requirements of cell proliferation, *Science 324*, 1029-1033.

[10] Koppenol, W. H., Bounds, P. L., and Dang, C. V. (2011) Otto Warburg's contributions to current concepts of cancer metabolism, *Nature reviews. Cancer 11*, 325-337.

[11] Ward, Patrick S., and Thompson, Craig B. (2012) Metabolic Reprogramming: A Cancer Hallmark Even Warburg Did Not Anticipate, *Cancer cell 21*, 297-308.

[12] Aon, M. A., Stanley, B. A., Sivakumaran, V., Kembro, J. M., O'Rourke, B., Paolocci, N., and Cortassa, S. (2012) Glutathione/thioredoxin systems modulate mitochondrial H2O2 emission: an experimental-computational study, *The Journal of general physiology 139*, 479-491.

[13] Liberti, M. V., and Locasale, J. W. (2016) The Warburg Effect: How Does it Benefit Cancer Cells?, *Trends in biochemical sciences 41*, 211-218.

[14] Jones, R. G., and Thompson, C. B. (2009) Tumor suppressors and cell metabolism: a recipe for cancer growth, *Genes & development 23*, 537-548.

[15] DeBerardinis, R. J., Lum, J. J., Hatzivassiliou, G., and Thompson, C. B. (2008) The biology of cancer: metabolic reprogramming fuels cell growth and proliferation, *Cell metabolism 7*, 11-20.

[16] Kennedy, K. M., and Dewhirst, M. W. (2010) Tumor metabolism of lactate: the influence and therapeutic potential for MCT and CD147 regulation, *Future Oncol 6*, 127-148.

[17] Feron, O. (2009) Pyruvate into lactate and back: from the Warburg effect to symbiotic energy fuel exchange in cancer cells, *Radiother Oncol 92*, 329-333.

[18] Antico Arciuch, V. G., Elguero, M. E., Poderoso, J. J., and Carreras, M. C. (2012) Mitochondrial regulation of cell cycle and proliferation, *Antioxidants & redox signaling 16*, 1150-1180.

[19] Coller, H. A. (2011) Cell biology. The essence of quiescence, *Science 334*, 1074-1075.

[20] Chen, W., Dong, J., Haiech, J., Kilhoffer, M. C., and Zeniou, M. (2016) Cancer Stem Cell Quiescence and Plasticity as Major Challenges in Cancer Therapy, *Stem Cells Int 2016*, 1740936.

[21] Malumbres, M. (2014) Cyclin-dependent kinases, *Genome Biol 15*, 122.
[22] Malumbres, M., Harlow, E., Hunt, T., Hunter, T., Lahti, J. M., Manning, G., Morgan, D. O., Tsai, L. H., and Wolgemuth, D. J. (2009) Cyclin-dependent kinases: a family portrait, *Nature cell biology 11*, 1275-1276.
[23] Malumbres, M., Sotillo, R., Santamaria, D., Galan, J., Cerezo, A., Ortega, S., Dubus, P., and Barbacid, M. (2004) Mammalian cells cycle without the D-type cyclin-dependent kinases Cdk4 and Cdk6, *Cell 118*, 493-504.
[24] Malumbres, M., and Barbacid, M. (2005) Mammalian cyclin-dependent kinases, *Trends in biochemical sciences 30*, 630-641.
[25] Sun, X., and Feinberg, M. W. (2015) Regulation of endothelial cell metabolism: just go with the flow, *Arterioscler Thromb Vasc Biol 35*, 13-15.
[26] Lemons, J. M., Feng, X. J., Bennett, B. D., Legesse-Miller, A., Johnson, E. L., Raitman, I., Pollina, E. A., Rabitz, H. A., Rabinowitz, J. D., and Coller, H. A. (2010) Quiescent fibroblasts exhibit high metabolic activity, *PLoS Biol 8*, e1000514.
[27] Tan, A. S., Baty, J. W., Dong, L. F., Bezawork-Geleta, A., Endaya, B., Goodwin, J., Bajzikova, M., Kovarova, J., Peterka, M., Yan, B., et al. (2015) Mitochondrial genome acquisition restores respiratory function and tumorigenic potential of cancer cells without mitochondrial DNA, *Cell metabolism 21*, 81-94.
[28] Weinberg, F., Hamanaka, R., Wheaton, W. W., Weinberg, S., Joseph, J., Lopez, M., Kalyanaraman, B., Mutlu, G. M., Budinger, G. R., and Chandel, N. S. (2010) Mitochondrial metabolism and ROS generation are essential for Kras-mediated tumorigenicity, *Proceedings of the National Academy of Sciences of the United States of America 107*, 8788-8793.
[29] Kluckova, K., Bezawork-Geleta, A., Rohlena, J., Dong, L., and Neuzil, J. (2013) Mitochondrial complex II, a novel target for anti-cancer agents, *Biochimica et biophysica acta 1827*, 552-564.
[30] Cheng, G., Zielonka, J., Ouari, O., Lopez, M., McAllister, D., Boyle, K., Barrios, C. S., Weber, J. J., Johnson, B. D., Hardy, M., et al. (2016) Mitochondria-Targeted Analogues of Metformin Exhibit Enhanced Antiproliferative and Radiosensitizing Effects in Pancreatic Cancer Cells, *Cancer research 76*, 3904-3915.
[31] Rohlena, J., Dong, L. F., and Neuzil, J. (2013) Targeting the mitochondrial electron transport chain complexes for the induction of apoptosis and cancer treatment, *Current pharmaceutical biotechnology 14*, 377-389.
[32] Green, R. (2017) Admirable Quia Cell Parts and Functions Flash Cards, *Transmission Electron Microscope Parts and Functions*.
[33] Armand, R., Channon, J. Y., Kintner, J., White, K. A., Miselis, K. A., Perez, R. P., and Lewis, L. D. (2004) The effects of ethidium bromide induced loss of mitochondrial DNA on mitochondrial phenotype and ultrastructure in a human leukemia T-cell line (MOLT-4 cells), *Toxicology and applied pharmacology 196*, 68-79.
[34] Yu, M., Shi, Y., Wei, X., Yang, Y., Zhou, Y., Hao, X., Zhang, N., and Niu, R. (2007) Depletion of mitochondrial DNA by ethidium bromide treatment inhibits the proliferation and tumorigenesis of T47D human breast cancer cells, *Toxicology letters 170*, 83-93.
[35] Murphy, M. P., and Smith, R. A. (2007) Targeting antioxidants to mitochondria by conjugation to lipophilic cations, *Annu Rev Pharmacol Toxicol 47*, 629-656.
[36] Birsoy, K., Wang, T., Chen, W. W., Freinkman, E., Abu-Remaileh, M., and Sabatini, D. M. (2015) An Essential Role of the Mitochondrial Electron Transport Chain in Cell Proliferation Is to Enable Aspartate Synthesis, *Cell 162*, 540-551.

[37] Sullivan, L. B., Gui, D. Y., Hosios, A. M., Bush, L. N., Freinkman, E., and Vander Heiden, M. G. (2015) Supporting Aspartate Biosynthesis Is an Essential Function of Respiration in Proliferating Cells, *Cell 162*, 552-563.
[38] Schagger, H., and Pfeiffer, K. (2000) Supercomplexes in the respiratory chains of yeast and mammalian mitochondria, *The EMBO journal 19*, 1777-1783.
[39] Acin-Perez, R., Fernandez-Silva, P., Peleato, M. L., Perez-Martos, A., and Enriquez, J. A. (2008) Respiratory active mitochondrial supercomplexes, *Molecular cell 32*, 529-539.
[40] Belevich, I., Bloch, D. A., Belevich, N., Wikstrom, M., and Verkhovsky, M. I. (2007) Exploring the proton pump mechanism of cytochrome c oxidase in real time, *Proceedings of the National Academy of Sciences of the United States of America 104*, 2685-2690.
[41] Lemarie, A., and Grimm, S. (2011) Mitochondrial respiratory chain complexes: apoptosis sensors mutated in cancer?, *Oncogene 30*, 3985-4003.
[42] Hirst, J., Carroll, J., Fearnley, I. M., Shannon, R. J., and Walker, J. E. (2003) The nuclear encoded subunits of complex I from bovine heart mitochondria, *Biochimica et biophysica acta 1604*, 135-150.
[43] Sazanov, L. A. (2015) A giant molecular proton pump: structure and mechanism of respiratory complex I, *Nat Rev Mol Cell Biol 16*, 375-388.
[44] Balsa, E., Marco, R., Perales-Clemente, E., Szklarczyk, R., Calvo, E., Landazuri, M. O., and Enriquez, J. A. (2012) NDUFA4 is a subunit of complex IV of the mammalian electron transport chain, *Cell metabolism 16*, 378-386.
[45] Baradaran, R., Berrisford, J. M., Minhas, G. S., and Sazanov, L. A. (2013) Crystal structure of the entire respiratory complex I, *Nature 494*, 443-448.
[46] Sun, F., Huo, X., Zhai, Y., Wang, A., Xu, J., Su, D., Bartlam, M., and Rao, Z. (2005) Crystal structure of mitochondrial respiratory membrane protein complex II, *Cell 121*, 1043-1057.
[47] Quinlan, C. L., Orr, A. L., Perevoshchikova, I. V., Treberg, J. R., Ackrell, B. A., and Brand, M. D. (2012) Mitochondrial complex II can generate reactive oxygen species at high rates in both the forward and reverse reactions, *The Journal of biological chemistry 287*, 27255-27264.
[48] Drose, S. (2013) Differential effects of complex II on mitochondrial ROS production and their relation to cardioprotective pre- and postconditioning, *Biochimica et biophysica acta 1827*, 578-587.
[49] Solmaz, S. R., and Hunte, C. (2008) Structure of complex III with bound cytochrome c in reduced state and definition of a minimal core interface for electron transfer, *The Journal of biological chemistry 283*, 17542-17549.
[50] Mulkidjanian, A. Y. (2005) Ubiquinol oxidation in the cytochrome bc1 complex: reaction mechanism and prevention of short-circuiting, *Biochimica et biophysica acta 1709*, 5-34.
[51] Lenaz, G., and Genova, M. L. (2010) Structure and organization of mitochondrial respiratory complexes: a new understanding of an old subject, *Antioxidants & redox signaling 12*, 961-1008.
[52] Alexandrov, L. B., Nik-Zainal, S., Wedge, D. C., Aparicio, S. A., Behjati, S., Biankin, A. V., Bignell, G. R., Bolli, N., Borg, A., Borresen-Dale, A. L., et al. (2013) Signatures of mutational processes in human cancer, *Nature 500*, 415-421.
[53] Richter, O. M., and Ludwig, B. (2003) Cytochrome c oxidase--structure, function, and physiology of a redox-driven molecular machine, *Reviews of physiology, biochemistry and pharmacology 147*, 47-74.

[54] Lee, I., Bender, E., and Kadenbach, B. (2002) Control of mitochondrial membrane potential and ROS formation by reversible phosphorylation of cytochrome c oxidase, *Molecular and cellular biochemistry 234-235*, 63-70.
[55] Symersky, J., Osowski, D., Walters, D. E., and Mueller, D. M. (2012) Oligomycin frames a common drug-binding site in the ATP synthase, *Proceedings of the National Academy of Sciences of the United States of America 109*, 13961-13965.
[56] Abrahams, J. P., Leslie, A. G. W., Lutter, R., and Walker, J. E. (1994) Structure at 2.8 A resolution of F1-ATPase from bovine heart mitochondria, *Nature 370*, 621-628.
[57] Jonckheere, A. I., Smeitink, J. A., and Rodenburg, R. J. (2012) Mitochondrial ATP synthase: architecture, function and pathology, *Journal of inherited metabolic disease 35*, 211-225.
[58] Benz, R., and McLaughlin, S. (1983) The molecular mechanism of action of the proton ionophore FCCP (carbonylcyanide p-trifluoromethoxyphenylhydrazone), *Biophys J 41*, 381-398.
[59] Chopineaux-Courtois, V., Reymond, F., Bouchard, G., Carrupt, P.-A., Testa, B., and Girault, H. H. (1999) Effects of Charge and Intramolecular Structure on the Lipophilicity of Nitrophenols, *Journal of the American Chemical Society 121*, 1743-1747.
[60] Tharmalingam, N., Jayamani, E., Rajamuthiah, R., Castillo, D., Fuchs, B. B., Kelso, M. J., and Mylonakis, E. (2017) Activity of a novel protonophore against methicillin-resistant Staphylococcus aureus, *Future Med Chem 9*, 1401-1411.
[61] Ikeda, K., Shiba, S., Horie-Inoue, K., Shimokata, K., and Inoue, S. (2013) A stabilizing factor for mitochondrial respiratory supercomplex assembly regulates energy metabolism in muscle, *Nat Commun 4*, 2147.
[62] Blaza, J. N., Serreli, R., Jones, A. J., Mohammed, K., and Hirst, J. (2014) Kinetic evidence against partitioning of the ubiquinone pool and the catalytic relevance of respiratory-chain supercomplexes, *Proceedings of the National Academy of Sciences of the United States of America 111*, 15735-15740.
[63] Acín-Pérez, R., Bayona-Bafaluy, M. P., Fernández-Silva, P., Moreno-Loshuertos, R., Pérez-Martos, A., Bruno, C., Moraes, C. T., and Enríquez, J. A. (2004) Respiratory Complex III Is Required to Maintain Complex I in Mammalian Mitochondria, *Molecular cell 13*, 805-815.
[64] Maranzana, E., Barbero, G., Falasca, A. I., Lenaz, G., and Genova, M. L. (2013) Mitochondrial respiratory supercomplex association limits production of reactive oxygen species from complex I, *Antioxidants & redox signaling 19*, 1469-1480.
[65] Acin-Perez, R., and Enriquez, J. A. (2014) The function of the respiratory supercomplexes: the plasticity model, *Biochimica et biophysica acta 1837*, 444-450.
[66] Stroh, C., Wang, H., Bash, R., Ashcroft, B., Nelson, J., Gruber, H., Lohr, D., Lindsay, S. M., and Hinterdorfer, P. (2004) Single-molecule recognition imaging microscopy, *Proceedings of the National Academy of Sciences of the United States of America 101*, 12503-12507.
[67] Letts, J. A., Fiedorczuk, K., and Sazanov, L. A. (2016) The architecture of respiratory supercomplexes, *Nature 537*, 644.
[68] Letts, J. A., Fiedorczuk, K., and Sazanov, L. A. (2016) The architecture of respiratory supercomplexes, *Nature 537*, 644-648.
[69] Habersetzer, J., Larrieu, I., Priault, M., Salin, B., Rossignol, R., Brethes, D., and Paumard, P. (2013) Human F1F0 ATP synthase, mitochondrial ultrastructure and OXPHOS impairment: a (super-)complex matter?, *PloS one 8*, e75429.

[70] Kovarova, N., Mracek, T., Nuskova, H., Holzerova, E., Vrbacky, M., Pecina, P., Hejzlarova, K., Kluckova, K., Rohlena, J., Neuzil, J., et al. (2013) High molecular weight forms of mammalian respiratory chain complex II, *PloS one 8*, e71869.
[71] Wittig, I., and Schagger, H. (2008) Structural organization of mitochondrial ATP synthase, *Biochimica et biophysica acta 1777*, 592-598.
[72] Giorgio, V., von Stockum, S., Antoniel, M., Fabbro, A., Fogolari, F., Forte, M., Glick, G. D., Petronilli, V., Zoratti, M., Szabo, I., et al. (2013) Dimers of mitochondrial ATP synthase form the permeability transition pore, *Proceedings of the National Academy of Sciences of the United States of America 110*, 5887-5892.
[73] Cogliati, S., Frezza, C., Soriano, M. E., Varanita, T., Quintana-Cabrera, R., Corrado, M., Cipolat, S., Costa, V., Casarin, A., Gomes, L. C., et al. (2013) Mitochondrial cristae shape determines respiratory chain supercomplexes assembly and respiratory efficiency, *Cell 155*, 160-171.
[74] Chaban, Y., Boekema, E. J., and Dudkina, N. V. (2014) Structures of mitochondrial oxidative phosphorylation supercomplexes and mechanisms for their stabilisation, *Biochimica et biophysica acta 1837*, 418-426.
[75] Loschen, G., Flohe, L., and Chance, B. (1971) Respiratory chain linked H(2)O(2) production in pigeon heart mitochondria, *FEBS letters 18*, 261-264.
[76] Boveris, A., Oshino, N., and Chance, B. (1972) The cellular production of hydrogen peroxide, *The Biochemical journal 128*, 617-630.
[77] Cadenas, E., and Davies, K. J. (2000) Mitochondrial free radical generation, oxidative stress, and aging, *Free radical biology & medicine 29*, 222-230.
[78] Chen, Q., Vazquez, E. J., Moghaddas, S., Hoppel, C. L., and Lesnefsky, E. J. (2003) Production of reactive oxygen species by mitochondria: central role of complex III, *The Journal of biological chemistry 278*, 36027-36031.
[79] Kareyeva, A. V., Grivennikova, V. G., Cecchini, G., and Vinogradov, A. D. (2011) Molecular identification of the enzyme responsible for the mitochondrial NADH-supported ammonium-dependent hydrogen peroxide production, *FEBS letters 585*, 385-389.
[80] Tretter, L., and Adam-Vizi, V. (2004) Generation of reactive oxygen species in the reaction catalyzed by alpha-ketoglutarate dehydrogenase, *J Neurosci 24*, 7771-7778.
[81] Seifert, E. L., Estey, C., Xuan, J. Y., and Harper, M. E. (2010) Electron transport chain-dependent and -independent mechanisms of mitochondrial H2O2 emission during long-chain fatty acid oxidation, *The Journal of biological chemistry 285*, 5748-5758.
[82] Mracek, T., Holzerova, E., Drahota, Z., Kovarova, N., Vrbacky, M., Jesina, P., and Houstek, J. (2014) ROS generation and multiple forms of mammalian mitochondrial glycerol-3-phosphate dehydrogenase, *Biochimica et biophysica acta 1837*, 98-111.
[83] Drahota, Z., Chowdhury, S. K., Floryk, D., Mracek, T., Wilhelm, J., Rauchova, H., Lenaz, G., and Houstek, J. (2002) Glycerophosphate-dependent hydrogen peroxide production by brown adipose tissue mitochondria and its activation by ferricyanide, *Journal of bioenergetics and biomembranes 34*, 105-113.
[84] Turrens, J. F. (2003) Mitochondrial formation of reactive oxygen species, *The Journal of physiology 552*, 335-344.
[85] Quinlan, C. L., Perevoshchikova, I. V., Hey-Mogensen, M., Orr, A. L., and Brand, M. D. (2013) Sites of reactive oxygen species generation by mitochondria oxidizing different substrates, *Redox biology 1*, 304-312.
[86] Zhao, W., Diz, D. I., and Robbins, M. E. (2007) Oxidative damage pathways in relation to normal tissue injury, *The British journal of radiology 80 Spec No 1*, S23-31.

[87] Murphy, Michael P. (2009) How mitochondria produce reactive oxygen species, *Biochemical Journal 417*, 1-13.
[88] Murphy, M. P. (2009) How mitochondria produce reactive oxygen species, *The Biochemical journal 417*, 1-13.
[89] Kalbacova, M., Vrbacky, M., Drahota, Z., and Melkova, Z. (2003) Comparison of the effect of mitochondrial inhibitors on mitochondrial membrane potential in two different cell lines using flow cytometry and spectrofluorometry, *Cytometry. Part A : the journal of the International Society for Analytical Cytology 52*, 110-116.
[90] Watabe, M., and Nakaki, T. (2007) ATP depletion does not account for apoptosis induced by inhibition of mitochondrial electron transport chain in human dopaminergic cells, *Neuropharmacology 52*, 536-541.
[91] Brand, M. D. (2016) Mitochondrial generation of superoxide and hydrogen peroxide as the source of mitochondrial redox signaling, *Free radical biology & medicine 100*, 14-31.
[92] Halliwell, B., and Cross, C. E. (1994) Oxygen-derived species: their relation to human disease and environmental stress, *Environmental health perspectives 102 Suppl 10*, 5-12.
[93] Fukai, T., and Ushio-Fukai, M. (2011) Superoxide dismutases: role in redox signaling, vascular function, and diseases, *Antioxidants & redox signaling 15*, 1583-1606.
[94] Ricci, J. E., Waterhouse, N., and Green, D. R. (2003) Mitochondrial functions during cell death, a complex (I-V) dilemma, *Cell death and differentiation 10*, 488-492.
[95] Rohlena, J., Dong, L. F., Ralph, S. J., and Neuzil, J. (2011) Anticancer drugs targeting the mitochondrial electron transport chain, *Antioxidants & redox signaling 15*, 2951-2974.
[96] Scialo, F., Fernandez-Ayala, D. J., and Sanz, A. (2017) Role of Mitochondrial Reverse Electron Transport in ROS Signaling: Potential Roles in Health and Disease, *Frontiers in physiology 8*, 428.
[97] Fato, R., Bergamini, C., Bortolus, M., Maniero, A. L., Leoni, S., Ohnishi, T., and Lenaz, G. (2009) Differential effects of mitochondrial Complex I inhibitors on production of reactive oxygen species, *Biochimica et biophysica acta 1787*, 384-392.
[98] Dröse, S., and Brandt, U. (2012) Molecular Mechanisms of Superoxide Production by the Mitochondrial Respiratory Chain, In *Mitochondrial Oxidative Phosphorylation: Nuclear-Encoded Genes, Enzyme Regulation, and Pathophysiology* (Kadenbach, B., Ed.), pp 145-169, Springer New York, New York, NY.
[99] Hirst, J., King, M. S., and Pryde, K. R. (2008) The production of reactive oxygen species by complex I, *Biochemical Society transactions 36*, 976-980.
[100] St-Pierre, J., Buckingham, J. A., Roebuck, S. J., and Brand, M. D. (2002) Topology of superoxide production from different sites in the mitochondrial electron transport chain, *The Journal of biological chemistry 277*, 44784-44790.
[101] Miwa, S., St-Pierre, J., Partridge, L., and Brand, M. D. (2003) Superoxide and hydrogen peroxide production by Drosophila mitochondria, *Free radical biology & medicine 35*, 938-948.
[102] Han, D., Canali, R., Rettori, D., and Kaplowitz, N. (2003) Effect of glutathione depletion on sites and topology of superoxide and hydrogen peroxide production in mitochondria, *Molecular pharmacology 64*, 1136-1144.
[103] Zhang, L., Yu, L., and Yu, C. A. (1998) Generation of superoxide anion by succinate-cytochrome c reductase from bovine heart mitochondria, *The Journal of biological chemistry 273*, 33972-33976.
[104] Moreno-Sanchez, R., Hernandez-Esquivel, L., Rivero-Segura, N. A., Marin-Hernandez, A., Neuzil, J., Ralph, S. J., and Rodriguez-Enriquez, S. (2013) Reactive oxygen species are

generated by the respiratory complex II--evidence for lack of contribution of the reverse electron flow in complex I, *FEBS J 280*, 927-938.
[105] Kluckova, K., Sticha, M., Cerny, J., Mracek, T., Dong, L., Drahota, Z., Gottlieb, E., Neuzil, J., and Rohlena, J. (2015) Ubiquinone-binding site mutagenesis reveals the role of mitochondrial complex II in cell death initiation, *Cell death & disease 6*, e1749.
[106] Chen, Y. R., and Zweier, J. L. (2014) Cardiac mitochondria and reactive oxygen species generation, *Circulation research 114*, 524-537.
[107] Liu, Y., Fiskum, G., and Schubert, D. (2002) Generation of reactive oxygen species by the mitochondrial electron transport chain, *Journal of neurochemistry 80*, 780-787.
[108] Cadenas, E., Boveris, A., Ragan, C. I., and Stoppani, A. O. (1977) Production of superoxide radicals and hydrogen peroxide by NADH-ubiquinone reductase and ubiquinol-cytochrome c reductase from beef-heart mitochondria, *Archives of biochemistry and biophysics 180*, 248-257.
[109] Turrens, J. F., and Boveris, A. (1980) Generation of superoxide anion by the NADH dehydrogenase of bovine heart mitochondria, *The Biochemical journal 191*, 421-427.
[110] Herrero, A., and Barja, G. (2000) Localization of the site of oxygen radical generation inside the complex I of heart and nonsynaptic brain mammalian mitochondria, *Journal of bioenergetics and biomembranes 32*, 609-615.
[111] Kushnareva, Y., Murphy, A. N., and Andreyev, A. (2002) Complex I-mediated reactive oxygen species generation: modulation by cytochrome c and NAD(P)+ oxidation-reduction state, *The Biochemical journal 368*, 545-553.
[112] Raha, S., McEachern, G. E., Myint, A. T., and Robinson, B. H. (2000) Superoxides from mitochondrial complex III: the role of manganese superoxide dismutase, *Free radical biology & medicine 29*, 170-180.
[113] Starkov, A. A., and Fiskum, G. (2001) Myxothiazol induces H(2)O(2) production from mitochondrial respiratory chain, *Biochemical and biophysical research communications 281*, 645-650.
[114] Muller, F., Crofts, A. R., and Kramer, D. M. (2002) Multiple Q-Cycle Bypass Reactions at the QoSite of the Cytochromebc1Complex†, *Biochemistry 41*, 7866-7874.
[115] Huang, L. S., Cobessi, D., Tung, E. Y., and Berry, E. A. (2005) Binding of the respiratory chain inhibitor antimycin to the mitochondrial bc1 complex: a new crystal structure reveals an altered intramolecular hydrogen-bonding pattern, *J Mol Biol 351*, 573-597.
[116] Nicholls, D. G., and Ferguson, S. J. (2013) 5 - Respiratory Chains, In *Bioenergetics (Fourth Edition)* (Nicholls, D. G., and Ferguson, S. J., Eds.), pp 91-157, Academic Press, Boston.
[117] Meinhardt, S. W., and Crofts, A. R. (1982) The site and mechanism of action of myxothiazol as an inhibitor of electron transfer in Rhodopseudomonas sphaeroides, *FEBS letters 149*, 217-222.
[118] Xiao, D., Powolny, A. A., Moura, M. B., Kelley, E. E., Bommareddy, A., Kim, S. H., Hahm, E. R., Normolle, D., Van Houten, B., and Singh, S. V. (2010) Phenethyl isothiocyanate inhibits oxidative phosphorylation to trigger reactive oxygen species-mediated death of human prostate cancer cells, *The Journal of biological chemistry 285*, 26558-26569.
[119] Neuzil, J., Dong, L. F., Rohlena, J., Truksa, J., and Ralph, S. J. (2013) Classification of mitocans, anti-cancer drugs acting on mitochondria, *Mitochondrion 13*, 199-208.
[120] Zhang, Z., Huang, L., Shulmeister, V. M., Chi, Y. I., Kim, K. K., Hung, L. W., Crofts, A. R., Berry, E. A., and Kim, S. H. (1998) Electron transfer by domain movement in cytochrome bc1, *Nature 392*, 677-684.

[121] Hunte, C., Koepke, J., Lange, C., Roßmanith, T., and Michel, H. (2000) Structure at 2.3 Å resolution of the cytochrome bc1 complex from the yeast Saccharomyces cerevisiae co-crystallized with an antibody Fv fragment, *Structure 8*, 669-684.
[122] Boveris, A., and Cadenas, E. (1975) Mitochondrial production of superoxide anions and its relationship to the antimycin insensitive respiration, *FEBS letters 54*, 311-314.
[123] Han, D., Williams, E., and Cadenas, E. (2001) Mitochondrial respiratory chain-dependent generation of superoxide anion and its release into the intermembrane space, *Biochemical Journal 353*, 411-416.
[124] Miwa, S., and Brand, M. D. (2005) The topology of superoxide production by complex III and glycerol 3-phosphate dehydrogenase in Drosophila mitochondria, *Biochimica et biophysica acta 1709*, 214-219.
[125] Muller, F. L., Liu, Y., and Van Remmen, H. (2004) Complex III releases superoxide to both sides of the inner mitochondrial membrane, *The Journal of biological chemistry 279*, 49064-49073.
[126] Martinez-Reyes, I., and Cuezva, J. M. (2014) The H(+)-ATP synthase: a gate to ROS-mediated cell death or cell survival, *Biochimica et biophysica acta 1837*, 1099-1112.
[127] Salomon, A. R., Voehringer, D. W., Herzenberg, L. A., and Khosla, C. (2000) Understanding and exploiting the mechanistic basis for selectivity of polyketide inhibitors of F(0)F(1)-ATPase, *Proceedings of the National Academy of Sciences of the United States of America 97*, 14766-14771.
[128] Salomon, A. R., Voehringer, D. W., Herzenberg, L. A., and Khosla, C. (2001) Apoptolidin, a selective cytotoxic agent, is an inhibitor of F0F1-ATPase, *Chemistry & biology 8*, 71-80.
[129] Wang, Y., and Hekimi, S. (2016) Understanding Ubiquinone, *Trends in cell biology 26*, 367-378.
[130] Ribas, V., Garcia-Ruiz, C., and Fernandez-Checa, J. C. (2014) Glutathione and mitochondria, *Front Pharmacol 5*, 151.
[131] Miriyala, S., Spasojevic, I., Tovmasyan, A., Salvemini, D., Vujaskovic, Z., St Clair, D., and Batinic-Haberle, I. (2012) Manganese superoxide dismutase, MnSOD and its mimics, *Biochimica et biophysica acta 1822*, 794-814.
[132] Burgering, B. M. (2008) A brief introduction to FOXOlogy, *Oncogene 27*, 2258-2262.
[133] Kim, Y. S., Gupta Vallur, P., Phaeton, R., Mythreye, K., and Hempel, N. (2017) Insights into the Dichotomous Regulation of SOD2 in Cancer, *Antioxidants (Basel) 6*, 86.
[134] Li, S., Yan, T., Yang, J. Q., Oberley, T. D., and Oberley, L. W. (2000) The role of cellular glutathione peroxidase redox regulation in the suppression of tumor cell growth by manganese superoxide dismutase, *Cancer research 60*, 3927-3939.
[135] Holley, A. K., Dhar, S. K., Xu, Y., and St Clair, D. K. (2012) Manganese superoxide dismutase: beyond life and death, *Amino Acids 42*, 139-158.
[136] Miriyala, S., Holley, A. K., and St Clair, D. K. (2011) Mitochondrial superoxide dismutase--signals of distinction, *Anticancer Agents Med Chem 11*, 181-190.
[137] Esworthy, R. S., Ho, Y. S., and Chu, F. F. (1997) The Gpx1 gene encodes mitochondrial glutathione peroxidase in the mouse liver, *Archives of biochemistry and biophysics 340*, 59-63.
[138] Maiorino, M., Scapin, M., Ursini, F., Biasolo, M., Bosello, V., and Flohe, L. (2003) Distinct promoters determine alternative transcription of gpx-4 into phospholipid-hydroperoxide glutathione peroxidase variants, *The Journal of biological chemistry 278*, 34286-34290.

[139] Oberley, T. D., Verwiebe, E., Zhong, W., Kang, S. W., and Rhee, S. G. (2001) Localization of the thioredoxin system in normal rat kidney, *Free radical biology & medicine 30*, 412-424.
[140] Embley, T. M., and Martin, W. (2006) Eukaryotic evolution, changes and challenges, *Nature 440*, 623-630.
[141] Tielens, A. G. M., Rotte, C., van Hellemond, J. J., and Martin, W. (2002) Mitochondria as we don't know them, *Trends in biochemical sciences 27*, 564-572.
[142] Green, D. R., and Reed, J. C. (1998) Mitochondria and apoptosis, *Science 281*, 1309-1312.
[143] Jurkovic, S., Osredkar, J., and Marc, J. (2008) Molecular impact of glutathione peroxidases in antioxidant processes, *Biochem Medica 18*, 162-174.
[144] Nohl, H., and Jordan, W. (2005) The Metabolic Fate of Mitochondrial Hydrogen Peroxide, *European Journal of Biochemistry 111*, 203-210.
[145] Meister, A., and Anderson, M. E. (1983) Glutathione, *Annual review of biochemistry 52*, 711-760.
[146] Wu, G., Fang, Y. Z., Yang, S., Lupton, J. R., and Turner, N. D. (2004) Glutathione metabolism and its implications for health, *The Journal of nutrition 134*, 489-492.
[147] Soderdahl, T., Enoksson, M., Lundberg, M., Holmgren, A., Ottersen, O. P., Orrenius, S., Bolcsfoldi, G., and Cotgreave, I. A. (2003) Visualization of the compartmentalization of glutathione and protein-glutathione mixed disulfides in cultured cells, *FASEB journal : official publication of the Federation of American Societies for Experimental Biology 17*, 124-126.
[148] Zimmermann, A. K., Loucks, F. A., Schroeder, E. K., Bouchard, R. J., Tyler, K. L., and Linseman, D. A. (2007) Glutathione binding to the Bcl-2 homology-3 domain groove: a molecular basis for Bcl-2 antioxidant function at mitochondria, *The Journal of biological chemistry 282*, 29296-29304.
[149] Markovic, J., Borras, C., Ortega, A., Sastre, J., Vina, J., and Pallardo, F. V. (2007) Glutathione is recruited into the nucleus in early phases of cell proliferation, *The Journal of biological chemistry 282*, 20416-20424.
[150] Fernandes, A. P., and Holmgren, A. (2004) Glutaredoxins: glutathione-dependent redox enzymes with functions far beyond a simple thioredoxin backup system, *Antioxidants & redox signaling 6*, 63-74.
[151] Hanschmann, E. M., Godoy, J. R., Berndt, C., Hudemann, C., and Lillig, C. H. (2013) Thioredoxins, glutaredoxins, and peroxiredoxins--molecular mechanisms and health significance: from cofactors to antioxidants to redox signaling, *Antioxidants & redox signaling 19*, 1539-1605.
[152] Gaber, A. (2014) The importance of Arabidopsis glutathione peroxidase 8 for protecting Arabidopsis plant and E. coli cells against oxidative stress, *GM Crops Food 5*, 20-26.
[153] Dayer, R., Fischer, B. B., Eggen, R. I., and Lemaire, S. D. (2008) The peroxiredoxin and glutathione peroxidase families in Chlamydomonas reinhardtii, *Genetics 179*, 41-57.
[154] Deponte, M. (2013) Glutathione catalysis and the reaction mechanisms of glutathione-dependent enzymes, *Biochimica et biophysica acta 1830*, 3217-3266.
[155] Couto, N., Wood, J., and Barber, J. (2016) The role of glutathione reductase and related enzymes on cellular redox homoeostasis network, *Free radical biology & medicine 95*, 27-42.
[156] Sena, L. A., and Chandel, N. S. (2012) Physiological roles of mitochondrial reactive oxygen species, *Molecular cell 48*, 158-167.

[157] Lu, J., and Holmgren, A. (2014) The thioredoxin antioxidant system, *Free radical biology & medicine 66*, 75-87.
[158] Cairns, R. A., Harris, I. S., and Mak, T. W. (2011) Regulation of cancer cell metabolism, *Nature reviews. Cancer 11*, 85-95.
[159] Cox, A. G., Winterbourn, C. C., and Hampton, M. B. (2009) Mitochondrial peroxiredoxin involvement in antioxidant defence and redox signalling, *The Biochemical journal 425*, 313-325.
[160] Wood, Z. A., Poole, L. B., and Karplus, P. A. (2003) Peroxiredoxin evolution and the regulation of hydrogen peroxide signaling, *Science 300*, 650-653.
[161] Yu, L., Wan, F., Dutta, S., Welsh, S., Liu, Z., Freundt, E., Baehrecke, E. H., and Lenardo, M. (2006) Autophagic programmed cell death by selective catalase degradation, *Proceedings of the National Academy of Sciences of the United States of America 103*, 4952-4957.
[162] Goodsell, D. S. (2004) *Catalase*.
[163] Nohl, H., and Jordan, W. (1980) The metabolic fate of mitochondrial hydrogen peroxide, *European journal of biochemistry / FEBS 111*, 203-210.
[164] Radi, R., Turrens, J. F., Chang, L. Y., Bush, K. M., Crapo, J. D., and Freeman, B. A. (1991) Detection of catalase in rat heart mitochondria, *The Journal of biological chemistry 266*, 22028-22034.
[165] Izawa, S., Inoue, Y., and Kimura, A. (1996) Importance of catalase in the adaptive response to hydrogen peroxide: analysis of acatalasaemic Saccharomyces cerevisiae, *The Biochemical journal 320 (Pt 1)*, 61-67.
[166] Shen, X., Sun, X., Sun, B., Li, T., Wu, G., Li, Y., Chen, L., Liu, Q., Cui, M., and Zhou, Z. (2018) ARRDC3 suppresses colorectal cancer progression through destabilizing the oncoprotein YAP, *FEBS letters 592*, 599-609.
[167] Circu, M. L., Stringer, S., Rhoads, C. A., Moyer, M. P., and Aw, T. Y. (2009) The role of GSH efflux in staurosporine-induced apoptosis in colonic epithelial cells, *Biochemical pharmacology 77*, 76-85.
[168] Son, Y., Kim, S., Chung, H.-T., and Pae, H.-O. (2013) Chapter Two - Reactive Oxygen Species in the Activation of MAP Kinases, In *Methods in enzymology* (Enrique, C., and Lester, P., Eds.), pp 27-48, Academic Press.
[169] Redza-Dutordoir, M., and Averill-Bates, D. A. (2016) Activation of apoptosis signalling pathways by reactive oxygen species, *Biochimica et biophysica acta 1863*, 2977-2992.
[170] Fuchs, Y., and Steller, H. (2011) Programmed cell death in animal development and disease, *Cell 147*, 742-758.
[171] Galluzzi, L., Bravo-San Pedro, J. M., Kepp, O., and Kroemer, G. (2016) Regulated cell death and adaptive stress responses, *Cellular and molecular life sciences : CMLS 73*, 2405-2410.
[172] Kroemer, G., Galluzzi, L., Vandenabeele, P., Abrams, J., Alnemri, E. S., Baehrecke, E. H., Blagosklonny, M. V., El-Deiry, W. S., Golstein, P., Green, D. R., et al. (2009) Classification of cell death: recommendations of the Nomenclature Committee on Cell Death 2009, *Cell death and differentiation 16*, 3-11.
[173] Galluzzi, L., and Vitale, I., and Aaronson, S. A., and Abrams, J. M., and Adam, D., and Agostinis, P., and Alnemri, E. S., and Altucci, L., and Amelio, I., and Andrews, D. W., et al. (2018) Molecular mechanisms of cell death: recommendations of the Nomenclature Committee on Cell Death 2018, *Cell death and differentiation 25*, 486-541.

[174] Liu, X., Yang, W., Guan, Z., Yu, W., Fan, B., Xu, N., and Liao, D. J. (2018) There are only four basic modes of cell death, although there are many ad-hoc variants adapted to different situations, *Cell Biosci 8*, 6.
[175] Mihaly, S. R., Sakamachi, Y., Ninomiya-Tsuji, J., and Morioka, S. (2017) Noncanocial cell death program independent of caspase activation cascade and necroptotic modules is elicited by loss of TGFbeta-activated kinase 1, *Sci Rep 7*, 2918.
[176] Chen, D., Yu, J., and Zhang, L. (2016) Necroptosis: an alternative cell death program defending against cancer, *Biochimica et biophysica acta 1865*, 228-236.
[177] Rabinowitz, J. D., and White, E. (2010) Autophagy and metabolism, *Science 330*, 1344-1348.
[178] Scherz-Shouval, R., Shvets, E., Fass, E., Shorer, H., Gil, L., and Elazar, Z. (2007) Reactive oxygen species are essential for autophagy and specifically regulate the activity of Atg4, *The EMBO journal 26*, 1749-1760.
[179] Santidrian, A. F., Matsuno-Yagi, A., Ritland, M., Seo, B. B., LeBoeuf, S. E., Gay, L. J., Yagi, T., and Felding-Habermann, B. (2013) Mitochondrial complex I activity and NAD+/NADH balance regulate breast cancer progression, *J Clin Invest 123*, 1068-1081.
[180] Zhang, Q., Raoof, M., Chen, Y., Sumi, Y., Sursal, T., Junger, W., Brohi, K., Itagaki, K., and Hauser, C. J. (2010) Circulating mitochondrial DAMPs cause inflammatory responses to injury, *Nature 464*, 104-107.
[181] Schulze-Osthoff, K., Bakker, A. C., Vanhaesebroeck, B., Beyaert, R., Jacob, W. A., and Fiers, W. (1992) Cytotoxic activity of tumor necrosis factor is mediated by early damage of mitochondrial functions. Evidence for the involvement of mitochondrial radical generation, *The Journal of biological chemistry 267*, 5317-5323.
[182] Zhang, D.-W., Shao, J., Lin, J., Zhang, N., Lu, B.-J., Lin, S.-C., Dong, M.-Q., and Han, J. (2009) RIP3, an Energy Metabolism Regulator That Switches TNF-Induced Cell Death from Apoptosis to Necrosis, *Science 325*, 332.
[183] Tait, S. W. G., Ichim, G., and Green, D. R. (2014) Die another way – non-apoptotic mechanisms of cell death, *Journal of cell science 127*, 2135.
[184] Cohen, G. M. (1997) Caspases: the executioners of apoptosis, *The Biochemical journal 326 (Pt 1)*, 1-16.
[185] Green, D., and Kroemer, G. (1998) The central executioners of apoptosis: caspases or mitochondria?, *Trends in cell biology 8*, 267-271.
[186] Garrido, C., and Kroemer, G. (2004) Life's smile, death's grin: vital functions of apoptosis-executing proteins, *Current opinion in cell biology 16*, 639-646.
[187] Kung, G., Konstantinidis, K., and Kitsis, R. N. (2011) Programmed necrosis, not apoptosis, in the heart, *Circulation research 108*, 1017-1036.
[188] Youle, R. J., and Strasser, A. (2008) The BCL-2 protein family: opposing activities that mediate cell death, *Nat Rev Mol Cell Biol 9*, 47-59.
[189] Stepczynska, A., Lauber, K., Engels, I. H., Janssen, O., Kabelitz, D., Wesselborg, S., and Schulze-Osthoff, K. (2001) Staurosporine and conventional anticancer drugs induce overlapping, yet distinct pathways of apoptosis and caspase activation, *Oncogene 20*, 1193-1202.
[190] Pong, K., Doctrow, S. R., Huffman, K., Adinolfi, C. A., and Baudry, M. (2001) Attenuation of staurosporine-induced apoptosis, oxidative stress, and mitochondrial dysfunction by synthetic superoxide dismutase and catalase mimetics, in cultured cortical neurons, *Experimental neurology 171*, 84-97.

[191] Zhang, X. D., Gillespie, S. K., and Hersey, P. (2004) Staurosporine induces apoptosis of melanoma by both caspase-dependent and -independent apoptotic pathways, *Molecular cancer therapeutics 3*, 187-197.
[192] Circu, M. L., and Aw, T. Y. (2010) Reactive oxygen species, cellular redox systems, and apoptosis, *Free radical biology & medicine 48*, 749-762.
[193] Brookes, P. S., Yoon, Y., Robotham, J. L., Anders, M. W., and Sheu, S. S. (2004) Calcium, ATP, and ROS: a mitochondrial love-hate triangle, *American journal of physiology. Cell physiology 287*, C817-833.
[194] Bernardi, P. (2013) The mitochondrial permeability transition pore: a mystery solved?, *Frontiers in physiology 4*, 95.
[195] Garrido, C., Galluzzi, L., Brunet, M., Puig, P. E., Didelot, C., and Kroemer, G. (2006) Mechanisms of cytochrome c release from mitochondria, *Cell death and differentiation 13*, 1423-1433.
[196] Adams, J. M., and Cory, S. (2007) The Bcl-2 apoptotic switch in cancer development and therapy, *Oncogene 26*, 1324-1337.
[197] Uren, R. T., Dewson, G., Bonzon, C., Lithgow, T., Newmeyer, D. D., and Kluck, R. M. (2005) Mitochondrial release of pro-apoptotic proteins: electrostatic interactions can hold cytochrome c but not Smac/DIABLO to mitochondrial membranes, *The Journal of biological chemistry 280*, 2266-2274.
[198] Li, L. Y., Luo, X., and Wang, X. (2001) Endonuclease G is an apoptotic DNase when released from mitochondria, *Nature 412*, 95.
[199] Ledgerwood, E. C., and Morison, I. M. (2009) Targeting the apoptosome for cancer therapy, *Clin Cancer Res 15*, 420-424.
[200] McIlwain, D. R., Berger, T., and Mak, T. W. (2015) Caspase functions in cell death and disease, *Cold Spring Harb Perspect Biol 7*.
[201] Salvesen, G. S. (2002) Caspases and apoptosis, *Essays Biochem 38*, 9-19.
[202] Chaitanya, G. V., Steven, A. J., and Babu, P. P. (2010) PARP-1 cleavage fragments: signatures of cell-death proteases in neurodegeneration, *Cell Commun Signal 8*, 31.
[203] Murphy, M. P. (2008) Targeting lipophilic cations to mitochondria, *Biochimica et biophysica acta 1777*, 1028-1031.
[204] Neuzil, J., Dong, L. F., Ramanathapuram, L., Hahn, T., Chladova, M., Wang, X. F., Zobalova, R., Prochazka, L., Gold, M., Freeman, R., et al. (2007) Vitamin E analogues as a novel group of mitocans: anti-cancer agents that act by targeting mitochondria, *Molecular aspects of medicine 28*, 607-645.
[205] Neuzil, J., Wang, X. F., Dong, L. F., Low, P., and Ralph, S. J. (2006) Molecular mechanism of 'mitocan'-induced apoptosis in cancer cells epitomizes the multiple roles of reactive oxygen species and Bcl-2 family proteins, *FEBS letters 580*, 5125-5129.
[206] Smith, R. A., Porteous, C. M., Gane, A. M., and Murphy, M. P. (2003) Delivery of bioactive molecules to mitochondria in vivo, *Proceedings of the National Academy of Sciences of the United States of America 100*, 5407-5412.
[207] Gane, E. J., Weilert, F., Orr, D. W., Keogh, G. F., Gibson, M., Lockhart, M. M., Frampton, C. M., Taylor, K. M., Smith, R. A., and Murphy, M. P. (2010) The mitochondria-targeted anti-oxidant mitoquinone decreases liver damage in a phase II study of hepatitis C patients, *Liver Int 30*, 1019-1026.
[208] Dong, L. F., Jameson, V. J., Tilly, D., Cerny, J., Mahdavian, E., Marin-Hernandez, A., Hernandez-Esquivel, L., Rodriguez-Enriquez, S., Stursa, J., Witting, P. K., et al. (2011)

Mitochondrial targeting of vitamin E succinate enhances its pro-apoptotic and anti-cancer activity via mitochondrial complex II, *The Journal of biological chemistry 286*, 3717-3728.
[209] Dong, L. F., Jameson, V. J., Tilly, D., Prochazka, L., Rohlena, J., Valis, K., Truksa, J., Zobalova, R., Mahdavian, E., Kluckova, K., et al. (2011) Mitochondrial targeting of alpha-tocopheryl succinate enhances its pro-apoptotic efficacy: a new paradigm for effective cancer therapy, *Free radical biology & medicine 50*, 1546-1555.
[210] Kovarova, J., Bajzikova, M., Vondrusova, M., Stursa, J., Goodwin, J., Nguyen, M., Zobalova, R., Pesdar, E. A., Truksa, J., Tomasetti, M., et al. (2014) Mitochondrial targeting of alpha-tocopheryl succinate enhances its anti-mesothelioma efficacy, *Redox report : communications in free radical research 19*, 16-25.
[211] Hubackova, S., Davidova, E., Rohlenova, K., Stursa, J., Werner, L., Andera, L., Dong, L., Terp, M. G., Hodny, Z., Ditzel, H. J., et al. (2018) Selective elimination of senescent cells by mitochondrial targeting is regulated by ANT2, *Cell death and differentiation*.
[212] Moreira, P. I., Custodio, J., Moreno, A., Oliveira, C. R., and Santos, M. S. (2006) Tamoxifen and estradiol interact with the flavin mononucleotide site of complex I leading to mitochondrial failure, *The Journal of biological chemistry 281*, 10143-10152.
[213] Boukalova, S., Stursa, J., Werner, L., Ezrova, Z., Cerny, J., Bezawork-Geleta, A., Pecinova, A., Dong, L., Drahota, Z., and Neuzil, J. (2016) Mitochondrial Targeting of Metformin Enhances Its Activity against Pancreatic Cancer, *Molecular cancer therapeutics 15*, 2875-2886.
[214] Andrzejewski, S., Gravel, S. P., Pollak, M., and St-Pierre, J. (2014) Metformin directly acts on mitochondria to alter cellular bioenergetics, *Cancer Metab 2*, 12.
[215] Hur, K. Y., and Lee, M. S. (2015) New mechanisms of metformin action: Focusing on mitochondria and the gut, *J Diabetes Investig 6*, 600-609.
[216] Loubiere, C., Clavel, S., Gilleron, J., Harisseh, R., Fauconnier, J., Ben-Sahra, I., Kaminski, L., Laurent, K., Herkenne, S., Lacas-Gervais, S., et al. (2017) The energy disruptor metformin targets mitochondrial integrity via modification of calcium flux in cancer cells, *Sci Rep 7*, 5040.
[217] Dawood, S., Broglio, K., Buzdar, A. U., Hortobagyi, G. N., and Giordano, S. H. (2010) Prognosis of women with metastatic breast cancer by HER2 status and trastuzumab treatment: an institutional-based review, *J Clin Oncol 28*, 92-98.
[218] Miller, K. D., Siegel, R. L., Lin, C. C., Mariotto, A. B., Kramer, J. L., Rowland, J. H., Stein, K. D., Alteri, R., and Jemal, A. (2016) Cancer treatment and survivorship statistics, 2016, *CA: a cancer journal for clinicians 66*, 271-289.
[219] Saura, C., Bendell, J., Jerusalem, G., Su, S., Ru, Q., De Buck, S., Mills, D., Ruquet, S., Bosch, A., Urruticoechea, A., et al. (2014) Phase Ib study of Buparlisib plus Trastuzumab in patients with HER2-positive advanced or metastatic breast cancer that has progressed on Trastuzumab-based therapy, *Clin Cancer Res 20*, 1935-1945.
[220] Schafer, Z. T., Grassian, A. R., Song, L., Jiang, Z., Gerhart-Hines, Z., Irie, H. Y., Gao, S., Puigserver, P., and Brugge, J. S. (2009) Antioxidant and oncogene rescue of metabolic defects caused by loss of matrix attachment, *Nature 461*, 109-113.
[221] Ding, Y., Liu, Z., Desai, S., Zhao, Y., Liu, H., Pannell, L. K., Yi, H., Wright, E. R., Owen, L. B., Dean-Colomb, W., et al. (2012) Receptor tyrosine kinase ErbB2 translocates into mitochondria and regulates cellular metabolism, *Nat Commun 3*, 1271.
[222] You, Y., Xu, Z., and Chen, Y. (2018) Doxorubicin conjugated with a trastuzumab epitope and an MMP-2 sensitive peptide linker for the treatment of HER2-positive breast cancer, *Drug Deliv 25*, 448-460.

[223] Dragowska, W. H., Ginj, M., Kozlowski, P., Yung, A., Ruth, T. J., Adam, M. J., Sossi, V., Bally, M. B., and Yapp, D. T. T. (2016) Overexpression of HER-2 in MDA-MB-435/LCC6 Tumours is Associated with Higher Metabolic Activity and Lower Energy Stress, *Scientific Reports 6*, 18537.

[224] Rohlena, J., Dong, L. F., Kluckova, K., Zobalova, R., Goodwin, J., Tilly, D., Stursa, J., Pecinova, A., Philimonenko, A., Hozak, P., et al. (2011) Mitochondrially targeted alpha-tocopheryl succinate is antiangiogenic: potential benefit against tumor angiogenesis but caution against wound healing, *Antioxidants & redox signaling 15*, 2923-2935.

[225] Flora, S. J., Bhatt, K., and Mehta, A. (2009) Arsenic moiety in gallium arsenide is responsible for neuronal apoptosis and behavioral alterations in rats, *Toxicology and applied pharmacology 240*, 236-244.

[226] Guy, C. T., Webster, M. A., Schaller, M., Parsons, T. J., Cardiff, R. D., and Muller, W. J. (1992) Expression of the neu protooncogene in the mammary epithelium of transgenic mice induces metastatic disease, *Proceedings of the National Academy of Sciences of the United States of America 89*, 10578-10582.

[227] Truksa, J., Dong, L. F., Rohlena, J., Stursa, J., Vondrusova, M., Goodwin, J., Nguyen, M., Kluckova, K., Rychtarcikova, Z., Lettlova, S., et al. (2015) Mitochondrially targeted vitamin E succinate modulates expression of mitochondrial DNA transcripts and mitochondrial biogenesis, *Antioxidants & redox signaling 22*, 883-900.

[228] Gnaiger, E., Kuznetsov, A., Schneeberger, S., Seiler, R., Brandacher, G., Steurer, W., and Margreiter, R. (2000) Mitochondria in the Cold, In *Life in the Cold* (Heldmaier, G., and Klingenspor, M., Eds.), pp 431-442, Springer Berlin Heidelberg.

[229] Rueden, C. T., Schindelin, J., Hiner, M. C., DeZonia, B. E., Walter, A. E., Arena, E. T., and Eliceiri, K. W. (2017) ImageJ2: ImageJ for the next generation of scientific image data, *BMC Bioinformatics 18*, 529.

[230] Schmitt, S., Saathoff, F., Meissner, L., Schropp, E. M., Lichtmannegger, J., Schulz, S., Eberhagen, C., Borchard, S., Aichler, M., Adamski, J., et al. (2013) A semi-automated method for isolating functionally intact mitochondria from cultured cells and tissue biopsies, *Analytical biochemistry 443*, 66-74.

[231] Frezza, C., Cipolat, S., and Scorrano, L. (2007) Organelle isolation: functional mitochondria from mouse liver, muscle and cultured fibroblasts, *Nature protocols 2*, 287-295.

[232] Vondrusova, M., Bezawork-Geleta, A., Sachaphibulkij, K., Truksa, J., and Neuzil, J. (2015) The effect of mitochondrially targeted anticancer agents on mitochondrial (super)complexes, *Methods in molecular biology 1265*, 195-208.

[233] Zerbetto, E., Vergani, L., and Dabbeni-Sala, F. (1997) Quantification of muscle mitochondrial oxidative phosphorylation enzymes via histochemical staining of blue native polyacrylamide gels, *Electrophoresis 18*, 2059-2064.

[234] Wittig, I., Carrozzo, R., Santorelli, F. M., and Schagger, H. (2007) Functional assays in high-resolution clear native gels to quantify mitochondrial complexes in human biopsies and cell lines, *Electrophoresis 28*, 3811-3820.

[235] Wittig, I., Karas, M., and Schagger, H. (2007) High resolution clear native electrophoresis for in-gel functional assays and fluorescence studies of membrane protein complexes, *Molecular & cellular proteomics : MCP 6*, 1215-1225.

[236] Zou, C., Wang, Y., and Shen, Z. (2005) 2-NBDG as a fluorescent indicator for direct glucose uptake measurement, *Journal of biochemical and biophysical methods 64*, 207-215.

[237] Grivennikova, V. G., Kareyeva, A. V., and Vinogradov, A. D. (2018) Oxygen-dependence of mitochondrial ROS production as detected by Amplex Red assay, *Redox biology 17*, 192-199.
[238] Weydert, C. J., and Cullen, J. J. (2010) Measurement of superoxide dismutase, catalase and glutathione peroxidase in cultured cells and tissue, *Nature protocols 5*, 51-66.
[239] Kim, K. H., and Sederstrom, J. M. (2015) Assaying Cell Cycle Status Using Flow Cytometry, *Curr Protoc Mol Biol 111*, 28 26 21-11.
[240] Spinazzi, M., Casarin, A., Pertegato, V., Salviati, L., and Angelini, C. (2012) Assessment of mitochondrial respiratory chain enzymatic activities on tissues and cultured cells, *Nature protocols 7*, 1235-1246.
[241] Schoors, S., De Bock, K., Cantelmo, A. R., Georgiadou, M., Ghesquiere, B., Cauwenberghs, S., Kuchnio, A., Wong, B. W., Quaegebeur, A., Goveia, J., et al. (2014) Partial and transient reduction of glycolysis by PFKFB3 blockade reduces pathological angiogenesis, *Cell metabolism 19*, 37-48.
[242] Siegel, R. L., Miller, K. D., and Jemal, A. (2018) Cancer statistics, 2018, *CA: a cancer journal for clinicians 68*, 7-30.
[243] DeSantis, C. E., Lin, C. C., Mariotto, A. B., Siegel, R. L., Stein, K. D., Kramer, J. L., Alteri, R., Robbins, A. S., and Jemal, A. (2014) Cancer treatment and survivorship statistics, 2014, *CA: a cancer journal for clinicians 64*, 252-271.
[244] Cheng, G., Zielonka, J., Ouari, O., Lopez, M., McAllister, D., Boyle, K., Barrios, C. S., Weber, J. J., Johnson, B. D., Hardy, M., et al. (2016) Mitochondria-Targeted Analogues of Metformin Exhibit Enhanced Antiproliferative and Radiosensitizing Effects in Pancreatic Cancer Cells, *Cancer research 76*, 3904.
[245] Slamon, D. J., Clark, G. M., Wong, S. G., Levin, W. J., Ullrich, A., and McGuire, W. L. (1987) Human breast cancer: correlation of relapse and survival with amplification of the HER-2/neu oncogene, *Science 235*, 177-182.
[246] Cardoso, C. M., Custodio, J. B., Almeida, L. M., and Moreno, A. J. (2001) Mechanisms of the deleterious effects of tamoxifen on mitochondrial respiration rate and phosphorylation efficiency, *Toxicology and applied pharmacology 176*, 145-152.
[247] Neuzil, J., Dyason, J. C., Freeman, R., Dong, L. F., Prochazka, L., Wang, X. F., Scheffler, I., and Ralph, S. J. (2007) Mitocans as anti-cancer agents targeting mitochondria: lessons from studies with vitamin E analogues, inhibitors of complex II, *Journal of bioenergetics and biomembranes 39*, 65-72.
[248] Lapuente-Brun, E., Moreno-Loshuertos, R., Acin-Perez, R., Latorre-Pellicer, A., Colas, C., Balsa, E., Perales-Clemente, E., Quiros, P. M., Calvo, E., Rodriguez-Hernandez, M. A., et al. (2013) Supercomplex assembly determines electron flux in the mitochondrial electron transport chain, *Science 340*, 1567-1570.
[249] Dong, L. F., Swettenham, E., Eliasson, J., Wang, X. F., Gold, M., Medunic, Y., Stantic, M., Low, P., Prochazka, L., Witting, P. K., et al. (2007) Vitamin E analogues inhibit angiogenesis by selective induction of apoptosis in proliferating endothelial cells: the role of oxidative stress, *Cancer research 67*, 11906-11913.
[250] Naderi, J., Hung, M., and Pandey, S. (2003) Oxidative stress-induced apoptosis in dividing fibroblasts involves activation of p38 MAP kinase and over-expression of Bax: resistance of quiescent cells to oxidative stress, *Apoptosis : an international journal on programmed cell death 8*, 91-100.

[251] Sarsour, E. H., Venkataraman, S., Kalen, A. L., Oberley, L. W., and Goswami, P. C. (2008) Manganese superoxide dismutase activity regulates transitions between quiescent and proliferative growth, *Aging Cell 7*, 405-417.
[252] Kops, G. J., Dansen, T. B., Polderman, P. E., Saarloos, I., Wirtz, K. W., Coffer, P. J., Huang, T. T., Bos, J. L., Medema, R. H., and Burgering, B. M. (2002) Forkhead transcription factor FOXO3a protects quiescent cells from oxidative stress, *Nature 419*, 316-321.
[253] Yan, B., Stantic, M., Zobalova, R., Bezawork-Geleta, A., Stapelberg, M., Stursa, J., Prokopova, K., Dong, L., and Neuzil, J. (2015) Mitochondrially targeted vitamin E succinate efficiently kills breast tumour-initiating cells in a complex II-dependent manner, *BMC Cancer 15*, 401.
[254] Viale, A., Pettazzoni, P., Lyssiotis, C. A., Ying, H., Sanchez, N., Marchesini, M., Carugo, A., Green, T., Seth, S., Giuliani, V., et al. (2014) Oncogene ablation-resistant pancreatic cancer cells depend on mitochondrial function, *Nature 514*, 628-632.
[255] Roesch, A., Vultur, A., Bogeski, I., Wang, H., Zimmermann, K. M., Speicher, D., Korbel, C., Laschke, M. W., Gimotty, P. A., Philipp, S. E., et al. (2013) Overcoming intrinsic multidrug resistance in melanoma by blocking the mitochondrial respiratory chain of slow-cycling JARID1B(high) cells, *Cancer cell 23*, 811-825.
[256] Trachootham, D., Zhou, Y., Zhang, H., Demizu, Y., Chen, Z., Pelicano, H., Chiao, P. J., Achanta, G., Arlinghaus, R. B., Liu, J., et al. (2006) Selective killing of oncogenically transformed cells through a ROS-mediated mechanism by beta-phenylethyl isothiocyanate, *Cancer cell 10*, 241-252.
[257] Trachootham, D., Alexandre, J., and Huang, P. (2009) Targeting cancer cells by ROS-mediated mechanisms: a radical therapeutic approach?, *Nature reviews. Drug discovery 8*, 579-591.
[258] Lee, S. R., Kim, J. R., Kwon, K. S., Yoon, H. W., Levine, R. L., Ginsburg, A., and Rhee, S. G. (1999) Molecular cloning and characterization of a mitochondrial selenocysteine-containing thioredoxin reductase from rat liver, *The Journal of biological chemistry 274*, 4722-4734.
[259] Ott, M., Robertson, J. D., Gogvadze, V., Zhivotovsky, B., and Orrenius, S. (2002) Cytochrome c release from mitochondria proceeds by a two-step process, *Proceedings of the National Academy of Sciences of the United States of America 99*, 1259-1263.
[260] Kagan, V. E., Tyurin, V. A., Jiang, J., Tyurina, Y. Y., Ritov, V. B., Amoscato, A. A., Osipov, A. N., Belikova, N. A., Kapralov, A. A., Kini, V., et al. (2005) Cytochrome c acts as a cardiolipin oxygenase required for release of proapoptotic factors, *Nat Chem Biol 1*, 223-232.
[261] Dong, Z., Shanmughapriya, S., Tomar, D., Siddiqui, N., Lynch, S., Nemani, N., Breves, S. L., Zhang, X., Tripathi, A., Palaniappan, P., et al. (2017) Mitochondrial Ca(2+) Uniporter Is a Mitochondrial Luminal Redox Sensor that Augments MCU Channel Activity, *Molecular cell 65*, 1014-1028 e1017.
[262] Brown, K. K., Eriksson, S. E., Arner, E. S., and Hampton, M. B. (2008) Mitochondrial peroxiredoxin 3 is rapidly oxidized in cells treated with isothiocyanates, *Free radical biology & medicine 45*, 494-502.
[263] Chen, Y., Cai, J., and Jones, D. P. (2006) Mitochondrial thioredoxin in regulation of oxidant-induced cell death, *FEBS letters 580*, 6596-6602.
[264] Cox, A. G., Brown, K. K., Arner, E. S., and Hampton, M. B. (2008) The thioredoxin reductase inhibitor auranofin triggers apoptosis through a Bax/Bak-dependent process that involves peroxiredoxin 3 oxidation, *Biochemical pharmacology 76*, 1097-1109.

[265] Conrad, M., Jakupoglu, C., Moreno, S. G., Lippl, S., Banjac, A., Schneider, M., Beck, H., Hatzopoulos, A. K., Just, U., Sinowatz, F., et al. (2004) Essential role for mitochondrial thioredoxin reductase in hematopoiesis, heart development, and heart function, *Molecular and cellular biology 24*, 9414-9423.

[266] Nonn, L., Williams, R. R., Erickson, R. P., and Powis, G. (2003) The absence of mitochondrial thioredoxin 2 causes massive apoptosis, exencephaly, and early embryonic lethality in homozygous mice, *Molecular and cellular biology 23*, 916-922.

[267] Li, Y., Huang, T. T., Carlson, E. J., Melov, S., Ursell, P. C., Olson, J. L., Noble, L. J., Yoshimura, M. P., Berger, C., Chan, P. H., et al. (1995) Dilated cardiomyopathy and neonatal lethality in mutant mice lacking manganese superoxide dismutase, *Nat Genet 11*, 376-381.

[268] Rogers, L. K., Tamura, T., Rogers, B. J., Welty, S. E., Hansen, T. N., and Smith, C. V. (2004) Analyses of glutathione reductase hypomorphic mice indicate a genetic knockout, *Toxicological sciences : an official journal of the Society of Toxicology 82*, 367-373.

[269] Ho, Y. S., Magnenat, J. L., Bronson, R. T., Cao, J., Gargano, M., Sugawara, M., and Funk, C. D. (1997) Mice deficient in cellular glutathione peroxidase develop normally and show no increased sensitivity to hyperoxia, *The Journal of biological chemistry 272*, 16644-16651.

[270] Birsoy, K., Possemato, R., Lorbeer, F. K., Bayraktar, E. C., Thiru, P., Yucel, B., Wang, T., Chen, W. W., Clish, C. B., and Sabatini, D. M. (2014) Metabolic determinants of cancer cell sensitivity to glucose limitation and biguanides, *Nature 508*, 108-112.

[271] Brindle, K. M., Bohndiek, S. E., Gallagher, F. A., and Kettunen, M. I. (2011) Tumor imaging using hyperpolarized 13C magnetic resonance spectroscopy, *Magn Reson Med 66*, 505-519.

[272] Shrayyef, M. Z., and Gerich, J. E. (2010) Normal Glucose Homeostasis, In *Principles of Diabetes Mellitus* (Poretsky, L., Ed.), pp 19-35, Springer US, Boston, MA.

[273] Hirayama, A., Kami, K., Sugimoto, M., Sugawara, M., Toki, N., Onozuka, H., Kinoshita, T., Saito, N., Ochiai, A., Tomita, M., et al. (2009) Quantitative metabolome profiling of colon and stomach cancer microenvironment by capillary electrophoresis time-of-flight mass spectrometry, *Cancer research 69*, 4918-4925.

[274] Goveia, J., Pircher, A., Conradi, L. C., Kalucka, J., Lagani, V., Dewerchin, M., Eelen, G., DeBerardinis, R. J., Wilson, I. D., and Carmeliet, P. (2016) Meta-analysis of clinical metabolic profiling studies in cancer: challenges and opportunities, *EMBO molecular medicine 8*, 1134-1142.

[275] Kroemer, G., Marino, G., and Levine, B. (2010) Autophagy and the integrated stress response, *Molecular cell 40*, 280-293.

[276] Haq, R., Shoag, J., Andreu-Perez, P., Yokoyama, S., Edelman, H., Rowe, G. C., Frederick, D. T., Hurley, A. D., Nellore, A., Kung, A. L., et al. (2013) Oncogenic BRAF regulates oxidative metabolism via PGC1alpha and MITF, *Cancer cell 23*, 302-315.